# UC Davis

## UC Davis Electronic Theses and Dissertations

### Title

Soil Viral Ecology in Fire Affected Ecosystems

### Permalink

https://escholarship.org/uc/item/1zw3f46w

### Author

Geonczy, Sara

### Publication Date

2024

### Supplemental Material

https://escholarship.org/uc/item/1zw3f46w#supplemental

Peer reviewed|Thesis/dissertation

eScholarship.org Powered by the California Digital Library
University of California

Soil Viral Ecology in Fire Affected Ecosystems

By

SARA EUGENIA GEONCZY
DISSERTATION

Submitted in partial satisfaction of the requirements for the degree of

DOCTOR OF PHILOSOPHY

in

Soils and Biogeochemistry

in the

OFFICE OF GRADUATE STUDIES

of the

UNIVERSITY OF CALIFORNIA

DAVIS

Approved:

_____

Joanne Emerson, Chair

_____

Valerie Eviner

_____

Jorge Rodrigues

Committee in Charge

2024

**Acknowledgements**

~ Everyone in the Emerson lab has played a role in helping me through the years, providing many fantastic iterations of awkward lab photos, and recovering millions of putative viruses: Joanne Emerson, Laura Zinke, Aurélie Bak, Winston Bess, Rose Bolle, Anneliek ter Horst, Alena Schroeder, Christian Santos-Medellín, Genesee Jason, Jess Sorensen, Jane Fudyma, Grant Gogul, Amethyst Ralph, Lissangel Martinez, Devyn Durham, Brandon Matsumoto, Ella Sieradzki, Luke Hillary, Lucie Jiraska

~ My friends and peers from the Soils and Biogeochemistry graduate group and beyond

~ The many professors who have helped shape my academic experience at UC Davis: Valerie Eviner, Jorge Rodrigues, Majdi Abou Najm, Kate Scow, Sanjai Parikh, Ron Amundson, Toby O'Geen, Amisha Poret-Peterson

~ My small and supportive family: Mama, Papa, Maria

## Table of Contents

**Abstract** ..... **v**

**Chapter One: Virome responses to heating of a forest soil suggest that most dsDNA viral particles do not persist at 90°C** ..... **1**

Abstract ..... 1

Introduction ..... 2

Materials and Methods ..... 5

Results ..... 12

Discussion ..... 19

Conclusion ..... 22

Data Availability ..... 22

Acknowledgements ..... 22

References ..... 23

Main Figures ..... 28

Supplementary Figures ..... 34

**Chapter Two: Locally heterogeneous soil viral, prokaryotic, and chemical responses to prescribed burn reflect patchy burn severity in a mixed conifer forest** ..... **36**

Abstract ..... 36

Introduction ..... 37

Materials and Methods ..... 39

Results and Discussion ..... 47

Conclusion ..... 54

Data Availability ..... 55
Acknowledgements ..... 55
References ..... 56
Main Figures ..... 60
Supplementary Figures ..... 64
**Chapter Three: Soil viral and prokaryotic communities shifted significantly after wildfire in chaparral and woodland habitats ..... 69**
Abstract ..... 69
Introduction ..... 70
Materials and Methods ..... 71
Results and Discussion ..... 77
Conclusion ..... 84
Data Availability ..... 85
Acknowledgements ..... 85
References ..... 85
Main Figures ..... 89
Supplementary Figures ..... 92

**Abstract**

The current increase in global fire activity, driven by climate change, land use change, and fire suppression policies, warrants a better understanding of fire's effects on soil microorganisms which drive major biogeochemical processes including carbon turnover and nutrient availability. Viruses of prokaryotes (bacteria and archaea), which are largely dsDNA viruses, apply pressure to microbial communities via infection and lysis and may also have distinct impacts on biogeochemical cycling apart from infection dynamics, making their own responses to fire (associated with host dynamics and/or based on their extracellular durability) important factors in understanding post-fire biogeochemistry. Incorporating soil viruses into the microbial community framework has begun to elucidate their roles in key soil processes and reveal similar and distinct responses to changing environmental conditions when compared to their host. Our ability to comprehensively interrogate dsDNA viral communities in soil has been possible with the development of size filtrated metagenomics, or viromics, which enriches samples in virus-like particles and enhances the ability to recover viruses through shotgun metagenomic sequencing. Using a viromics-based approach, the following three studies investigate soil viral communities in fire-affected systems with three different angles and scopes, in response to: (1) laboratory-based heating, (2) a field-based prescribed burn, and (3) a field-based wildfire.

In the first study, research was focused on isolating and understanding the effects of heating in soil, which is one of the main direct impacts from fire and is also relevant in other practices, such as solarization. Prior to this work, little was known about the effects of high temperatures on soil viruses. In this study, three data types (DNase-treated viromes, non-DNase-treated viromes, and 16S rRNA gene amplicon sequencing) were leveraged to measure the responses of soil viral and prokaryotic communities to heating to 30°C, 60°C, or 90°C, in comparison to field and control conditions. This experiment investigated: (1) the responses of dsDNA viral communities to heating of soils from two horizons (O and A) from the same forest

soil profile, (2) the extent to which specific viral taxa could be identified as heat-sensitive or heat-tolerant across replicates and soil horizons, and (3) prokaryotic and virus-host dynamics in response to heating. Both viral and prokaryotic communities responded similarly to the treatment variables, and within both soil horizons, viral and prokaryotic communities clustered into three groups, based on beta-diversity patterns: the ambient community (field, control, and 30°C samples), the 60°C, and the 90°C communities. As DNase-treated viromic DNA yields were below detection limits at 90°C, it was inferred that most viral capsids were compromised after the 90°C treatment, indicating a maximum temperature threshold between 60°C and 90°C for most viral particles in these soils. Groups of heat-tolerant and heat-sensitive vOTUs were also identified across both soil sources. Overall, it was determined that over 70% of viral populations, like their prokaryotic counterparts, could withstand temperatures as high as 60°C, with shifts in relative abundance explaining most community compositional differences across heating treatments.

In the second study, the response of viral communities to prescribed burning, a management strategy for maintaining forest health and mitigating devastating wildfires, was investigated. Soil viral community responses to a spring prescribed burn in a mixed conifer forest were assessed, as was the extent to which soil chemical properties and/or prokaryotic host communities could explain the observed patterns. With a before-after control-impact (BACI) design, two replicate soil samples were collected at each of two depths (0-3 cm and 3-6 cm) from four treatment (burn) plots and two control plots, at five timepoints (two before and three after the burn) over two months. From these 120 samples, 91 viromes were sequenced, and 198,402 viral 'species' (vOTUs) were recovered. Viral communities differed most significantly by location, regardless of treatment, and along with prokaryotic communities, exhibited a heterogenous response to fire. This response was correlated with soil chemical changes attributed to the burn, leading to the development of a chemistry-based burn severity index for this study. Low viromic DNA yields (a proxy for viral particle abundances) at high burn severity

suggested loss of viral biomass. The relative abundances of Firmicutes, Actinobacteria, and the viruses predicted to infect them significantly increased along the burn severity gradient, suggesting survival of spore-formers and viral infection of these abundant taxa.

In the third study, soil samples were collected over the course of one year after a wildfire in Mediterranean chaparral and woodland habitats in northern California. The principal goal of the study was to compare temporal responses within each habitat to unburned controls. Wildfire resulted in substantial shifts in viral community composition in both habitats. There were significant changes in the relative abundances of viruses predicted to infect bacteria from spore-forming phyla, which were at higher abundance in burned samples. Additionally, a substantial proportion of vOTUs in both burned habitats was also found in a burned Mediterranean forest, which may indicate some conserved traits in post-fire ecosystems.

Overall, from the results of these three studies, there are significant shifts in viral community composition in response to fire and fire-related impacts (heating). Measuring responses to biologically relevant temperature changes helped to elucidate how the direct impacts of heating from a disturbance like fire might be immediately shifting communities based on temperature persistence thresholds of extracellular virions. The prescribed burn study in a forest ecosystem introduced the heterogeneity of fire as an ecosystem process and reinforced the importance of measuring burn severity, specifically based on soil chemical property changes. The burn severity index helped to reveal clear shifts in viral community composition, with evidence of decreased viral particle abundances, decreased viral richness, and changes in relative abundances of viruses that infected specific phyla, particularly host phyla that also changed in relative abundance in the prokaryotic communities. Lastly, under the least controlled fire scenario, our third study found a clear difference in viral and prokaryotic communities between soils affected by wildfire and unburned controls.

**Chapter One**: **Virome responses to heating of a forest soil suggest that most dsDNA viral particles do not persist at 90°C**


## Abstract

Many fundamental characteristics of soil viruses remain underexplored, including the effects of high temperatures on viruses and their hosts, as would be encountered under disturbances like wildland fire, prescribed burning, and soil solarization. In this study, we leveraged three data types (DNase-treated viromes, non-DNase-treated viromes, and 16S rRNA gene amplicon sequencing) to measure the responses of soil viral and prokaryotic communities to heating to 30°C, 60°C, or 90°C, in comparison to field and control conditions. We investigated (1) the response of dsDNA viral communities to heating of soils from two horizons (O and A) from the same forest soil profile, (2) the extent to which specific viral taxa could be identified as heat-sensitive or heat-tolerant across replicates and soil horizons, and (3) prokaryotic and virus-host dynamics in response to heating. We found that both viral and prokaryotic communities responded similarly to the treatment variables. Community composition differed most significantly by soil source (O or A horizon). Within both soil horizons, viral and prokaryotic communities clustered into three groups, based on beta-diversity patterns: the ambient community (field, control, and 30°C samples) and the 60°C and 90°C communities. As DNase-treated viromic DNA yields were below detection limits at 90°C, we infer that most viral capsids were compromised after the 90°C treatment, indicating a maximum temperature threshold between 60°C and 90°C for most viral particles in these soils. We also identified groups of heat-tolerant and heat-sensitive vOTUs across both soil sources. Overall, we found that over 70% of viral populations, like their prokaryotic counterparts, could withstand temperatures as high as 60°C, with shifts in relative abundance explaining most community compositional differences across heating treatments.

## Introduction

Soil viral ecology is a growing field that explores how viruses interact with their hosts and the environment, which can help characterize their role in soil functions (1–4). Many soil functions, particularly biogeochemical cycling, are driven by microbial processes that immobilize, mineralize, and otherwise transform key chemical elements (5,6), with viral infection presumed to impact these processes in largely unknown ways. Prokaryotic viruses target bacteria and archaea, impacting host metabolic activity and leading to cell lysis through various forms of infection dynamics (7). Viruses are also theorized to play a direct part in nutrient cycling, separate from their impact on microorganisms, for example as stoichiometrically enriched sources of phosphorus (8). Since viruses must remain viable to infect their host, uncovering basic characteristics of soil viruses, such as temperature thresholds, is needed in order to better understand the role of viruses in complex biogeochemical processes.

The temperature range that an organism can tolerate while remaining viable is a defining characteristic that influences ecological responses to changing environmental conditions and can impact biogeographical patterns. For soil organisms, certain disturbances can increase soil temperatures outside the range of an average diurnal cycle. Soil solarization can increase temperatures up to more than 50°C at 5 cm depth (9). Soils under forest slash burn piles can reach up to 138 ± 28°C at 5 cm depth (10). Controlled surface burns can increase soil temperatures to over 400°C at 2 cm (11). Temperature tolerance determines which organisms can or cannot survive these disturbances and contributes to community compositional changes (12). While more is known about prokaryotic temperature tolerances in soil (13,14), studying the temperature tolerances of the viruses of these prokaryotes can help us to better understand virus-host dynamics and post-disturbance ecological responses.

High temperatures are known to inactivate viruses and compromise viral capsids, releasing nucleic acids into the environment (2,15–17). Upper thresholds for persistence vary, and prokaryotic viruses have been found in extreme thermal environments, serving as the only

entities that can continue to apply biological pressure on microorganisms at high temperatures (18). Studies of sewage and sludge have also shown that phages can be more resistant to thermally induced inactivation than bacteria (19). In dairy production studies, temperate phages of *Lactococcus* spp. have been shown to survive temperatures as high as 97°C after 5 minutes of heating, with even more heat-resistant dairy bacteriophages still being discovered (20–22). However, much less is known about the response of soil prokaryotic viruses to soil heating. In a study of peat soil prokaryotic viruses, soil warming up to 9°C above ambient temperature was not shown to significantly change viral community composition after two years (23). In a study looking at viral community shifts in a hyperthermophilic composting plant, considered a model system for better understanding decomposition of organic matter in soil, there were distinct viral communities in the composting phases, including a hyperthermophilic phase between 80 to 90°C and a thermophilic phase at around 55°C (24).

The degree of temperature change from heating in soil depends on a suite of physicochemical characteristics, including soil moisture, organic matter content, and mineralogy (25–29). Soil also does not heat evenly, and there is evidence of stratified microbial survival in soil based on depth (30). Studies in soils show that there is a range of prokaryotic survival thresholds that varies by temperature and duration of heating, likely owing to different adaptations of prokaryotes, as well as the heterogeneity of soils which impacts the extent of heat penetration (14). For instance, organic soils that typically comprise the upper section of a soil profile, considered the O horizon, have high organic matter content and generally higher water holding capacity. In forests, mineral soils that directly underlie an O horizon are typically considered the A horizon and have lower organic matter content (31,32). This makes it important to study the impact of increased temperature on various soil types, with special attention to different horizons within a soil profile, with distinct properties, such as mineralogy and water holding capacity, that intrinsically respond differently to heating (33–36).

Fortunately, the ability to investigate the temperature tolerance of viruses in soil is

enabled via viromics. Viromics is a size-fractionated metagenomic approach that enriches for virus-like-particles (VLPs), in many cases specifically enriching for dsDNA viruses (4,37). Viral particles are brought into solution via mechanical and chemical means to remove most free virions from the soil matrix, including those that were adhered to soil particles or occluded in aggregate pores. DNase treatment, the addition of a DNA-degrading enzyme, cleans samples by removing the vast majority of DNA occurring outside a virion capsid prior to DNA extraction (38,39). This leaves samples that are enriched in extracellular virions (not prophages or viruses in the intracellular stage of their replication cycle) with intact capsids that are theoretically viable, or at least more likely to be viable than virions with compromised capsids. Thus, DNase-treated viromics is a way to measure active viral community dynamics (39). However, when considering viromes that have not been treated with DNase, sequences can be recovered not only from virions that remained intact and potentially viable, but also from viruses that have been compromised (40), which can provide further insights into persistence under changing environmental conditions.

Viromes, whether treated with DNase or not, also enrich for small prokaryotic cells that are able to pass through a 0.22 μm filtration step, including those belonging to the superphylum Patescibacteria, which are ultra-small bacteria with small genome sizes (40–42). Thus, 16S rRNA gene amplicon sequencing of viromes can also reveal dynamics of small bacteria, in which the signal is otherwise obscured with total DNA extraction. Viromes not treated with DNase can also potentially reveal microbial mortality through characterization of relic DNA of prokaryotes (40). This can be especially useful if paired with sequencing results from total DNA, which would include prokaryotes both potentially active (cells intact) and dead.

In this study, we leveraged these three sample types (DNase-treated viromes, non-DNase-treated viromes, and total DNA) to measure the responses of soil viral and prokaryotic communities to heating treatments of target temperatures between 30°C and 90°C and to deduce virus-host dynamics. Primarily, we used DNase-treated viromes to characterize

presumed active viral communities, and we used total DNA for prokaryotic communities. We used non-DNase-treated viromes to yield additional insights into the inactive/relic fraction of viruses and prokaryotes (e.g., for additional evidence as to which species succumbed at which temperature thresholds), as well as to infer the responses of small bacteria to increasing temperature. From both total DNA and the non-DNase-treated viromes, we generated 16S rRNA gene amplicon sequencing data to characterize prokaryotic communities. The three main questions that we address in this study are: (1) How do dsDNA viral communities respond to heating of soils from two horizons (O and A) from the same soil profile? (2) To what extent are specific viral taxa consistently heat-sensitive or heat-tolerant across replicates and soil types? and (3) What are the prokaryotic and virus-host dynamics in response to heating?

## Materials and Methods

*Soil Sampling:*

Soils for this study was collected from Blodgett Forest Research Station in California, USA (38°54.905' N, 120°39.640' W, elevation 4299 ft) on April 18, 2022. This location was chosen due to a field experiment in the same area set up one year prior, which studied the impact of prescribed burning on soil viral ecology. Building on evidence that spatial variability obscures treatment effects in soil virus studies (43–45), we sought to constrain spatial variability as much as possible by collecting 2 kg of each of two soil types (O and A horizon) from one 40 x 70 x 6 cm block and homogenizing and sieving (8 mm) each soil type. This specific location was selected because of its soil profile characteristics, where the O horizon corresponded to a depth of 0-3 cm with an abrupt horizon boundary above the underlying A horizon, which went beyond a depth of 6 cm. We determined the characteristics of the soil horizons using a soil probe.

*Selection of Experimental Parameters:*

For experimental soil heating, we chose 10°C as the control temperature, which

approximated field temperatures without a heating disturbance. To determine this temperature, temperature measurements were taken just prior to soil collection using a soil thermometer inserted at 3 and 6 cm depths in random locations within the soil collection area (**Supplementary Table 1**). In addition, temperatures were measured at six nearby plots (four burn plots and two control plots) over a period of 6 days before and after a prescribed burn in the previous year as part of the aforementioned ongoing study. For this, we used temperature probes (Extech SDL200 4-Channel Data Logging Thermometer, Extech TP873 Bead Wire Type K Temperature Probe, -30 to 300°C) inserted at 1, 2, 4, and 6 cm in soil profile with at least one logging unit per plot (**Supplementary Table 2**), allowing us to select three biologically and ecologically relevant temperatures for the heating treatments. We chose 90°C for the highest temperature, due to evidence of some viral persistence at these temperatures (18,20–22,24), 60°C for the second-highest temperature, as prokaryotic community shifts would be expected due to some mortality at that temperature (33), and 30°C for the lower temperature, as this represents elevated temperatures seen in some heating disturbances (solarization, surface burning) but is lower than most known survival thresholds for prokaryotes and virions. We selected 30 minutes as the heating time to sufficiently heat up the soil to a stable temperature and to mimic short-term heating disturbances as may happen naturally in prescribed burning.

*Laboratory microcosms subjected to soil heating:*

The experimental treatments were as follows: six samples (three technical replicates per horizon) were processed for DNA extraction the day after field collection without any heating treatment, after storage at 4°C for approximately 12 hours. These are considered “field” samples because they were processed shortly after field sampling. Each of the other sample sets (three samples per horizon per set) were randomly divided into two 36-hour treatment periods that occurred in succession. This time was chosen so that samples could be processed within a two-day period (12 samples per day). At the beginning of each treatment period, samples were placed in a New Brunswick Excella E-24R light-penetrable incubator (Eppendorf, Hamburg, Germany)

at 10°C to maintain soil at the control temperature. At the beginning of the 36 hours, samples were subjected to 30 minutes of heating by removing tubes from the incubator and placing them in 50 ml modular heating blocks (VWR #13259-254, Radnor, PA, USA) that were pre-heated to one of three temperatures (30, 60, or 90°C).

Soil samples were added up to the 20 mL line of 50 mL bioreaction centrifuge tubes (VWR #76211-286), which maximized the amount of soil exposed to the heating block. Due to differences in bulk density (0.15 g/cm$^3$ for the O horizon soil and 0.39 g/cm$^3$ for the A horizon soil), each sample weighed on average 6.39 g for the organic soil and 9.77 g for the mineral soil. The tubes had vented caps with 0.22 μm membranes, which allowed for free gas exchange while maintaining aseptic conditions. After 30 minutes, the samples were returned to the 10°C incubator. A sample set remained in the 10°C incubator for the entire 36 hours and was considered the "control" sample set. For each treatment, an additional sample (not processed for downstream measurements) was used for measuring the soil temperature in the center of the tube at the start and at 10 min intervals throughout the 30-minute heating incubation. Once the 36 hours were complete, the samples were collected for DNA extraction. Samples were heated and processed in a random order to minimize batch effects.

*Viromic DNA extraction and quantification:*

We extracted viromic DNA from all samples, as previously described (45). Briefly, to each soil sample, we initially added 9 mL of protein-supplemented phosphate-buffered saline solution (PPBS: 2% bovine serum albumin, 10% phosphate-buffered saline, 1% potassium citrate, and 150 mM $MgSO_4$, pH 6.5). Samples were vortexed until homogenized and then placed on a horizontal shaker at 300 RPM at 4°C for 10 min. Supernatant was transferred into a new tube and then 9 mL of PPBS was added to the soil remaining in the original tube, repeating the process for a total of three soil resuspensions and elutions, ending with a total of three volumes of supernatant pooled together in a new centrifuge tube (approximately 27 mL). The pooled supernatant was then centrifuged at 8 min at 7840 RPM, 4°C, with the progressively

cleaner supernatant collected and the concentrated soil particles discarded, for a total of three centrifugation and supernatant collection steps. The final supernatant was filtered through a 5 μm polyethersulfone (PES) membrane filter (PALL, Port Washington, NY, USA) to filter out larger soil particles and then the filtrate went through a 0.22 μm PES membrane filter (PALL) to exclude most cellular organisms (apart from ultra-small bacteria (40,41)). Virus-sized particles and DNA remaining in the filtrate were concentrated into a pellet using the Optima LE-80K ultracentrifuge with a 50.2 Ti rotor (Beckman-Coulter, Brea, CA, USA) at 32,000 RPM at 4°C for 2 h 25 min. The pellet was resuspended in 200 μL of 0.02 μm filtered ultrapure water and split into two tubes, with one half treated with DNase which included an incubation at 37°C for 30 min after adding 10 units of RQ1 RNase-free DNase (Promega, Madison, WI, USA) and one half not treated with DNase (considered non-DNase-treated virome samples). For all virome samples, DNA was extracted using the DNeasy PowerSoil Pro kit (Qiagen, Hilden, Germany), following the manufacturer's protocol, with the addition of a 10 min incubation at 65°C prior to cell lysis, which also served as the 'stop' incubation for the DNase treatment. DNA quantification was performed using the Qubit dsDNA HS Assay and Qubit 4 fluorometer (ThermoFisher, Waltham, MA, USA), and samples with yields above 0.1 ng/μl were prepared for library construction and sequencing.

*Total DNA extraction and quantification:*

For each sample, 0.25 g of soil was added directly to the DNeasy PowerSoil Pro kit (Qiagen) for DNA extraction, following the manufacturer's protocol, with the addition of a 10 min incubation at 65°C prior to cell lysis. DNA quantification was performed using the Qubit dsDNA HS Assay and Qubit 4 fluorometer (ThermoFisher).

*Shotgun virome library preparation and sequencing:*

Sequencing of all viromes was performed by the DNA Technologies and Expression Analysis Core at the University of California, Davis Genome Center (Davis, CA, USA). Metagenomic libraries were constructed with the DNA Hyper Prep kit (Kapa Biosystems-Roche,

Basel, Switzerland) and sequenced (paired-end, 150 bp) using the Illumina NovaSeq S4 platform to a requested depth of 10 Gbp per virome.

*Amplicon library preparation and sequencing:*

We performed 16S rRNA gene amplicon sequencing on all total DNA extractions and on all the non-DNase treated viromes using a dual-indexing strategy (46). We used the Platinum Hot Start PCR Master Mix (ThermoFisher) with the 515F/806R universal primer set for amplification of the V4 region of the 16S rRNA gene. We followed Earth Microbiome Project's PCR protocol (47), which included an initial denaturation step at 94°C for 3 min, 35 cycles of 94°C for 45 s, 50°C for 60 s, and 72°C for 90 s, and a final extension step at 72°C for 10 min. We cleaned libraries with AmpureXP magnetic beads (Beckman Coulter), quantified amplicons with a Qubit 4 fluorometer (ThermoFisher), and then pooled all bead-purified products together in equimolar concentrations. Libraries were sequenced by the DNA Technologies and Expression Analysis Core at the University of California, Davis Genome Center, paired-end (250 bp) on the Illumina MiSeq platform.

*Soil physicochemical measurements:*

We calculated gravimetric soil moisture nine times for each soil horizon, by weighing out 10 g of soil into aluminum weigh dishes and measuring the weight after 24 hours in a drying oven at 105°C. Three replicate samples of field-condition soil (not dried) of each horizon and one sample for each post-heat treatment (at 30, 60, and 90°C temperatures) were sent to Ward Laboratories (Kearney, Nebraska, USA) for a suite of soil chemistry analyses under the Haney Soil Health Analysis package (48), which is summarized in **Supplementary Table 3**. The measurements included: soil pH and soluble salts (1:1 soil/water suspension), organic matter (percentage weight loss-on-ignition), soil respiration (Solvita® $CO_2$-Burst method: soil was dried at 50°C and sieved at 2 mm, then 40 g soil was incubated for 24 hours in a 50 mL container with perforated bottom allowing for rewetting with 25 mL distilled water in a 250 mL glass jar sealed with a Solvita® paddle, and after 24 hours, $CO_2$-C was quantified with a

Solvita® digital reader with the units of mg CO2-C/kg soil), water extractable total N and organic C (quantified by shaking 4 g of soil with 40 mL of distilled water for 10 min and filtering with a Whatman 2V), Haney-(H3A: combination of citric, malic, and oxalic acids) extracted ammonium (NH4-N), nitrate (NO3-N), and inorganic phosphorus (orthophosphate: PO4-P) (the latter quantified with flow injection analysis), and H3A-extracted total phosphorus (P), potassium (K), zinc (Zn), iron (Fe), manganese (Mn), copper (Cu), sulfur (S), calcium (Ca), magnesium (Mg), sodium (Na), and Aluminum (Al) (quantified using inductively coupled argon plasma, or ICAP, atomic emission spectroscopy). Calculations included inorganic N (sum of H3A-extracted NH4-N and NO3-N), organic N (water-extractable total N minus inorganic N), organic P (total P minus inorganic P), microbially active carbon (soil respiration divided by water extractable organic C, expressed as percentage), organic C : organic N, and organic N : inorganic N.

*Virome bioinformatic processing:*

Raw reads were trimmed using Trimmomatic v0.39 (49) with a minimum q-score of 30 and a minimum read length of 50 bases. We used BBMap v39.01 (50) to remove PhiX sequences. Each virome was assembled separately with MEGAHIT v1.2.9 (51) in the metalarge mode with a minimum contig length of 10,000 bp. Assembled contigs were analyzed with VIBRANT v1.2.0 (52) with the -virome flag to identify viral contigs. All output viral contigs (low, medium, and high quality) from all samples were iteratively clustered to form a representative, dereplicated set of vOTUs. We first used CD-HIT v4.8.1 (53) to cluster viral contigs at 95% shared nucleotide identity and 85% alignment coverage (breadth). We then consolidated the resulting contigs into species-level viral operational taxonomic units (vOTUs) with dRep v3.2.2 (54), using the default algorithm for secondary clustering comparisons, default average nucleotide identity (ANI) threshold to form secondary clusters (0.95), and 0.85 minimum level of overlap between genomes when doing secondary comparisons. Quality-filtered raw reads from all viromes were then mapped against the dereplicated set of vOTUs using Bowtie 2 v2.4.1

(55) in sensitive mode. Lastly, we used CoverM v0.5.0 (56) to quantify vOTU abundance and generated a trimmed mean coverage table and a count table for downstream analyses (0.75 minimum covered fraction). Host taxonomy of the entire set of dereplicated vOTUs was predicted using iPHoP v1.1.0 (57), with a minimum cutoff score of 90 (**Supplementary Table 4**).

*16S rRNA gene amplicon sequence bioinformatic processing:*

We used DADA2 v1.12.1 (58) to demultiplex 16S rRNA gene amplicon reads and perform quality assessment, read merging, and chimera removal. For quality filtering, we used the filterAndTrim() function with the following parameters: truncLen = c(0,0), maxN = 0, maxEE = c(2,2), truncQ = 2, rm.phix = TRUE. All other processing was with default settings. Amplicon sequence variants (ASVs) were assigned taxonomy by using the DADA2 RDP classifier, using the SILVA database v138.1 as reference (59).

*Statistical and ecological analyses:*

All ecological and statistical analyses were performed using R v4.3.0 (60). Input for all analyses of viral communities or vOTUs was the trimmed mean coverage vOTU table. We normalized the vOTU abundance table by using the decostand function (method = “total”, MARGIN = 2) from the Vegan package v2.6-4 (61) and removed singletons (vOTUs detected in only one sample). We used a DADA2-generated abundance table for 16S rRNA gene amplified single variants (ASVs), filtered out mitochondria and chloroplasts, and removed singletons (ASVs that only appeared in a single sample). We calculated Bray-Curtis dissimilarities with vegdist (method = “bray”) and performed PERMANOVAs with adonis, both functions from Vegan. We used the cmdscale function to perform multidimensional scaling and retrieve true eigenvalues and calculate PCoA points. We created upset plots using ComplexUpset v1.3.5 and using species abundance tables that were transformed into presence-absence tables (62). To determine enrichment of vOTUs along the temperature gradient, we performed a differential abundance analysis, using the tool DESeq2 v1.38.3 (63). We performed differential abundance

comparisons among all temperatures within horizon and sample type subgroups, then adjusted P-values using the Bonferroni method to determine overall significance of differentially abundant contigs. To identify trend groups among these contigs, we used k-means clustering. Statistical analyses are documented in **Supplementary Tables 5-6**.

*Gene-sharing Network:*

We predicted protein content for each vOTU using Prodigal v2.6.3 (metagenome mode) (64) and used the amino acid file output for gene-sharing network analysis with the tool vConTACT v2.0 (65). We used Diamond for protein alignment (66) and the MCL algorithm for clustering proteins. We used the Fruchterman-Reingold algorithm from the Ggally package (67) to visualize the resulting network, additionally highlighting a subnetwork with neighborhoods that were enriched in significantly differentially abundant vOTUs.

## Results

*Study Design and Dataset Features*

To evaluate the extent to which extractable viral and prokaryotic community composition differed in response to heating treatments and to constrain the threshold temperature(s) for likely decay of most viral particles, we performed a laboratory heating experiment on soils from two horizons (O and A horizons) from a mixed conifer forest (**Figure 1A).** The soil from each horizon was divided into five sample groups, each with three technical replicates (**Figure 1B**). The 'field' sample group was processed within 24 hours of sample collection for viromics and total DNA extraction to capture viral and prokaryotic communities present in the field. The remaining sample groups were subjected to a 36-hour incubation at 10°C, with three of the sample groups elevated to higher temperatures (30, 60, or 90°C) for 30 minutes at the beginning of the incubation. The fourth set of samples remained in the 10°C incubation for the entire 36 hours and is considered the control group. The temperature at the center of the test tube reached 84.4°C for the O horizon soil and 83.0°C for the A horizon soil

when placed in the 90°C heating block, 58.0°C for the O horizon soil and 57.9°C for the A horizon soil in the 60°C heating block, and 29°C for the O horizon soil and 28.8°C for the A horizon soil in the 30°C heating block (**Figure 1C**). As expected, the soil did not heat evenly, so when reporting the intended temperature as the heating block temperature (e.g. 90°C), we acknowledge that not all of the soil reached that temperature.

We sought to characterize the temperature responses of viral particles, microorganisms, and relic DNA to determine which viruses and organisms likely remained viable and which likely did not persist across the temperature gradient. We performed a suite of DNA extraction and sequencing approaches to compare the viral particle, prokaryotic, and relic DNA fractions. Two types of viromes were prepared by sequencing DNA from the post-0.22 μm (viromic) DNA fraction: prior to DNA extraction, each <0.22 μm viral concentrate was split in half, with one half treated with DNase ('DNase-treated'), and the other half not treated with DNase (henceforth referred to as 'non-DNase treated'), for a total of 60 extracted viromes from 30 samples. Based on our prior work (39,40), the DNase-treated viromes capture primarily intact viral particles, whereas the non-DNase treated viromes capture a combination of intact viral particles, compromised viral particles, extracellular DNA potentially reflecting dead microbes and viruses, and small cells that passed through the 0.22 μm filter. DNA yields were below detection limits (less than 0.1 ng/μl) from all six DNase-treated viromes (both soil horizons) at 90°C, and thus we were able to sequence 54 of the 60 prepared viromes (**Figure 3G**). From the 54 sequenced viromes, 145,914 contigs >10 kbp were assembled, 141,638 of which were identified as viral via VIBRANT (52). These viral contigs clustered into 18,869 representative vOTU sequences (**Supplementary Table 7**), and we analyzed a final dataset of 18,538 vOTUs after removing singletons (vOTUs only appearing in a single sample).

To investigate prokaryotic communities, we generated 16S rRNA gene amplicon sequences from both total DNA, which captures a combination of active, dormant, and dead prokaryotes (68,69), and from non-DNase viromes, which would include relic (extracellular)

DNA that co-precipitated with viral particles, as well as an enrichment of small-celled microorganisms (40,41). We were able to perform 16S rRNA gene amplicon sequencing on all 30 total DNA samples and all 30 non-DNase viromes, together yielding 24,270 ASVs (**Supplementary Table 8**), which reduced to 6,679 ASVs after rarefying to a common depth of 25,000 reads per sample and removing singletons.

*Viral and prokaryotic community composition differed most significantly by soil source (between O and A horizons) and secondarily along a temperature gradient*

Considering the full dataset of 54 sequenced viromes, soil viral communities differed most significantly by soil source (between O and A horizons, $p < 0.001$ by PERMANOVA) (**Figure 2A**). When considering DNase-treated viromes, the largest fraction of vOTUs was shared between the two horizons (39%), but the fraction that was distinct to each horizon was still substantial (32% and 29% in O and A horizons, respectively) (**Figure 2B**), showing compositional distinction between the two soil sources. Despite close physical proximity, the distinct physicochemical features of each soil horizon (e.g., microbially active carbon, pH, organic matter, available nitrogen) presumably contributed to the differences in viral community composition (**Figure 2C**). A robust comparison of temperature responses by soil horizon would have required biological replicates from different locations, which was not our goal in this study. Rather, our interest was to compare two distinct soil sources, empirically confirmed here as distinct in both viral and physicochemical composition, to determine whether two different soil sources would yield similar measured responses to temperature.

Within each soil source (O or A horizon), viral communities differed significantly based on temperature treatment ($p < 0.001$ for O horizon, $p < 0.001$ for A horizon by PERMANOVA) (**Figures 3A & B**). In both horizons, viromes significantly separated into three treatment groups: one group with field, control, and 30°C viromes (hereafter referred to as the "ambient" community), a second with 60°C viromes, and a third with 90°C viromes, noting that the 90°C temperature group only included non-DNase viromes in both horizons, as DNase-treated

viromes yielded no detectable DNA at that temperature. In DNase-treated viromes from both horizons, the vast majority of vOTUs was detected in all treatment groups (82% in O horizon and 73% in A horizon), suggesting persistence of most viral species up to 60°C (the highest temperature from which DNase-treated viromes were recovered). The next largest group of vOTUs (8% in O horizon and 7% in A horizon) was present in all treatments, except for the highest temperature, which in this case was 60°C (**Figures 3C & D** and **Supplementary Figures 1A-D),** suggesting temperature-induced decay of those viral populations between 30°C and 60°C. These results show that in the DNase-treated viromes, the presence or absence of unique vOTUs is likely not the main driver separating ambient and 60°C communities.

When considering the non-DNase viromes, recalling that these viromes likely contained genomes from compromised virions, the same trend was apparent in the O and A horizon, with most (43% for O and 37% for A) unique vOTUs shared across the ambient community (field, control and 30°C) and all treatment groups (60°C and 90°C). The ambient community and 60°C had the second most shared vOTUs (35% for O and 16% for A). The ambient community alone had the third most shared vOTUs in the O horizon (11%), but in the A horizon, the number of vOTUs shared among ambient samples (5.4% of total number of vOTUs) was not the third most-ranking intersection (**Figures 3E & F**). Consistent with increasing decay of viral particles in the 60°C and 90°C treatments from both horizons, there were significant differences based on temperature treatment on DNase-treated and non-DNase-treated viromic DNA yields ($p < 0.05$ by Kruskal-Wallis rank sum test) (**Figure 3G**). Together, these results suggest that treatment up to 30°C had no significant effect on viral particle abundance or viral community composition, but both DNA yields and community composition changed significantly at 60°C and again at 90°C. Differences between the ambient viral communities and the two higher temperature treatment groups were largely due to differences in the relative abundances of vOTUs present across treatments, rather than successional community changes, though there were a small number of vOTUs distinct to specific treatment conditions.

*Significantly differentially abundant vOTUs clustered into heat-sensitive and heat-tolerant trait groups*

We performed differential abundance analysis on vOTUs in DNase-treated viromes (likely intact virions) to determine which vOTUs were enriched or depleted as temperature increased. We identified 2,413 vOTUs (13% of total number of vOTUs in DNase-treated viromes) that were significantly differentially abundant across all pairwise temperature comparisons. We then tracked the change in the mean relative abundance of these vOTUs in all replicates within a temperature group and within a horizon over the temperature gradient. Two distinct trend groups emerged for both horizons: vOTUs that increased in abundance as temperature increased, labeled as "heat tolerant," and vOTUs that decreased in abundance as temperature increased, labeled as "heat sensitive" (**Figures 4A & B**). We then investigated the extent to which membership in each trend group was preserved between the two soil horizons. While the majority of vOTUs (74%) were uniquely found in a particular trend group in only one of the soil horizons, 454 vOTUs were heat-sensitive (19% of total) and 149 heat-tolerant (6% of total) in both the O and A horizons (**Figure 4C**).

Finally, we investigated whether the trait of heat sensitivity or tolerance was taxonomically conserved by performing network analyses to place vOTUs into viral network neighborhoods. We identified 1,995 network neighborhoods, which consisted of vOTUs with at least one shared predicted protein with at least one other vOTU in the same neighborhood (**Figure 4D**). We identified 41 neighborhoods that were enriched in heat-sensitive vOTUs in both horizons, 31 enriched in heat-tolerant vOTUs in both horizons, 48 enriched in heat-sensitive vOTUs in only the A horizon, and 41 enriched in heat-tolerant vOTUs in only the O horizon. We did not identify any neighborhoods that were enriched in heat-sensitive vOTUs in only the O horizon, heat-tolerant vOTUs in only the A horizon, or containing vOTUs with mixed traits between the two horizons. To further investigate taxonomic associations of heat-tolerant vOTUs, we identified a subnetwork with clusters that had a significant proportion of these

members. These clusters had a total of 250 nodes (vOTUs, **Figure 4E**), suggesting some taxonomic similarity among vOTUs that persist at higher temperatures. Only two RefSeq viruses were found in this subnetwork, and they were both viruses of Proteobacteria, suggesting that other viruses in the subnetwork might also infect Proteobacteria.

*Prokaryotic community responses to heat treatments were similar to those of viral communities*

We assessed prokaryotic community responses to heat treatments by leveraging 16S rRNA gene amplicon data from both total DNA and non-DNase-treated viromes. Although the recovered prokaryotic communities were significantly different in the total and <0.22 μm (viromic) size fractions, the patterns in response to temperature were similar for each fraction in each horizon (**Figures 5A&B**). Like the viral communities, soil prokaryotic communities were most significantly distinct by soil source (soil horizon) ($p < 0.001$ by PERMANOVA) (**Supplementary Figure 2A**). Within each soil type, prokaryotic community composition also differed significantly with temperature, separating into the same three temperature groups as for the viral communities: field/control/30°C (ambient community), 60°C, and 90°C. Similar to the viral communities, we can consider the prokaryotic ambient community to be best represented in the field, control, and 30°C samples, with significant compositional shifts as the temperature increased to 60°C and then 90°C ($p < 0.001$ for O horizon, for both sample types independently and $p < 0.001$ for A horizon for both sample types independently by PERMANOVA) (**Supplementary Figures 2B-E**).

Underlying the prokaryotic community compositional patterns were taxonomic shifts that largely reflected similarity across the ambient conditions and changes in the relative abundances of specific taxa at 60°C and again at 90°C. In total DNA from the O horizon, the relative abundances of Acidobacteriota, Actinobacteria, Bacteroidota, Myxococcota, and Proteobacteria were significantly impacted by heat treatment (Kruskal-Wallis rank sum test, $p < 0.05$) (**Figure 5C**), as were all of those taxa, except for Myxococcota, in the A horizon (Kruskal-

Wallis rank sum test, $p < 0.05$) (**Figure 5D**). For the >0.22 μm 'viromic' fraction in the O horizon, the relative abundances of the same taxa as in total DNA from the O horizon (Acidobacteriota, Actinobacteria, Myxococcota, and Proteobacteria), as well as Firmicutes and Patescibacteria, were significantly impacted by temperature treatment (Kruskal-Wallis rank sum test, $p < 0.05$) (**Figure 5E**). Finally, in the A horizon, >0.22 μm 'viromic' fraction, the relative abundances of 11 of the 12 most abundant phyla in the dataset (all but Planctomycetota) differed significantly by temperature treatment (Kruskal-Wallis rank sum test, $p < 0.05$) (**Figure 5F**). There were some consistent shifts across both soil horizons and sample type (total DNA or non-DNase-treated virome), including an increase in the relative abundances of Actinobacteria and Firmicutes with increasing temperature. Additionally, Proteobacteria decreased in relative abundance as temperature increased, except for in the >0.22 μm 'viromic' fraction from the O horizon, where there was no significant trend. There were also distinct differences in each subgroup of soil horizon and DNA fraction. In the total DNA samples from the O horizon, there was a slightly higher enrichment of Bacteroidota in the ambient temperature group (on average 8.5% relative abundance), which decreased at higher temperatures (on average 1.8% at 60°C and 2.9% at 90°C). In the >0.22 μm 'viromic' fraction, the most notable taxon was the Patescibacteria (synonymous with Candidate Phyla Radiation), which are small-celled bacteria known to be enriched in 0.2 μm filtered soil samples (40,41). The Patescibacteria dominated the prokaryotic sequences recovered from the ambient temperature group in the O horizon (on average 70% relative abundance) and were also detected at lower but still high abundance in ambient samples from the A horizon (7%), decreasing significantly in the O horizon (15% at 60°C and 5.8% at 90°C) and in the A horizon (0.6% at 60°C and 0.3% at 90°C) as temperature increased. Overall, prokaryotic communities exhibited similar beta-diversity trends to viruses, in terms of both differences by soil type (O vs. A horizon) and across the temperature gradient, suggesting that, in addition to the direct impacts of temperature, viral communities could be shifting in response to host communities on the

timescale of this experiment.

To determine whether there was differential survival between viruses and their hosts, we first sought to link the two using iPHoP, a machine learning tool that predicts hosts for viruses of prokaryotes via a series of sequencing-based markers (Roux et al., 2023). Phylum-level taxonomic information of predicted hosts was assigned to 1,934 vOTUs, or 10% of the vOTUs in this dataset. Based on the Kruskal-Wallis rank sum test, there were significant differences across the temperature gradient in the relative abundance of vOTUs with a predicted host of Actinobacteria ($p = 0.019$) or Cyanobacteria ($p = 0.02$) in the O horizon and Actinobacteria ($p = 0.02$) or Proteobacteria ($p = 0.02$) in the A horizon (**Supplementary Figures 1E&F**). While we had intended to leverage the 16S rRNA gene sequencing data to compare specific, linked virus-host responses to temperature, meaningful data analysis was not possible, due to limited host prediction. We did find that most of the predicted host phyla were also found in the ASV profiles in the respective horizon.

## Discussion

This study revealed a likely upper limit to viral persistence between 60 and 90°C for most, if not all, viral species in the studied soils. Given that DNA yields for DNase-treated viromes were below detection limits for all six samples that underwent heating treatment at 90°C and that these DNase-treated viromes likely captured predominantly intact virions (39,40), we can infer substantial or complete depletion of intact soil viral particles at 90°C. The depletion threshold presumably occurred between 60°C and 90°C, or possibly with an upper limit as low as 83°C, which was the lowest maximum temperature achieved in the center of the microcosms incubated at 90°C. We can thus assume a maximum viability threshold between 83°C and 90°C for most soil viruses from these forest soils. This threshold is aligned with a study that focused on 24 viruses of thermophilic *Bacillus* strains isolated from compost, soil, silage, and rotting straw, in which the ability to form plaques was possible at 50°C but not at

70°C (70). Additionally, while studies have shown heat resistance in viral isolates at above 90°C (22), there is evidence that virus inactivation occurs faster in complex matrices, such as soil (15). Performing heating treatments with higher resolution between 60°C and 90°C and at multiple heating durations will likely reveal more precise temperature thresholds for different groups of dsDNA prokaryotic viruses in soil.

Although data are limited for viruses, thermotolerance for prokaryotes is much better understood, and in general, the inferred viral thermotolerances here are consistent with those of prokaryotes. In response to heat treatment, within both soil types, both viruses and prokaryotes clustered into three groups, with community composition similar across the ambient community (field, control, and 30°C samples) and at 60°C and again at 90°C. Changes in vOTU relative abundances better explained separation among viral communities along the temperature gradient than did compositional turnover, with most viral species detectable across the temperature gradient. This suggests that thermotolerance up to at least 60°C is widespread among most viral 'species' in these soils. Since the largest intersection of vOTUs was present in all treatment groups in the DNase-treated viromes (which included all but the 90°C samples), we infer that most vOTUs in these soil samples were tolerant at 60°C. The idea of viral and prokaryotic ambient communities having high thermotolerance seems to be supported by other studies focused on microbial populations. For example, in composting systems where the optimal growth temperatures for most strains were found to be 30 to 40°C, thermotolerance (up to 60°C, the maximum study temperature) was ubiquitous among all major phyla (Actinobacteria, Firmicutes, Proteobacteria), with most microorganisms considered eurythermal (adaptable to and able to tolerate a wide range of temperatures) (71). In terms of prokaryotic trends in response to temperature change, the increase in relative abundance of Firmicutes at 90°C is also consistent with prior studies, with members of the Firmicutes exhibiting persistence in hostile habitats, spore-forming capabilities, and a relatively high growth rate, comprising the majority of thermotolerant strains with high thermal plasticity (71).

The increase in relative abundance of Chloroflexi at 90°C in this study is consistent with increasing relative abundance of this phylum with increasing temperature in Costa Rican hot springs that reached up to 63°C (72). The significant decrease of Patescibacteria at higher temperatures (a result only evident in the prokaryotic data from the viromes, which enrich for small cells) also may be due to the lower number of functional genes related to stress response in their small genomes, as compared to other bacteria with larger genome sizes (42). The detection of viruses in this study that were more significantly abundant at 60°C suggests that some of these viruses may exhibit heat tolerance, similar to prior discoveries of heat-tolerant prokaryotic phyla. However, the connection between viruses and their hosts and whether they exhibit differential or parallel survival with increasing temperature requires further investigation.

In this study, we found that both viral and prokaryotic communities exhibited similar beta-diversity patterns according to soil source. Community composition differed most significantly by soil source (O or A horizon). Viral community differences between O and A horizons have not been extensively studied in other soils, but viral communities are known to differ by soil depth (23,73,74), consistent with differences between horizons found in this study. For prokaryotes, the observed compositional differences were consistent with known differences between soil horizons. For example, as in this study, Acidobacteria, Proteobacteria, and Actinobacteria are ubiquitous in forest organic and mineral soils, with Bacteroidetes more prominent in organic soils and Firmicutes and Chloroflexi more prominent in mineral soils (75,76). While considered rare in soil (77), here Patescibacteria represented a substantial proportion (up to 80%) of the prokaryotes detected in the O horizon 'viromic' (< 0.22 μm) fraction. They were also more prominent in organic compared to mineral soils, which may be due to their tendency to metabolize simple metabolites like glucose and pyruvate which may be more available in organic matter rich soils (42).

## Conclusion

Results from this study indicate a maximum viability threshold between 83°C and 90°C for most soil viruses from these forest soil samples. Among the intact (and presumably viable) virions recovered from DNase-treated viromes, most identified vOTUs were detected across the entire temperature gradient from 10°C to 60°C, suggesting that thermotolerance up to at least 60°C is widespread among most viral 'species' in these soils. While distinct viral and prokaryotic communities were found in the O and A horizon of the same soil profile, community shifts followed the same trend, with community composition similar in the ambient community (field, control, and 30°C samples) and at 60°C and again at 90°C. In our review of heat-tolerant and heat-sensitive vOTUs, many viruses were found to be tolerant or sensitive in one, not both, horizons. More robust testing of different soil types may reveal which soil characteristics may alter the thermotolerance of a virus. Lastly, leveraging our < 0.22 μm non-DNase treated viromes allowed us to gain insight on temperature sensitivities of ultrasmall bacteria. We found that Patescibacteria, a phylum of small-celled bacteria, were vulnerable at higher temperatures. Collectively, DNase-treated and non-DNase treated viromes along with total DNA metagenomes can be useful when characterizing different fractions of the microbial community, including intact viruses, compromised viruses, relic DNA, and ultrasmall cells, which can be especially insightful for studying microbial responses to changing environmental conditions.

## Data Availability

All raw sequences have been deposited in the NCBI Sequence Read Archive under the BioProject accession PRJNA1093237. The database of dereplicated vOTUs is available at https://zenodo.org/records/11043663. All scripts are available at https://github.com/seugeo/soilheating.

## Acknowledgements

This chapter was submitted for peer-reviewed publication with the following coauthors:

Luke Hillary, Christian Santos-Medellín, Jane Fudyma, Jess Sorensen, and Joanne Emerson. Additionally, we thank Brandon Matsumoto for help with sample collection, staff at the Blodgett Forest Research Station (Kane Russell, Amy Mason, and Ariel Thomson) for advising on field sampling logistics and coordinating site visits, resource support from the Traxler Lab at UC Berkeley (Monika Fischer, Neem Patel), and statistical analysis advice from Lucie Jiraska. Thanks to Valerie Eviner and Jorge Rodrigues for helpful comments on a draft version of this chapter. Funding for this work was provided by the U.S. Department of Energy (DOE), Office of Science, Office of Biological and Environmental Research (BER), Genomic Science Program, award number DE-SC0021198 (grant to JBE). SEG was also supported by the National Science Foundation Graduate Research Fellowship, the University of California Eugene Cota-Robles Fellowship, and the College of Agriculture and Environmental Sciences (UC Davis) Dean's Circle Award.

## References

1.Emerson JB. Soil Viruses: A New Hope. mSystems. 2019 May 28;4(3):e00120-19, /msystems/4/3/msys.00120-19.atom.

2.Kimura M, Jia ZJ, Nakayama N, Asakawa S. Ecology of viruses in soils: Past, present and future perspectives. Soil Science and Plant Nutrition. 2008 Feb;54(1):1–32.

3.Kuzyakov Y, Mason-Jones K. Viruses in soil: Nano-scale undead drivers of microbial life, biogeochemical turnover and ecosystem functions. Soil Biology and Biochemistry. 2018 Dec;127:305–17.

4.Trubl G, Hyman P, Roux S, Abedon ST. Coming-of-Age Characterization of Soil Viruses: A User's Guide to Virus Isolation, Detection within Metagenomes, and Viromics. Soil Syst. 2020 Apr 21;4(2):23.

5.Kuypers MMM, Marchant HK, Kartal B. The microbial nitrogen-cycling network. Nat Rev Microbiol. 2018 May;16(5):263–76.

6.Lladó S, López-Mondéjar R, Baldrian P. Forest Soil Bacteria: Diversity, Involvement in Ecosystem Processes, and Response to Global Change. Microbiol Mol Biol Rev. 2017;81(2).

7.Labrie SJ, Samson JE, Moineau S. Bacteriophage resistance mechanisms. Nature Reviews Microbiology. 2010 May;8(5):317–27.

8.Jover LF, Effler TC, Buchan A, Wilhelm SW, Weitz JS. The elemental composition of virus particles: implications for marine biogeochemical cycles. Nat Rev Microbiol. 2014 Jul;12(7):519–28.

9.Oz H, Coskan A, Atilgan A. Determination of Effects of Various Plastic Covers and Biofumigation on Soil Temperature and Soil Nitrogen Form in Greenhouse Solarization: New Solarization Cover Material. J Polym Environ. 2017 Jun 1;25(2):370–7.

10.Busse MD, Shestak CJ, Hubbert KR. Soil heating during burning of forest slash piles and wood piles. International Journal of Wildland Fire 22(6): 786-796. 2013;22:786–96.

11.Massman WJ, Frank JM. Effect of a controlled burn on the thermophysical properties of a dry soil using a new model of soil heat flow and a new high temperature heat flux sensor. International Journal of Wildland Fire 13: 427-442. 2004;427–42.

12.Siliakus MF, van der Oost J, Kengen SWM. Adaptations of archaeal and bacterial membranes to variations in temperature, pH and pressure. Extremophiles. 2017 Jul 1;21(4):651–70.

13.Donhauser J, Niklaus PA, Rousk J, Larose C, Frey B. Temperatures beyond the community optimum promote the dominance of heat-adapted, fast growing and stress resistant bacteria in alpine soils. Soil Biology and Biochemistry. 2020 Sep 1;148:107873.

14.Pingree MRA, Kobziar LN. The myth of the biological threshold: A review of biological responses to soil heating associated with wildland fire. Forest Ecology and Management. 2019 Jan;432:1022–9.

15.Bertrand I, Schijven JF, Sánchez G, Wyn-Jones P, Ottoson J, Morin T, et al. The impact of temperature on the inactivation of enteric viruses in food and water: a review: Virus inactivation. Journal of Applied Microbiology. 2012 Jun;112(6):1059–74.

16.Jończyk E, Kłak M, Międzybrodzki R, Górski A. The influence of external factors on bacteriophages—review. Folia Microbiol. 2011 May;56(3):191–200.

17.Williamson KE, Fuhrmann JJ, Wommack KE, Radosevich M. Viruses in Soil Ecosystems: An Unknown Quantity Within an Unexplored Territory. Annu Rev Virol. 2017 Sep 29;4(1):201–19.

18.Breitbart M, Wegley L, Leeds S, Schoenfeld T, Rohwer F. Phage community dynamics in hot springs. Appl Environ Microbiol. 2004 Mar;70(3):1633–40.

19.Mocé-Llivina L, Muniesa M, Pimenta-Vale H, Lucena F, Jofre J. Survival of bacterial indicator species and bacteriophages after thermal treatment of sludge and sewage. Appl Environ Microbiol. 2003 Mar 1;69(3):1452–6.

20.Atamer Z, Dietrich J, Müller-Merbach M, Neve H, Heller KJ, Hinrichs J. Screening for and characterization of Lactococcus lactis bacteriophages with high thermal resistance. International Dairy Journal. 2009 Apr 1;19(4):228–35.

21.Buzrul S, Öztürk P, Alpas H, Akcelik M. Thermal and chemical inactivation of lactococcal bacteriophages. LWT - Food Science and Technology. 2007 Dec;40(10):1671–7.

22.Guglielmotti DM, Mercanti DJ, Reinheimer JA, Quiberoni A del L. Review: Efficiency of Physical and Chemical Treatments on the Inactivation of Dairy Bacteriophages. Front Microbiol. 2012 Jan 11;2:282.

23.Ter Horst AM, Santos-Medellín C, Sorensen JW, Zinke LA, Wilson RM, Johnston ER, et al. Minnesota peat viromes reveal terrestrial and aquatic niche partitioning for local and global viral populations. Microbiome. 2021 Nov 26;9(1):233.

24.Liao H, Liu C, Ai C, Gao T, Yang QE, Yu Z, et al. Mesophilic and thermophilic viruses are associated with nutrient cycling during hyperthermophilic composting. The ISME Journal. 2023 Jun 1;17(6):916–30.

25.Bruns TD, Chung JA, Carver AA, Glassman SI. A simple pyrocosm for studying soil microbial response to fire reveals a rapid, massive response by Pyronema species. Suen G, editor. PLoS ONE. 2020 Mar 4;15(3):e0222691.

26.Dooley SR, Treseder KK. The effect of fire on microbial biomass: a meta-analysis of field studies. Biogeochemistry. 2012 Jul;109(1–3):49–61.

27.Janzen C, Tobin-Janzen T. Microbial Communities in Fire-Affected Soils. In: Dion P, Nautiyal CS, editors. Microbiology of Extreme Soils [Internet]. Berlin, Heidelberg: Springer Berlin Heidelberg; 2008 [cited 2020 May 6]. p. 299–316. (Varma A, editor. Soil Biology; vol. 13). Available from: http://link.springer.com/10.1007/978-3-540-74231-9_14

28.Lucas-Borja ME, Miralles I, Ortega R, Plaza-Álvarez PA, Gonzalez-Romero J, Sagra J, et al. Immediate fire-induced changes in soil microbial community composition in an outdoor experimental controlled system. Science of The Total Environment. 2019 Dec;696:134033.

29.Mataix-Solera J, Guerrero C, García-Orenes F, Bárcenas GM, Torres MP. Forest fire effects on soil microbiology. Fire effects on soils and restoration strategies. 2009;5:133–75.

30.Palmer B, Pietrasiak N, Cobb P, Lipson D. Using simulated wildland fire to assess microbial survival at multiple depths from biocrust and bare soils. Frontiers in Microbiology. 2023;14.

31.Neary DG, Ryan KC, DeBano LF. Wildland fire in ecosystems: effects of fire on soils and water. Gen Tech Rep RMRS-GTR-42-vol4 Ogden, UT: US Department of Agriculture, Forest Service, Rocky Mountain Research Station 250 p [Internet]. 2005 [cited 2024 Apr 6];042. Available from:

https://www.fs.usda.gov/research/treesearch/20912

32.Osman KT. Forest Soils. In: Osman KT, editor. Soils: Principles, Properties and Management [Internet]. Dordrecht: Springer Netherlands; 2013 [cited 2024 Feb 12]. p. 229–51. Available from: https://doi.org/10.1007/978-94-007-5663-2_14

33.Busse MD, Hubbert KR, Moghaddas EEY. Fuel reduction practices and their effects on soil quality. Gen Tech Rep PSW-GTR-241 Albany, CA: US Department of Agriculture, Forest Service, Pacific Southwest Research Station 156 p [Internet]. 2014 [cited 2024 Apr 6];241. Available from: https://www.fs.usda.gov/research/treesearch/45914

34.Certini G. Effects of fire on properties of forest soils: a review. Oecologia. 2005 Mar;143(1):1–10.

35.Johnson DW, Turner J. Tamm Review: Nutrient cycling in forests: A historical look and newer developments. Forest Ecology and Management. 2019 Jul 15;444:344–73.

36.van Wagtendonk JW, Sugihara NG, Stephens SL, Thode AE, Shaffer KE, Fites-Kaufman J, editors. Fire in California's ecosystems. Second edition. Oakland, California: University of California Press; 2018. 550 p.

37.Santos-Medellin C, Zinke LA, ter Horst AM, Gelardi DL, Parikh SJ, Emerson JB. Viromes outperform total metagenomes in revealing the spatiotemporal patterns of agricultural soil viral communities. ISME J. 2021 Jul;15(7):1956–70.

38.Göller PC, Haro-Moreno JM, Rodriguez-Valera F, Loessner MJ, Gómez-Sanz E. Uncovering a hidden diversity: optimized protocols for the extraction of dsDNA bacteriophages from soil. Microbiome. 2020 Feb 11;8(1):17.

39.Sorensen JW, Zinke LA, ter Horst AM, Santos-Medellín C, Schroeder A, Emerson JB. DNase Treatment Improves Viral Enrichment in Agricultural Soil Viromes. mSystems. 2021 Sep 7;6(5):10.1128/msystems.00614-21.

40.Santos-Medellín C, Blazewicz SJ, Pett-Ridge J, Firestone MK, Emerson JB. Viral but not bacterial community successional patterns reflect extreme turnover shortly after rewetting dry soils. Nat Ecol Evol. 2023 Sep 28;1–14.

41.Nicolas AM, Jaffe AL, Nuccio EE, Taga ME, Firestone MK, Banfield JF. Soil Candidate Phyla Radiation Bacteria Encode Components of Aerobic Metabolism and Co-occur with Nanoarchaea in the Rare Biosphere of Rhizosphere Grassland Communities. mSystems. 2021 Aug 17;6(4):10.1128/msystems.01205-20.

42.Tian R, Ning D, He Z, Zhang P, Spencer SJ, Gao S, et al. Small and mighty: adaptation of superphylum Patescibacteria to groundwater environment drives their genome simplicity. Microbiome. 2020 Apr 6;8(1):51.

43.Durham DM, Sieradzki ET, ter Horst AM, Santos-Medellín C, Bess CWA, Geonczy SE, et al. Substantial differences in soil viral community composition within and among four Northern California habitats. ISME Commun [Internet]. 2022 Dec 1 [cited 2024 Mar 30];2(1). Available from: https://dx.doi.org/10.1038/s43705-022-00171-y

44.Fudyma JD, ter Horst AM, Santos-Medellín C, Sorensen J, Gogul G, Hillary LS, et al. Exploring viral particle, soil, and extraction buffer physicochemical characteristics and their impacts on extractable viral communities. Soil Biology and Biochemistry. 2024 Mar 29;109419.

45.Santos-Medellín C, Estera-Molina K, Yuan M, Pett-Ridge J, Firestone MK, Emerson JB. Spatial turnover of soil viral populations and genotypes overlain by cohesive responses to moisture in grasslands. Proceedings of the National Academy of Sciences. 2022 Nov 8;119(45):e2209132119.

46.Edwards J, Santos-Medellín C, Sundaresan V. Extraction and 16S rRNA Sequence Analysis of Microbiomes Associated with Rice Roots. Bio Protoc. 2018 Jun 20;8(12):e2884.

47.Thompson LR, Sanders JG, McDonald D, Amir A, Ladau J, Locey KJ, et al. A communal catalogue reveals Earth's multiscale microbial diversity. Nature. 2017;551(7681):457–63.

48.Haney Test Interpretation Guide v1.0 [Internet]. [cited 2024 Apr 10]. Available from: https://www.wardlab.com/wp-content/uploads/2020/02/Haney-Rev-1.0-Interpretation-Guide-PDF-1.pdf

49.Bolger AM, Lohse M, Usadel B. Trimmomatic: a flexible trimmer for Illumina sequence data. Bioinformatics. 2014 Aug 1;30(15):2114–20.

50.Bushnell B. BBTools software package. 2014 [cited 2023 Oct 25]. BBMap. Available from: https://sourceforge.net/projects/bbmap/

51.Li D, Liu CM, Luo R, Sadakane K, Lam TW. MEGAHIT: an ultra-fast single-node solution for large and complex metagenomics assembly via succinct de Bruijn graph. Bioinformatics. 2015 May 15;31(10):1674–6.

52.Kieft K, Zhou Z, Anantharaman K. VIBRANT: automated recovery, annotation and curation of microbial viruses, and evaluation of viral community function from genomic sequences. Microbiome. 2020 Jun 10;8(1):90.

53.Huang Y, Niu B, Gao Y, Fu L, Li W. CD-HIT Suite: a web server for clustering and comparing biological sequences. Bioinformatics. 2010 Mar 1;26(5):680–2.

54.Olm MR, Brown CT, Brooks B, Banfield JF. dRep: a tool for fast and accurate genomic comparisons that enables improved genome recovery from metagenomes through de-replication. ISME J. 2017 Dec;11(12):2864–8.

55.Langmead B, Trapnell C, Pop M, Salzberg SL. Ultrafast and memory-efficient alignment of short DNA sequences to the human genome. Genome Biology. 2009 Mar 4;10(3):R25.

56.Woodcroft BJ. CoverM [Internet]. 2023. Available from: https://github.com/ wwood/CoverM

57.Roux S, Camargo AP, Coutinho FH, Dabdoub SM, Dutilh BE, Nayfach S, et al. iPHoP: An integrated machine learning framework to maximize host prediction for metagenome-derived viruses of archaea and bacteria. PLOS Biology. 2023 Apr 21;21(4):e3002083.

58.Callahan BJ, McMurdie PJ, Rosen MJ, Han AW, Johnson AJA, Holmes SP. DADA2: High-resolution sample inference from Illumina amplicon data. Nat Methods. 2016 Jul;13(7):581–3.

59.Quast C, Pruesse E, Yilmaz P, Gerken J, Schweer T, Yarza P, et al. The SILVA ribosomal RNA gene database project: improved data processing and web-based tools. Nucleic Acids Research. 2013 Jan 1;41(D1):D590–6.

60.R Core Team. R: A language and environment for statistical computing. [Internet]. R Foundation for Statistical Computing, Vienna, Austria.; 2023. Available from: https://www.R-project.org/

61.Oksanen J, Simpson GL, Blanchet FG, Kindt R, Legendre P, Minchin PR, et al. vegan: Community Ecology Package [Internet]. 2022 [cited 2022 Jul 6]. Available from: https://CRAN.R-project.org/package=vegan

62.Krassowski M. ComplexUpset: Create Complex UpSet Plots Using “ggplot2” Components [Internet]. 2021 [cited 2022 Sep 22]. Available from: https://CRAN.R-project.org/package=ComplexUpset

63.Love MI, Huber W, Anders S. Moderated estimation of fold change and dispersion for RNA-seq data with DESeq2. Genome Biology. 2014 Dec 5;15(12):550.

64.Hyatt D, Chen GL, LoCascio PF, Land ML, Larimer FW, Hauser LJ. Prodigal: prokaryotic gene recognition and translation initiation site identification. BMC Bioinformatics. 2010 Mar 8;11(1):119.

65.Jang HB, Bolduc B, Zablocki O, Kuhn JH, Roux S, Adriaenssens EM, et al. Taxonomic assignment of uncultivated prokaryotic virus genomes is enabled by gene-sharing networks. Nat Biotechnol. 2019 Jun;37(6):632–9.

66.Buchfink B, Reuter K, Drost HG. Sensitive protein alignments at tree-of-life scale using DIAMOND. Nat Methods. 2021 Apr;18(4):366–8.

67.Schloerke B, Cook D, Larmarange J, Briatte F, Marbach M, Thoen E, et al. GGally: Extension to “ggplot2” [Internet]. 2024 [cited 2024 Apr 10]. Available from: https://cloud.r-project.org/web/packages/GGally/index.html

68.Burkert A, Douglas TA, Waldrop MP, Mackelprang R. Changes in the Active, Dead, and Dormant Microbial Community Structure across a Pleistocene Permafrost Chronosequence. Applied and Environmental Microbiology. 2019 Mar 22;85(7):e02646-18.

69.Carini P, Marsden PJ, Leff JW, Morgan EE, Strickland MS, Fierer N. Relic DNA is abundant in soil and

obscures estimates of soil microbial diversity. Nat Microbiol. 2016 Dec 19;2(3):1–6.

70.Sharp RJ, Ahmad SI, Munster A, Dowsett B, Atkinson T. The Isolation and Characterization of Bacteriophages Infecting Obligately Thermophilic Strains of Bacillus. Microbiology. 1986;132(6):1709–22.

71.Moreno J, López-González JA, Arcos-Nievas MA, Suárez-Estrella F, Jurado MM, Estrella-González MJ, et al. Revisiting the succession of microbial populations throughout composting: A matter of thermotolerance. Science of The Total Environment. 2021 Jun 15;773:145587.

72.Uribe-Lorío L, Brenes-Guillén L, Hernández-Ascencio W, Mora-Amador R, González G, Ramírez-Umaña CJ, et al. The influence of temperature and pH on bacterial community composition of microbial mats in hot springs from Costa Rica. MicrobiologyOpen. 2019;8(10):e893.

73.Emerson JB, Roux S, Brum JR, Bolduc B, Woodcroft BJ, Jang HB, et al. Host-linked soil viral ecology along a permafrost thaw gradient. Nature Microbiology. 2018 Aug;3(8):870–80.

74.Liang X, Wagner RE, Zhuang J, DeBruyn JM, Wilhelm SW, Liu F, et al. Viral abundance and diversity vary with depth in a southeastern United States agricultural ultisol. Soil Biology and Biochemistry. 2019 Oct;137:107546.

75.Baldrian P, Kolařík M, Štursová M, Kopecký J, Valášková V, Větrovský T, et al. Active and total microbial communities in forest soil are largely different and highly stratified during decomposition. ISME J. 2012 Feb;6(2):248–58.

76.Uroz S, Ioannidis P, Lengelle J, Cébron A, Morin E, Buée M, et al. Functional Assays and Metagenomic Analyses Reveals Differences between the Microbial Communities Inhabiting the Soil Horizons of a Norway Spruce Plantation. PLOS ONE. 2013 Feb 13;8(2):e55929.

77.Liu T, Wu X, Li H, Alharbi H, Wang J, Dang P, et al. Soil organic matter, nitrogen and pH driven change in bacterial community following forest conversion. Forest Ecology and Management. 2020 Dec 1;477:118473.

## Main Figures

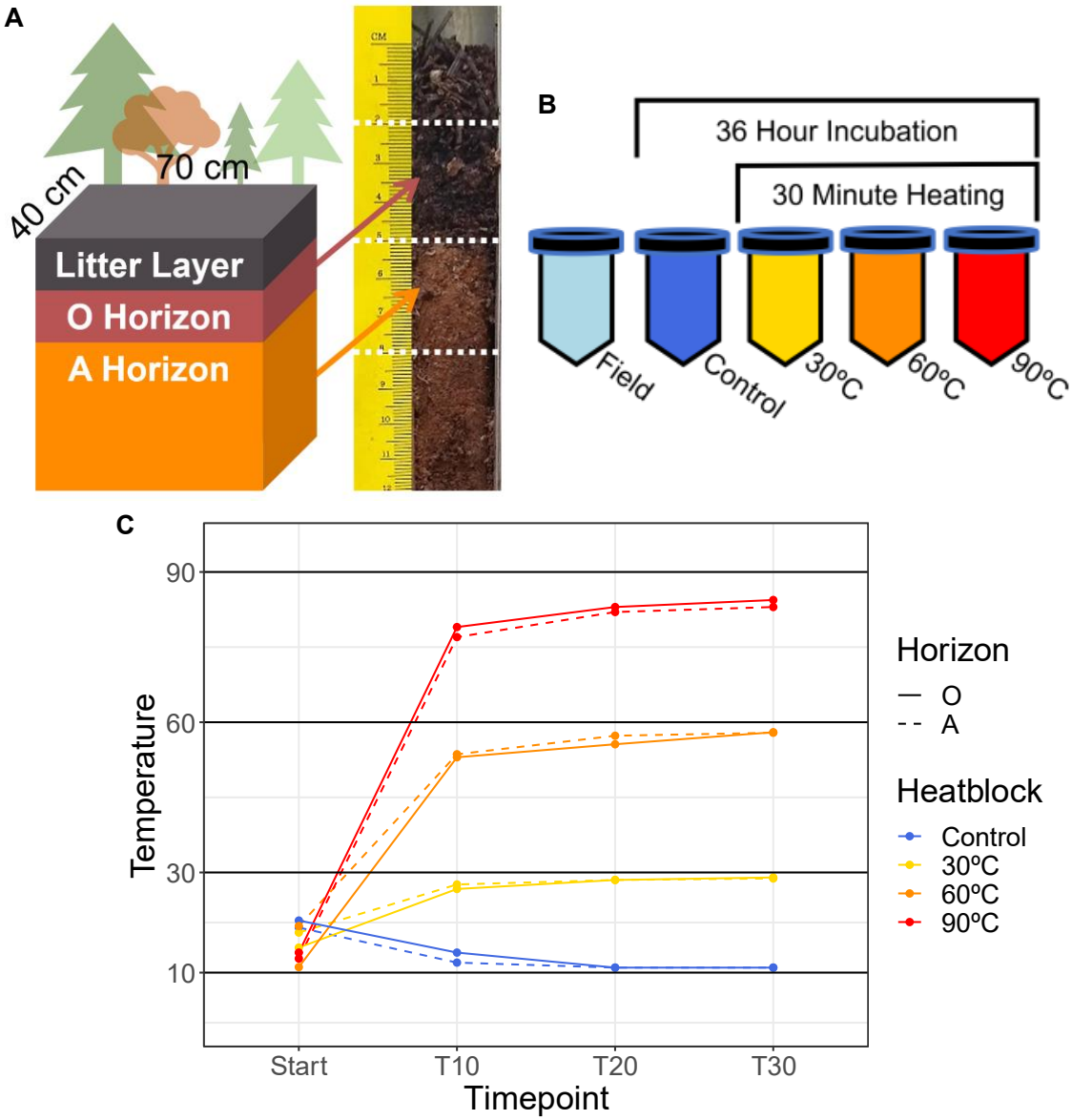


**Figure 1. Dataset Features**, **A**. Graphic depicts surface area of soil collection, arrows point to photo of a representative soil probe in the sample collection area, showing soil quality and sample depth of each horizon. The color of the horizons in the graphic is maintained in subsequent figures. **B**. Each of the five treatments is represented by a unique color that will be maintained throughout subsequent figures. Field samples were processed without an incubation step, while all other samples were incubated for 36 hours, with three sample sets elevated to different target temperatures (30, 60, or 90°C) over 30 minutes during the 36-hour incubation. **C**. Microcosm soil temperature over time (10-minute intervals), from start to 30 minutes (T30) for all incubated samples. Control samples were not added to a heat block. The rest were placed in a heat block preheated to the indicated temperature.

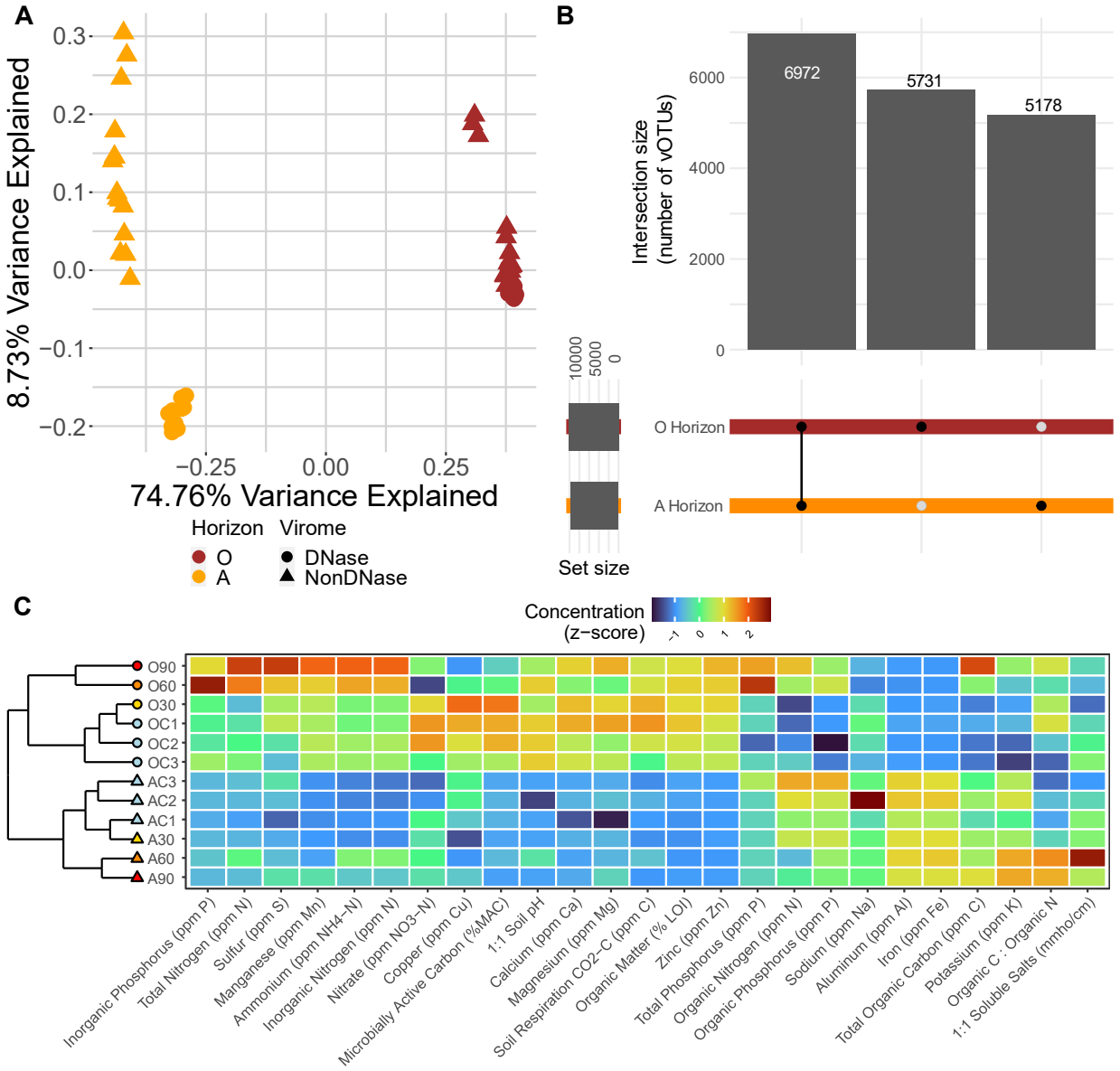


**Figure 2. Differences in viral community composition by soil type**, **A**. Unconstrained analyses of principal coordinates (PCoA) performed on vOTU Bray-Curtis dissimilarities calculated across all viromes, with colors indicating soil source and shapes indicating virome type. **B**. UpSet plot of vOTU detection in each horizon in DNase-treated viromes, with filled circles indicating detection in a particular horizon and intersection size indicating the number of vOTUs with a given detection pattern (one of the two horizons or both). **C**. Hierarchical clustering of soil samples based on soil chemical data, with three replicates of each horizon in the field treatment and one replicate of each horizon in the 30, 60, and 90°C treatments. Sample labels begin with horizon (A or O), followed by "F" for field or the incubation temperature. The corresponding heatmap shows the z-transformation of each environmental measurement across samples.

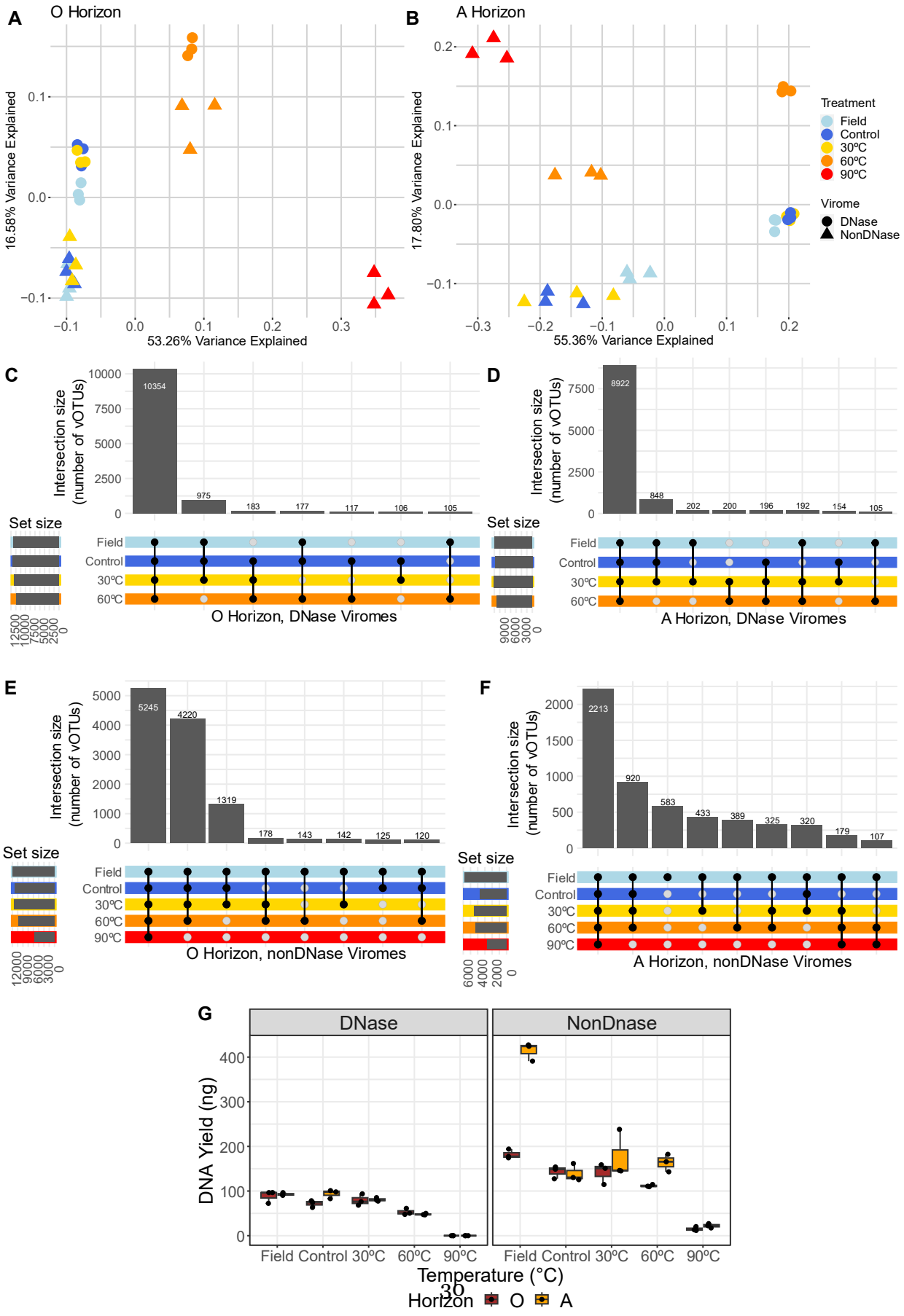
A
O Horizon
16.58% Variance Explained
53.26% Variance Explained
B
A Horizon
17.80% Variance Explained
55.36% Variance Explained
Treatment
Field
Control
30ºC
60ºC
90ºC
Virome
DNase
NonDNase
C
Intersection size
(number of vOTUs)
10354
975
183
177
117
106
105
Set size
Field
Control
30ºC
60ºC
O Horizon, DNase Viromes
D
8922
848
202
200
196
192
154
105
A Horizon, DNase Viromes
E
5245
4220
1319
178
143
142
125
120
90ºC
O Horizon, nonDNase Viromes
F
2213
920
583
433
389
325
320
179
107
A Horizon, nonDNase Viromes
G
DNase
NonDnase
DNA Yield (ng)
Field Control 30ºC 60ºC 90ºC
Temperature (°C)
Horizon O A

**Figure 3. Viral community composition shifts based on heating treatments**, **A/B**. Unconstrained analyses of principal coordinates (PCoA) performed on vOTU Bray-Curtis dissimilarities calculated across all viromes from the O (**A**) and A (**B**) horizons, with colors indicating treatment (field, control, or heat) and shapes indicating virome type. **C-F**. UpSet plots of DNase-treated viromes in O (**C**) and A (**D**) horizons and of non-DNase-treated viromes in O (**E**) and A (**F**) horizons, with filled circles indicating vOTU detection in at least two replicates of a particular treatment (field, control, or heat) and intersection size indicating number of vOTUs with a given detection pattern. **G**. DNA yields for DNase- (left facet) and non-DNase- (right facet) treated viromes from each horizon for each treatment. Box boundaries correspond to 25th and 75th percentiles, and whiskers extend to ±1.5x the interquartile range.

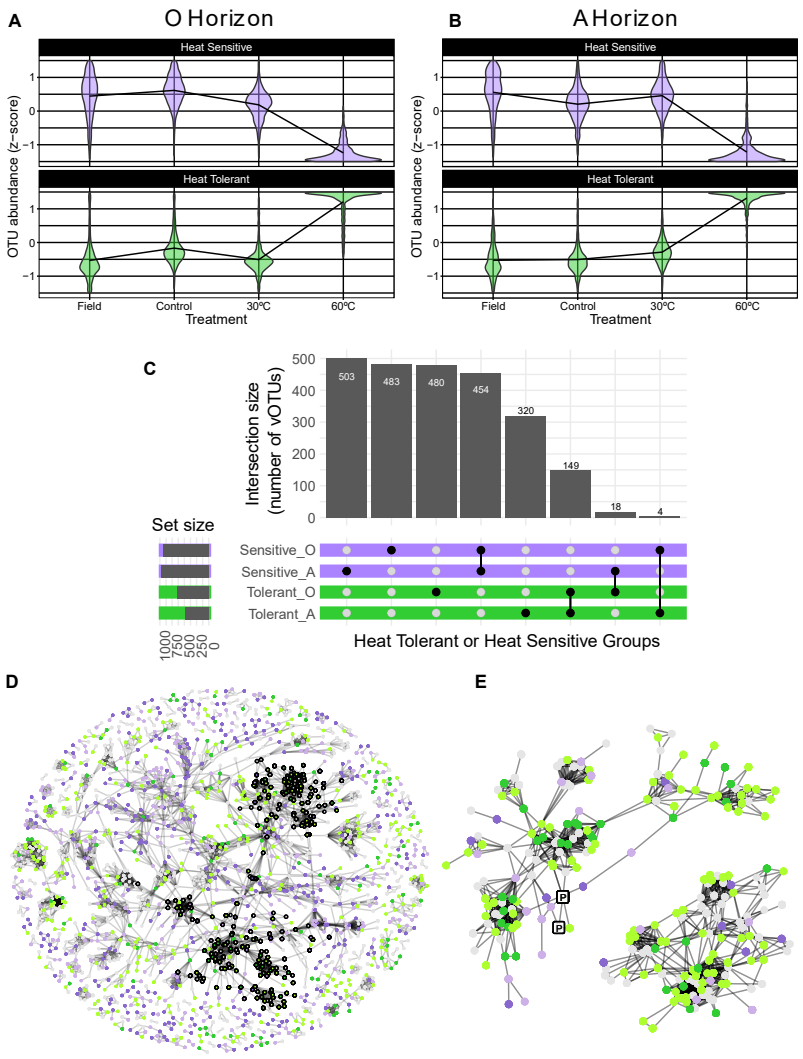


**Figure 4. Patterns of differentially abundant vOTUs based on heat treatments, A/B.** Violin plots visualizing distribution of vOTUs (z-score relative abundance) detected as significantly differentially abundant based on heat treatment in DNase-treated viromes from O (**A**) and A (**B**) horizons, with vOTUs enriched in the ambient samples (field, control, and 30°C) in the upper facet ("Heat Sensitive") and vOTUs enriched in the 60°C samples ("Heat Tolerant") in the lower facet. Trend line indicates mean z-score. **C**. UpSet plot of differentially abundant vOTUs in DNase-treated viromes, with filled circles indicating membership in a trend group in a particular horizon and intersection size indicating number of vOTUs with a given detection pattern. **D**. Gene-sharing network displaying significant overlaps in predicted protein content (edges) between vOTUs (nodes). Node color represents membership in trend group of both (darker shade) or one (lighter shade) of the soil horizons. Gray nodes indicate vOTUs that were not significantly differentially abundant based on temperature treatment. Black outlines around nodes indicate a subnetwork of local neighborhoods with significant overrepresentation of "Heat Tolerant" vOTUs. **E**. Gene-sharing subnetwork from **D**, with the two vOTUs significantly linked to RefSeq viruses isolated from Proteobacteria hosts (tagged with letter "P").

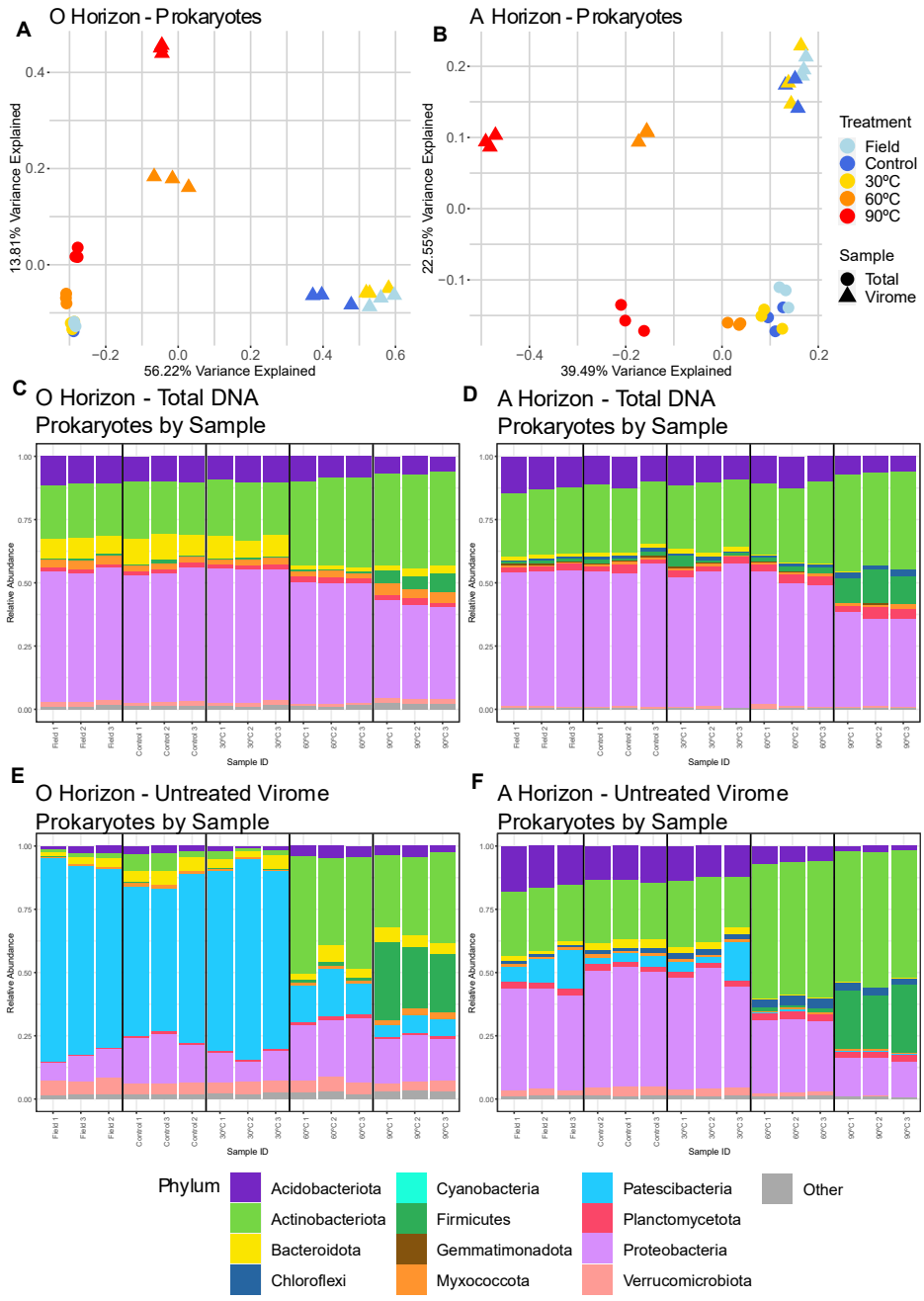


**Figure 5. Prokaryotic community compositional trends according to heat treatment**
Unconstrained analyses of principal coordinates (PCoA) performed on Bray-Curtis dissimilarities calculated from 16S rRNA gene amplicon sequence variant (ASV) relative abundances, with shape indicating sample type (total DNA or non-DNase-treated virome) and color indicating heat treatment in the O (**A**) and A (**B**) horizons. Phylum-level relative abundances in 16S rRNA gene profiles from total DNA amplicon libraries in the O (**C**) and A (**D**) horizons and from non-DNase virome libraries in the O (**E**) and A (**F**) horizons. Each stacked bar plot corresponds to a replicate within a treatment type, and the 12 most abundant phyla are colored, with all other low abundance phyla collapsed into an "other" group.

## Supplementary Figures

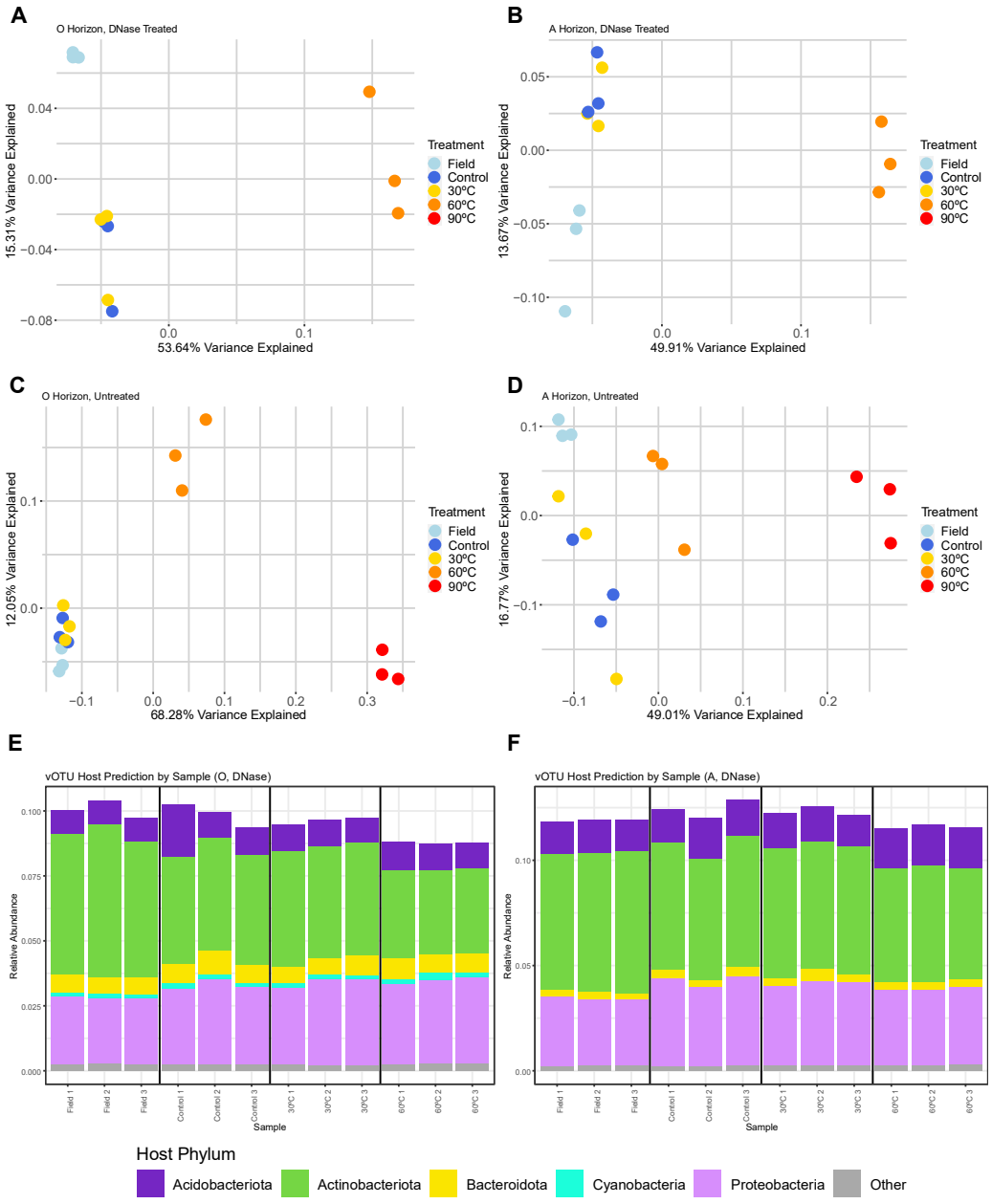


**Supplementary Figure 1. Viral community composition and predicted host abundances based on treatments**, **A-D**. Unconstrained analyses of principal coordinates (PCoA) performed on vOTU Bray-Curtis dissimilarities calculated across DNase-treated viromes from the O (**A**) and A (**B**) horizons and across non-DNase-treated viromes from the O (**C**) and A (**D**) horizons, with colors indicating treatment and shapes indicating virome type. **E-F**. Relative abundances of vOTUs with a phylum-level predicted host in DNase-treated viromes in the O (**E**) and A (**F**) horizons. Each stacked bar plot corresponds to a replicate within a treatment type, and the 5 most abundant host phyla are colored, with all other low abundance host phyla collapsed into an "other" group.

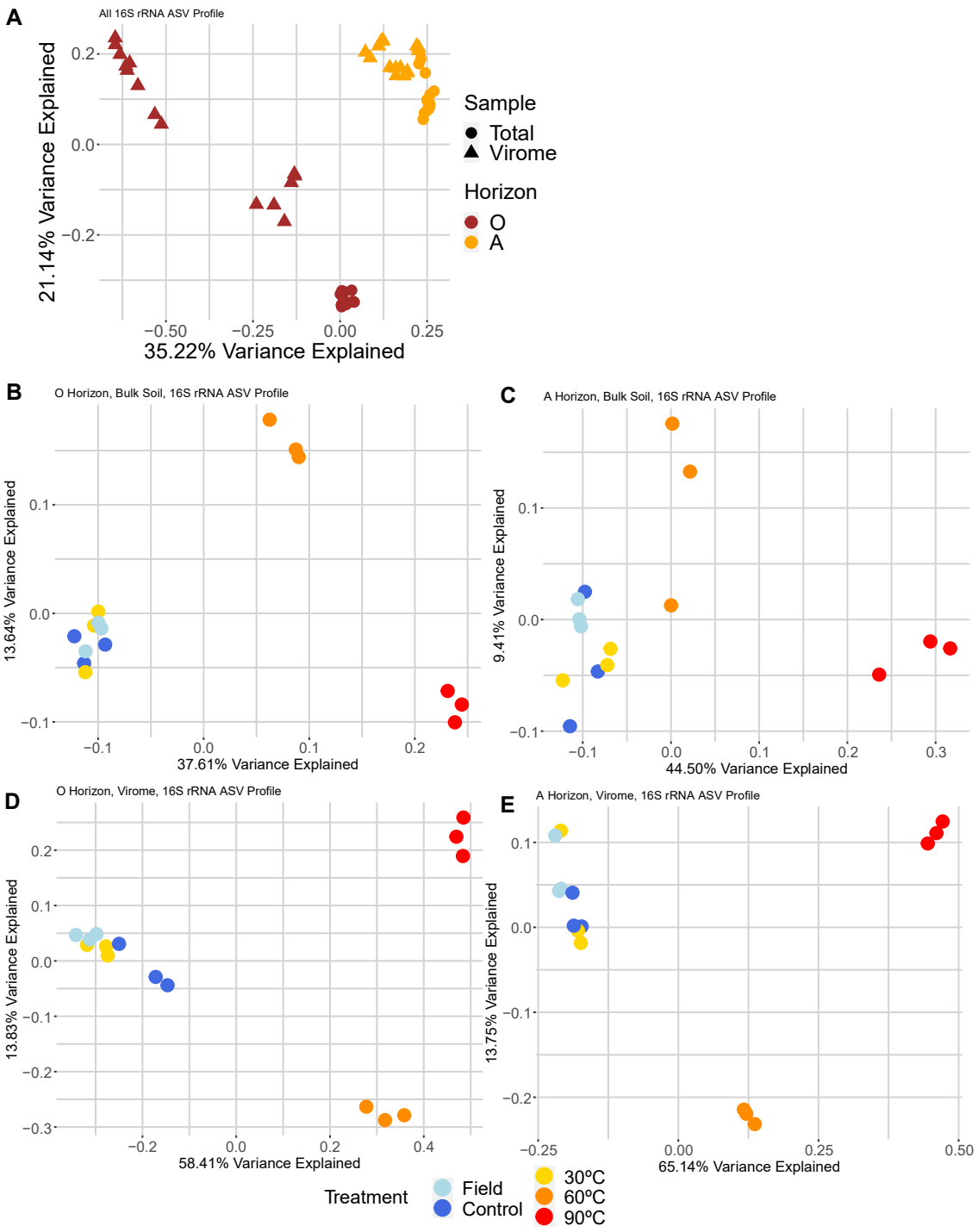


**Supplementary Figure 2. 16S rRNA gene ASV community composition based on soil type and treatments, A.** Unconstrained analyses of principal coordinates (PCoA) performed on vOTU Bray-Curtis dissimilarities calculated across all total DNA and non-DNase-treated viromes. Colors indicate horizon and shapes indicate sample type. **B-E.** PCoA performed on vOTU Bray-Curtis dissimilarities calculated across total DNA samples in the O (**B**) and A (**C**) horizons and across non-DNase-treated viromes in the O (**D**) and A (**E**) horizons. Colors indicate treatment and shapes indicate sample type.

## Chapter Two: Locally heterogeneous soil viral, prokaryotic, and chemical responses to prescribed burn reflect patchy burn severity in a mixed conifer forest


### Abstract

Prescribed burning, a management strategy to mitigate devastating wildfires, imparts physical, chemical, and biological changes to soil, with effects on viruses and virus-host dynamics largely unexplored, despite known viral contributions to biogeochemical processes. Using a viromic (<0.2 μm size fraction metagenomic) approach, we assessed how soil viral communities responded to a spring prescribed burn in a mixed conifer forest and whether soil chemical properties and/or prokaryotic host communities could explain the observed patterns. With a before-after control-impact (BACI) design, two replicate soil samples were collected at each of two depths (0-3 cm and 3-6 cm) from four treatment (burn) plots and two control plots, at five timepoints (two before and three after the burn) over two months. From these 120 samples, 91 viromes were sequenced, and 198,402 viral 'species' (vOTUs) were recovered. Viral communities differed most significantly by location, regardless of treatment, and along with prokaryotic communities, exhibited a heterogenous response to fire. This response was correlated with soil chemical changes attributed to the burn, leading us to develop a chemistry-based burn severity index. Low viromic DNA yields (a proxy for viral particle abundances) at high burn severity suggest loss of viral biomass. The relative abundances of Firmicutes, Actinobacteria, and the viruses predicted to infect them significantly increased along the burn severity gradient, suggesting survival of spore-formers and viral infection of these abundant, fire-responsive taxa. Overall, locally heterogenous soil viral and prokaryotic responses to prescribed burn were explained by patchy burn severity, ever over short distances after the same fire, as captured in the soil chemical data.

## Introduction

Prescribed burning is a management practice that aims to reintroduce fire as an ecological process in areas where fire has otherwise been suppressed, while at the same time aiding in the prevention of catastrophic wildfires (1–5). This practice is one aspect of regulating forest biogeochemical cycling (6), given that forests are a substantial carbon sink (7), but disturbances like wildfires can make forests a potential carbon source (8). Naturally, there is interest in the impact of prescribed burning on soil microorganisms, which are integral to key soil processes that mediate carbon turnover and nutrient availability in forest ecosystems (9–11). While most studies have focused on fungi and bacteria, the impact of prescribed burning on abundant soil viruses (12) has only recently been considered and is largely unexplored (13).

Viruses apply selective pressure on cellular organisms via infection and lysis and may also have distinct impacts on biogeochemical cycling apart from infection dynamics (14). For example, in marine ecosystems, viruses are known to affect biogeochemical cycling through conversion of living microbial biomass into dissolved organic matter, contributing to an estimated 10-40% of total bacterial mortality daily, including 10% of phytoplankton (15). Incorporating soil viruses into the microbial community framework has begun to elucidate their role in key soil processes (16), which would presumably be impacted by disturbances like fire.

In response to varying degrees of fire, including prescribed burning, there can be significant effects on soil biota biomass, abundance, richness, evenness, and diversity across many ecosystems (17–20). Heating directly impacts soil biota survival (21), and changes to soil properties, including short-term reduction in organic matter and increases in pH, mineral phosphorus, total nitrogen, potassium, calcium, and magnesium, can also impact microbial communities (21–23). These changes are especially evident at the soil surface (24,25). Heat penetration is typically only surface level, down to 2-3 cm depending on soil moisture, texture, and compaction, and the nature of the fire itself (26,27), with prescribed burning in forests typically reaching higher temperatures than in other ecosystems (28). Post-fire community

changes show distinct microbial zones along a soil profile (29), indicating the importance of depth-resolved studies in soil post-fire. Pyrophilous taxa (microorganisms that positively respond to fire) have also been identified (18,20,30). While viruses are known to be sensitive to heating (31–33), the effects of fire on soil viral communities are largely unknown. In particular, questions remain in understanding whether viruses and their hosts exhibit similar survival patterns, and to what extent infection dynamics play a role in community compositional changes that could impact biogeochemical cycling.

Burn severity, the degree of fire-induced change to soil (34), is a factor of fire intensity and duration (21) and is a key metric when understanding fire's effects on microbial communities (20,35). However, the characteristic heterogeneity of burn severity across the landscape can be difficult to capture at a small scale relevant to microorganisms (19). Prescribed fires are designed to be of low severity and are considered most effective at reducing surface fuel with low tree mortality (36). While summer and fall burning are more congruent with the natural timing of fires as an ecosystem process, changing environmental conditions have shortened the window for safe and effective burns even in the fall, with increasing consideration of winter and spring prescribed burns (37,38). These early season burns, when fuel moisture and soil moisture levels are higher, are less effective at consuming fuel and tend to have a greater degree of patchiness than late season burns (39), which may confer greater ecosystem resilience due to unburned refugia (5).

Here, we investigated the impact of prescribed burning on dsDNA viral communities in a forest soil in response to a spring prescribed burn, while simultaneously considering the burn impact on putative prokaryotic hosts (via 16S rRNA gene amplicon sequencing) and soil chemical properties. Leveraging a viromic (< 0.2 μm viral size fraction metagenomic) approach (40), we assessed how viral communities changed in response to the prescribed burn, whether the response differed between two near-surface depths (0-3 cm and 3-6 cm) and to what extent soil chemical properties and/or microbial community composition (including of specific taxa

predicted to be preyed upon by the most abundant viruses) could explain the observed patterns.

## Materials and Methods

*Study site description:*

We set up six 5 x 5 m square plots across two 20-acre forest units at the Blodgett Forest Research Station in California, USA (GPS coordinates in **Supplementary Table 9**). The two units have similar vegetation and management history, including over 100 years of fire exclusion (41). Three plots were in a forest unit that was planned to burn in a spring prescribed burn. The other three plots were in a unit that was not planned to be burned, and thus these plots were initially selected to represent control plots, but one plot in the control area burned (see "Prescribed Burn Treatment" section for further details). There was an attempt to locate plots approximately the same distance away from each other in each unit but based on our plot criteria (similar characteristics in terms of litter quality and quantity, slope, and without trees or shrubs directly growing in the plot), our choices were constrained and the distance between plots varied. Within each forest unit, the distance between plots was between 63 - 148 m in the burn unit and 89 - 271 m in the control unit. Between both units, the maximum distance between plots was 558 m and the minimum distance was 283 m. All plots were located in the Holland-Musick loams which consisted of fine-loamy soil with extensive profile development and an O horizon that extended from the surface to 5 to 8 cm deep (42). The vegetation surrounding all plots is considered mixed-conifer and includes a mix of firs (predominantly Douglas fir), pines (predominantly ponderosa), incense cedar, and oaks (tan oak and black oak).

*Prescribed burn treatment:*

Three days prior to the prescribed burn (2021 April 19), we buried two data logging units 30 cm below the surface (Extech SDL200 4-Channel Data Logging Thermometer, Waltham, MA, USA) just outside each burn plot on opposite sides and one data logging unit just outside one side of each control plot. The data logging units had temperature probes (Extech TP873 Bead Wire Type K Temperature Probe, -30 to 300°C) inserted at 1, 2, 4, and 6 cm depth in the

soil profile. These data logging units tracked soil temperature over the course of six days, capturing temperature fluctuations before, during, and after the prescribed burn (**Supplementary Table 10**). One of the dataloggers for B3 completely burned and one datalogger for B2 had a corrupt SD card, so we were unable to retrieve a second set of temperature data for these two plots.

Although the unit with our control plots was not planned to be burned, to determine whether the conditions were appropriate for a prescribed burn in the treatment plots, test burn was conducted on 12 April 2021 in the unit where our control plots were located. To protect the control plots, a fire line was cut around the perimeter of each plot to exclude fire, with a 5-10 foot buffer from the edge of the plots. Additionally, there was an individual with water at each plot to monitor and ensure fire did not enter any control plot during the burn. Unfortunately, one of the control plots burned as a result of this test burn, due to spread of the test fire after monitoring had been completed, leaving only two control plots instead of the planned three for post-burn control samples. This fire behavior was consistent with the official prescribed burn, where spot fires were found over one month after the burn was set, marking an unusual season for prescribed burning.

The prescribed burn occurred on 21 April 2021 and was considered a first entry spring burn that primarily used a strip head ignition pattern (linear strips of fire ignited on the ground evenly and closely together with the intention of homogenizing fire behavior and effects (5)). No ignitions occurred within the treatment plots, and fire was allowed to move into plots from outside the plot boundaries. The fire was maintained as a surface fire with limited individual or small group tree torching. Ignitions of both units (the test burn and the official prescribed burn) occurred during the same burn window (time period with acceptable burning conditions) under similar weather conditions, resulting in similar fire behavior and effects across units. This reinforced our decision to consider samples collected from the burned control plot in the same treatment group as the other three burn plots.

*Soil sampling:*

Each plot was divided into two halves (subplots) along the middle so that we could sample two replicates in each plot (one from each subplot) at each of five timepoints (14 and 3 days before the burn and 7, 14, and 30 days after the burn). Each subplot was then divided into eight equal-sized square sampling units (two columns of four sampling units in each subplot). At each timepoint over the course of the study, we took soil samples in the middle of corresponding sampling units of each plot (e.g. the top right of the right subplot and the top right of the left subplot for a single timepoint). The distance between replicate samples within each plot was approximately 3.75 m. At each sampling location, we collected soil at two depths, between 0 and 3 cm and between 3 and 6 cm, for a total of 4 samples per timepoint per plot. We homogenized and sieved (8 mm) all samples separately, yielding a total of 24 samples for each timepoint and a total of 120 samples for the entire study. The samples were stored on ice and transported back to the lab the same day as collection and promptly placed at 4°C until further sample processing, which started within 48 hours.

*Field metadata collection:*

We inventoried the trees and shrubs surrounding each plot and collected a representative sample of litter to determine the mix of vegetation contributing to litter quality and quantity (**Supplementary Table 9**). During sample collection, in-field soil temperature measurements were taken for each depth at each sampling location. We tested water repellency by wetting a sample with a single drop of deionized water and counting how many seconds it took until the drop had fully infiltrated into the soil (43). We also measured litter depth (or ash depth if it was post-burn) and O horizon depth (**Supplementary Table 11**). Additionally, we have precipitation data for March to June 2021 (**Supplementary Table 12**).

*Soil chemical measurements:*

We calculated the gravimetric soil moisture of each sample, by weighing out 10 g of soil into an aluminum weigh dish and measuring the weight after 24 hours in a drying oven at

105°C. A suite of soil chemistry analyses under the Haney Soil Health Test package (44,45), was performed by Ward Laboratories (Kearney, Nebraska, USA) (**Supplementary Table 13**). For the first sampling timepoint, the replicates of each depth in each plot were combined and 200 g of each homogenized field-condition soil (not dried) was submitted to determine average measurements for both samples, while for all subsequent timepoints, 200 g of field-condition soil of each individual sample was submitted for separate measurements. The measurements included: soil pH and soluble salts (1:1 soil/water suspension), organic matter (percentage weight loss-on-ignition), soil respiration (Solvita® CO2-Burst method: soil was dried at 50°C and sieved at 2 mm, then 40 g soil was incubated for 24 hours in a 50 mL container with perforated bottom allowing for rewetting with 25 mL distilled water in a 250 mL glass jar sealed with a Solvita® paddle, and after 24 hours, CO2-C was quantified with a Solvita® digital reader with the units of mg CO2-C/kg soil), water extractable total N and organic C (quantified by shaking 4 g of soil with 40 mL of distilled water for 10 min and filtering with a Whatman 2V), Haney-(H3A: combination of citric, malic, and oxalic acids) extracted ammonium (NH4-N), nitrate (NO3-N), and inorganic phosphorus (orthophosphate: PO4-P) (the latter quantified with flow injection analysis), and H3A-extracted total phosphorus (P), potassium (K), zinc (Zn), iron (Fe), manganese (Mn), copper (Cu), sulfur (S), calcium (Ca), magnesium (Mg), sodium (Na), and Aluminum (Al) (quantified using inductively coupled argon plasma, or ICAP, atomic emission spectroscopy). Calculations included inorganic N (sum of H3A-extracted NH4-N and NO3-N), organic N (water-extractable total N minus inorganic N), organic P (total P minus inorganic P), microbially active carbon (soil respiration divided by water extractable organic C, expressed as percentage), organic C : organic N, and organic N : inorganic N.

*Viromic DNA extraction and quantification:*

Within 72 hours of sample collection, we extracted viromic DNA from all samples (of the 24 samples per timepoints, 12 were randomly selected for processing each day, starting the day after collection), as previously described (33,46). Briefly, to 10 g of each soil sample, we added 9

mL of protein-supplemented phosphate-buffered saline solution (PPBS: 2% bovine serum albumin, 10% phosphate-buffered saline, 1% potassium citrate, and 150 mM $MgSO_4$, pH 6.5). Samples were vortexed until homogenized and then placed on a horizontal shaker at 300 RPM at 4°C for 10 min. Supernatant was transferred into a new tube and then 9 mL of PPBS was added to the soil remaining in the original tube, repeating the process for a total of three soil resuspensions and elutions, ending with a total of three volumes of supernatant pooled together in a new centrifuge tube. The pooled supernatant was then centrifuged at 8 min at 7840 RPM at 4°C, collecting the progressively clearer supernatant and discarding the concentrated soil particles, for a total of three centrifugations and supernatant collections. The final supernatant was filtered through a 5 μm polyethersulfone (PES) membrane filter (PALL, Port Washington, NY, USA) to filter out larger soil particles and then the filtrate went through a 0.22 μm PES membrane filter (PALL) to exclude most cellular organisms (apart from ultra-small bacteria (47,48)). Viral-sized particles and DNA remaining in the filtrate were concentrated into a pellet using an Optima LE-80K ultracentrifuge with a 50.2 Ti rotor (Beckman-Coulter, Brea, CA, USA) at 32,000 RPM at 4°C for 2 h 25 min. The pellet was resuspended in 200 μL of 0.02 μm filtered ultrapure water and treated with DNase which included an incubation at 37°C for 30 min after adding 10 units of RQ1 RNase-free DNase (Promega, Madison, WI, USA). We then extracted DNA using the DNeasy PowerSoil Pro kit (Qiagen, Hilden, Germany), following the manufacturer's protocol, with the addition of a 10 min incubation at 65°C prior to cell lysis, which also served as the 'stop' incubation for the DNase treatment. DNA quantification was performed using the Qubit dsDNA HS Assay and Qubit 4 fluorometer (ThermoFisher, Waltham, MA, USA). For timepoints 1-4, samples with yields above 0.05 ng/μl or 0.49 ng/g soil (above detection limit) were prepared for library construction and sequencing. For timepoint 5 (30 days after the burn), viromic DNA yields for 10 of the total 24 samples were below detection limits (including two of the 8 control samples), so the decision was made not to sequence any of the viromes for that timepoint.

*Total DNA extraction and quantification:*

For each sample, 0.25 g of soil was added directly to the DNeasy PowerSoil Pro kit (Qiagen) for total DNA extraction, following the manufacturer's protocol, with the addition of a 10 min incubation at 65°C prior to cell lysis. DNA quantification was performed using the Qubit dsDNA HS Assay kit and Qubit 4 fluorometer (ThermoFisher).

*Shotgun virome library preparation and sequencing:*

Sequencing of all viromes was performed by the DNA Technologies and Expression Analysis Core at the University of California, Davis Genome Center (Davis, CA, USA). Metagenomic libraries were constructed with the DNA Hyper Prep kit (Kapa Biosystems-Roche, Basel, Switzerland) and sequenced (paired-end, 150 bp) using the NovaSeq S4 (Illumina, San Diego, CA, USA) platform to a requested depth of 10 Gbp per virome.

*Amplicon library preparation and sequencing:*

We performed 16S rRNA gene amplicon sequencing on all total DNA extractions with a dual-indexing strategy (49). We used the Platinum Hot Start PCR Master Mix (ThermoFisher) with the 515F/806R universal primer set for amplification of the V4 region of the 16S rRNA gene. We followed Earth Microbiome Project's PCR protocol (50), which included an initial denaturation step at 94°C for 3 min, 35 cycles of 94°C for 45 s, 50°C for 60 s, and 72°C for 90 s, and a final extension step at 72°C for 10 min. Three of the samples had an undetectable total DNA yield and only one attempt at amplification was tried, all of them failing to amplify (BSM25, USM26, BSM31). Two other samples had detectable total DNA yields, but failed four attempts at amplification (BSM11, UDM33). We cleaned libraries with AmpureXP magnetic beads (Beckman-Coulter), quantified amplicons with a Qubit dsDNA HS Assay kit and Qubit 4 fluorometer (ThermoFisher), and then pooled all bead-purified products together in equimolar concentrations. The libraries were submitted to the DNA Technologies and Expression Analysis Core at the University of California, Davis Genome Center and sequenced (paired-end, 250 bp) using the MiSeq (Illumina) platform.

*Comparison to experimental heating:*

For our bioinformatics processing and data analysis, we also included soil viromes from a laboratory heating experiment performed on samples collected one year later (April 2022) at the same location of one of the control plots (plot U1), with samples subjected to different heat treatments in the laboratory (33). We included these samples to increase the number of recoverable vOTUs via read mapping (parameters described below) and for comparative analyses (parameters the same as for within-study comparisons, unless otherwise indicated).

*Virome bioinformatic processing:*

Viromes were processed as in our prior study (33). Briefly, raw reads were trimmed using Trimmomatic v0.39 (51) with a minimum q-score of 30 and a minimum read length of 50 bases. We used BBMap v39.01 (52) to remove PhiX sequences (k-mer size = 31 and hdist = 1). Each virome was assembled separately with MEGAHIT v1.2.9 (53) in the metalarge mode with a minimum contig length of 10,000 bp. Assembled contigs were analyzed with VIBRANT v1.2.0 (54) with the -virome flag to identify viral contigs. We used CD-HIT v4.8.1 (55) to cluster all output viral contigs at 95% shared nucleotide identity and 85% alignment coverage (breadth). Quality-filtered raw reads from all viromes were then mapped against the representative set of vOTUs using Bowtie 2 v2.4.1 (56) in sensitive mode. Lastly, we used CoverM v0.5.0 (57) to quantify vOTU relative abundances in each sample from the mapped read coverage and generated a trimmed mean coverage table with ≥75% horizontal (breadth) coverage threshold for vOTU detection and a count table with absolute number of reads aligned to each contig for downstream analyses. Host taxonomy for the entire set of dereplicated vOTUs was predicted using iPHoP v1.1.0 (58), with the iPHoP_db_Sept21_rw database and default parameters (minimum cutoff score of 90) (**Supplementary Table 14**).

*16S rRNA gene amplicon sequence bioinformatic processing:*

We used DADA2 v1.12.1 (59) to process 16S rRNA gene amplicon reads. We quality filtered reads with the filterAndTrim() function with the following parameters: truncLen =

c(0,0), maxN = 0, maxEE = c(2,2), truncQ = 2, rm.phix = TRUE. Default settings were used to perform error rate inference, dereplication, denoising, read merging, and chimera removal. Amplicon sequence variants (ASVs) were assigned taxonomy via the DADA2 RDP classifier106, using the SILVA database v138.1 as reference (60).

*Statistical and ecological analyses:*

All ecological and statistical analyses were performed with R v4.3.0 (61). Input for all analyses of viral communities or of vOTUs (e.g., vOTU detection patterns across samples, vOTU relative abundances) was the trimmed mean coverage vOTU table. We normalized the vOTU table by using the decostand function (method = "total", MARGIN = 2) from the Vegan package v2.6-6.1 (62) and removed singletons (vOTUs detected in only one sample). With a DADA2-generated relative abundance table for 16S rRNA gene amplified single variants (ASVs), we filtered out mitochondria and chloroplasts and removed singletons (ASVs that only appeared in a single sample). One sample (BSM27) did not meet the rarefaction threshold, so it was removed from further analysis. The following Vegan functions were used: vegdist (method = "bray") to calculate Bray-Curtis dissimilarities, adonis2 to perform PERMANOVA, and mantel to perform Mantel tests. We performed Kruskal-Wallis rank sum tests on means, followed by pairwise Wilcox Tests if the Kruskal-Wallis test was significant, with the Bonferroni p-value adjustment method for multiple comparisons. We determined correlation of paired samples between two variables with the cor.test function (Spearman method). We used the cmdscale function to perform multidimensional scaling and retrieve true eigenvalues and calculate PCoA point values. We performed PCA analysis with the princomp function (base R). We created upset plots with ComplexUpset v1.3.5, using vOTU or ASV relative abundance tables that were transformed into presence-absence tables (63). To determine the spatial distance between plots, we used the package geosphere v1.5-18 (64). We used the rcorr function from the package Hmisc v5.1-3 to determine correlations between relative abundances and chemical properties (65) and the pheatmap function from the package pheatmap v1.0.12 to visualize the correlations (66).

Statistical analyses are documented in **Supplementary Tables 15-18**.

## Results and Discussion

*Study design and dataset features*

To determine the responses of soil dsDNA viral and prokaryotic communities to a prescribed burn, we designed a before-after control-impact (BACI) (67,68) field study with four treatment plots (burned) and two control plots (did not burn) (**Figure 6A**). We sought to compare communities with and without burn treatment, both over time (before-after) and within timepoints (control-impact). In each of the six plots, we collected two replicate soil profiles with samples at two depths at 5 timepoints (14 and 3 days before and 7, 14, and 30 days after the prescribed burn, henceforth T1-5), for a total of 120 samples (**Figure 6B**).

We extracted DNA from DNase-treated viromes (91 viromes sequenced from the first four timepoints) and performed 16S rRNA gene amplicon sequencing on total DNA (115 samples amplified and sequenced from all timepoints). Fifteen viromes, or 12.5% of the total dataset had viromic DNA yields below detection limits (< 0.05 ng/µl, or < 0.49 ng/g soil), which was insufficient for sequencing. Ten of those viromes were from T5 (30 days post fire in soils approaching dryness, a condition previously shown to result in low-to-undetectable viromic yields (48)), with 8 from treatment plots and 2 from control plots. Due to low statistical power for treatment-control comparisons at T5, we decided against sequencing any of the viromes from that timepoint, resulting in a total of 29 viromes not sequenced from the full set of 120. We accounted for this 'censored data' (69) in our analysis of DNA yields (where the actual value for viromes with yields below detection limits was an unknown between 0 and 0.49 ng/g soil), and we report results from the sequenced viromes, with attempts to account for the missing data in our analyses and interpretations where possible.

We assembled 327,006 contigs > 10 kbp that were identified as likely viruses using VIBRANT (54) and clustered them at 95% average nucleotide identity (ANI) with the 141,638 contigs assembled from our laboratory heating experiment on soils from the same site (33) to a

final count of 272,017 'species-level' (70) vOTUs (**Supplementary Table 19**). The total number of vOTUs in the current study was reduced to 198,402 after removing vOTUs only detected in the heating experiment and removing singletons (vOTUs only detected in one virome). From the 16S rRNA gene amplicon sequencing data, we recovered 9,210 ASVs from both studies (**Supplementary Table 20**), which reduced to 4,136 ASVs after rarefying to a common depth of 18,500 reads per sample, removing singletons (ASVs that were detected in only one sample), and removing ASVs only detected in the heating experiment.

*Viromic DNA yields decreased significantly in post-burn samples*

The first evidence that burn treatment had an impact on viral communities came from significant changes in viromic DNA yields, a proxy for viral particle abundances (33,48) (**Figure 7A**). Viromic DNA yields for both burn and control plots significantly changed over time at each depth (Kruskal-Wallis, $p < 0.05$), but a pairwise Wilcoxon test showed significant yield decreases in post-fire timepoints compared to pre-fire timepoints in the burn plots only ($p.adj < 0.05$) and no significant differences between any of the timepoints in the control plots. Surface soils (0-3 cm) had more significant pairwise comparisons between timepoints than soils from 3-6 cm (5 versus 3 of a total of 8 comparisons for each depth), potentially indicating greater impact from the fire in the surface soils as might be expected based on previously observed surface-limited impacts from fire (24-27). At T3, the first timepoint after the fire, viromic DNA yields were significantly lower in burn versus control plots at 0-3 cm only and at T5, they were significantly lower at 3-6 cm only. Otherwise, within each timepoint, there were no significant differences in viromic DNA yields between burn and control plots (which was expected for pre-fire timepoints, but not necessarily for post-fire timepoints) and between depths within each treatment. Since all viromes with DNA yields below detection limits are considered censored data (with an unknown yield value between 0 and the lower detection threshold of 0.05 ng/µl or 0.49 ng/g soil), we set those values to 0 ng/g soil (the lower bound) and, in a repeat analysis to 0.49 ng/g soil (the upper bound), and there was no difference in the statistical results.

Across timepoints, soil moisture levels at both depths had changed significantly for burn plots and at the surface depth for control plots (Kruskal-Wallis, $p < 0.05$). While most of our sampling occurred after recent precipitation events, T5 did not (**Supplementary Figure 3A**). However, only in burn plots did pairwise Wilcoxon tests show a significant decrease in soil moisture at T5 compared with T1-T3 in both depths (p.adj < 0.05) (**Figure 7B**), indicating that fire likely exacerbated drying conditions. Low-to-undetectable viromic DNA yields at T5 are consistent with prior work suggesting lower viral biomass in dryer soils (48). Given that all but two viromes with DNA yields below detection limits were from post-fire treatment plots, along with significant decreases in both viromic DNA yields and soil moisture in burn plots only, we infer that the reduction of soil viral particle abundances can be attributed to burn treatment, both directly and in tandem with drying soil conditions.

*Spatial location better explained viral community composition than did burn treatment*

When considering the full viromic dataset across plots, treatments (burned and unburned), timepoints, and depth, plot (sample location) was the most significant factor driving viral community composition (explaining 17.32% ($R^2$) of the total variation in the data, $p = 0.001$ by PERMANOVA) (**Figures 8A-B**). The remaining variables were significant but explained much lower percentages of the variation. Timepoint and disturbance explained 4.95% and 1.73% of the total variation respectively (both $p = 0.001$ by PERMANOVA), and depth explained 1.31% of the variation ($p = 0.011$ by PERMANOVA). A linear regression of within-timepoint pairwise viral community Bray-Curtis similarities and spatial distances across pre-fire samples (all plots, two timepoints) revealed a slight but highly significant negative correlation at both T1 and T2 ($p < 0.001$ for both) (**Supplementary Figures 3B-C**), suggesting a distance-decay relationship, with communities farther apart more different than those closer together before any treatment had been applied. This relationship held after burn treatment ($p < 0.001$ for both T3 and T4) (**Supplementary Figures 3D-E**). Of the 198,402 vOTUs detected in more than one virome, the majority (57%) were detected in only one plot (**Figure 8C**), with only

1,100 vOTUs (0.55%) detected in all plots. These viral community compositional differences by plot, a subtle but significant distance-decay relationship across the sampled area, and the restricted detection of most vOTUs in single plots suggest that strong dispersal limitation and spatial structuring overlayed potential burn treatment effects at this site, consistent with other studies that have demonstrated strong spatial structuring of soil viral communities (40,71).

*Viral and prokaryotic community responses to burn treatment were evident in 'high-severity' samples*

To determine the extent to which soil chemical properties consistently shifted in response to burn treatment, we performed a series of analyses that compared responses of individual environmental variables and, separately, the suite of all measured variables together between burned and unburned samples. For most measured properties, there was substantial variation across post-fire treatment (burned) samples when compared to both types of control samples (from pre-fire burn plots and from unburned control plots) (**Supplementary Figures 4A-I**). The heterogeneity in measured chemical parameters is consistent with the heterogeneity in measured maximum temperatures achieved in each plot, including differences on both sides of plot B1 (474.8°C on one side and 62.6°C on the other side) (**Supplementary Figure 5A**). In a principal components analysis (PCA) of ten burn-relevant chemical properties (soil pH, organic matter, soil moisture, organic phosphorus, inorganic phosphorus, inorganic nitrogen, organic nitrogen : inorganic nitrogen, magnesium, calcium, and potassium (21–23)), all unburned samples (control samples and burn plots pre-fire) clustered closely together, while the post-fire treatment samples had a large spread, with some clustering with the unburned samples and the remaining distributed along the PCA1 axis, which explained 47% percent of the variance in the data (**Figure 9A**). This variability is indicative of a heterogenous, or patchy, soil chemical response to fire, and this patchiness is a known property of spring prescribed burns (39).

Given the patchy soil chemical response to burn, we sought to create a burn severity index for our dataset that could be leveraged as an explanatory factor for differences in the viral

and/or prokaryotic community responses across burned samples. We constructed a new PCA plot with the same subset of burn-relevant chemical properties, using burned samples alone (**Figure 9B**). The direction and magnitude of the loadings that contributed to the variation captured by PCA1 (shown as vectors in the PCA) aligned with known post-fire chemical changes (**Supplementary Figure 4J**) including an increase in pH and available nutrients and a decrease in organic matter and soil moisture (21–23). Therefore, we used the PCA1 scores from the PCA with burned samples only (**Figure 9B**) as a proxy for burn severity, assigning samples with lower values as less severely burned and samples with higher values as more severely burned. This allowed us to further interrogate impacts of burn treatment on viral and prokaryotic community composition beyond our binary burned vs. unburned comparisons.

We next investigated whether burn treatment effects were significantly different with depth in post-burn samples, as we hypothesized that, because heat typically penetrates only to about 3 cm even in high severity fires (26,27), there would be more substantial impacts to the viral communities at 0-3 cm compared to 3-6 cm. When comparing paired samples (samples from the same location but different depths), burn severity was higher at 0-3 cm than at 3-6 cm for 21 out of the 24 pairs (87.5%) (**Supplementary Figure 5B**), which confirms that, at least in terms of chemical changes, surface soils had a greater response than soils below 3 cm. However, the pairwise Bray-Curtis dissimilarities between viromes from both depths within the same vertical soil profile were not significantly different (Kruskal-Wallis, $p = 0.5835$) for any interaction of time and treatment, meaning that viral community differences across sample sets were similar at both depths, regardless of whether the samples were collected before or after the prescribed burn or from a control or treatment plot (**Supplementary Figure 5C**). We suspect that this lack of significant differences in viral community composition with depth in the burned samples is at least partially attributable to the missing virome sequencing data from mostly higher severity burned samples, due to insufficient viromic DNA yields.

Among burned samples, viral richness was negatively correlated with burn severity for

viromes at both depths ($p < 0.05$) (**Figure 9C**), however, while prokaryotic richness had a negative correlation at both depths (which corresponds with other studies noting a decreased richness after fire (17)), neither finding was significant (**Figure 9D**). Burn severity was significantly, but weakly correlated with viral community structure (Mantel statistic $r = 0.2689$, $p = 0.001$) (**Figure 9E**) and more strongly correlated with prokaryotic community structure (Mantel statistic $r = 0.5053$, $p = 0.001$) (**Figure 9F**). Burn severity has also been found to impact bacterial community composition after fire (72). Again, the missing virome data (largely from samples at the upper end of the burn severity index, **Figure 10B**) could explain why the correlation with burn severity was not as strong for viral communities than for prokaryotic communities, for which we had a more complete dataset. When considering viromic DNA yields, the likelihood of yields below detection limits significantly increased with increasing burn severity (binomial generalized linear model, $p < 0.05$), further reinforcing our interpretation that burn treatment was correlated with lower viral particle abundances. Decreased viromic DNA yields have previously been associated with soils with low moisture content (48) and soils that have experienced high temperatures (33), and here there was likely the interplay of both conditions that contributed to low viral particle abundances in more severely burned soils.

*Viruses and their predicted prokaryotic hosts responded similarly to fire, with viruses of the most fire-responsive taxa peaking in relative abundance at high burn severity*

We next sought to identify burn treatment-influenced shifts in the relative abundances of prokaryotic taxa and of the viruses predicted to infect them. When considering phylum-level prokaryotic taxonomy, trends were most clear when arranging samples along the burn severity gradient (**Figure 10A**), rather than by time or treatment group (**Supplementary Figures 6A-B**). The relative abundances of phyla Actinobacteriota, Chloroflexota, and Firmicutes had significant positive correlations with burn severity (Spearman's, $p < 0.05$), with Firmicutes having a particularly high positive correlation ($rho = 0.84$). Stress-tolerant traits in these phyla, such as spore formation and performing well under drought conditions for members of the

Actinobacteriota (73) and thermotolerance and spore formation in some members of both the Chloroflexota and Firmicutes (74,75), could explain their potential proliferation in burned soils, which has also been seen in other post-fire studies (particularly Actinobacteria and Firmicutes) (19,30) and in forest soils also collected at Blodgett that had been heated to 60°C and 90°C (33). The relative abundances of phyla Acidobacteriota, Bacteroidota, and Proteobacteria had significant negative correlations with burn severity (Spearman's rho > 0.75, $p < 0.05$). The reduction in Proteobacteria is counter to other post-fire studies, which typically report an increase in relative abundance, with the Proteobacteria Massilia even being assigned as pyrophilous (20,30,76). A correlation analysis of phylum-level prokaryotic relative abundances and soil chemical properties across all samples (including non-burned controls) revealed that Firmicutes and Actinobacteriota were significantly correlated in the same direction with many of the same properties that explained variation captured in PC1 (our burn severity index) and that Acidobacteriota, Proteobacteria, and Bacteroidota were significantly negatively correlated. (**Supplementary Figure 6C**).

Next, we investigated phylum-level host predictions, inherently coarse-grained but also more robust than predictions at finer taxonomic scales (58), to see whether viruses and their hosts exhibited similar dynamics in response to burn and/or across the burn severity range. On a per-sample basis, we were able to predict a host for a minimum of 7% of vOTUs and a maximum of 44% of vOTUs, with an average of 20% and a significantly higher percentage of predictions in soils with higher burn severity (Spearman's rho: 0.67, $p < 0.05$). As with prokaryotes, no clear trends in phylum-level host prediction were revealed based on timepoint or burn treatment (**Supplementary Figure 6E**), but with burn severity, clearer patterns emerged (**Figure 10B**). The relative abundances of viruses predicted to infect members of phylum Actinobacteriota or Firmicutes (two of the three prokaryotic phyla significantly positively correlated with burn severity) had a significant positive correlation with burn severity. Conversely, the relative abundances of viruses with a predicted host in the phylum

Acidobacteriota, Proteobacteriota, or Verrucomicrobiota (including two of the three prokaryotic phyla significantly negatively correlated with burn severity) had significant negative correlations with burn severity. A correlation analysis of relative abundances of viruses grouped by phylum-level host predictions and soil chemical properties across all samples (including non-burned controls) revealed that viruses predicted to infect Firmicutes, Actinobacteriota, and Myxococcota were significantly correlated in the same direction as most of the same properties that explained variation captured in PC1 (our burn severity index) (**Supplementary Figure 6D**). This indicates that viral populations have some level of interaction with both changes in host abundance and soil chemical changes in a post-burn environment, warranting further exploration of these groups of viruses as positive and negative post-fire responders.

**Conclusion**

This study interrogated soil viral community responses to a prescribed burn, revealing a heterogenous response aligned with burn severity. Viral communities were significantly spatially structured with plot location explaining greater viral community compositional variation than burn treatment, depth, or time. Our empirically defined proxy for burn severity, generated from a suite of burn-relevant chemical properties measured precisely at each sampling location, was key to revealing trends in viral and prokaryotic community composition and taxon relative abundances that were otherwise obscured. When accounting for burn severity, viral community richness and beta-diversity differed significantly according to the degree of burn. The relative abundances of four bacterial phyla significantly increased (Firmicutes and Actinobacteria, including known spore-formers) or decreased (Acidobacteriota and Proteobacteria) along the burn severity gradient, and the relative abundances of viruses predicted to infect these phyla responded in the same way as their putative hosts, suggesting increased viral predation of the most abundant (and, presumably, the most active) bacterial taxa. Increasing burn severity also corresponded with a greater number of low-to-undetectable viromic DNA yields, indicating decreasing viral particle abundances with higher burn severity. Our study reinforces the need to

include robust measurements of treatment-related properties, such as soil chemistry, with sample-specific resolution for assessing viral community responses to prescribed burning or to other inherently heterogenous disturbances. Had we only considered coarse, binary 'burned vs. unburned' treatment conditions here, we would have lacked the resolution to explain the heterogenous soil viral and prokaryotic community responses to the prescribed burn, which were attributable to highly localized burn severity differences. Our analyses have provided evidence for a more nuanced soil community response to fire, not just to burn overall, but to the specific degree of burn severity experienced by the very patch of soil that harbored the sampled communities, which could have been different from the conditions of other nearby soils in the same fire.

**Data Availability**

All raw sequences have been deposited in the NCBI Sequence Read Archive under the BioProject accession PRJNA1113186. The database of dereplicated vOTUs is available at https://zenodo.org/records/12562444. All scripts are available at https://github.com/seugeo/forestsoilviromes.

**Acknowledgements**

This chapter will be submitted for peer-reviewed publication with the following anticipated coauthors: Luke Hillary, Jess Sorensen, and Joanne Emerson. Additionally, we thank Patricia Lazicki, Jane Fudyma, and Christian Santos-Medellín for help with sample collection, staff at the Blodgett Forest Research Station (Ariel Thomson Roughton, Rob York, and Amy Mason) for advising on field sampling logistics, coordinating site visits, and coordinating the prescribed burn, resource support from the Traxler Lab at UC Berkeley (Monika Fischer, Neem Patel), and advice on statistical analysis from Andrew Blandino (UC Davis Statistical Laboratory), Amisha Poret-Peterson (USDA Agricultural Research Service), Valerie Eviner (UC Davis Department of Plant Sciences), and Cole Smith. Thanks to Valerie Eviner and Jorge Rodrigues for helpful comments on a draft version of the manuscript. Funding

for this work was provided by the U.S. Department of Energy (DOE), Office of Science, Office of Biological and Environmental Research (BER), Genomic Science Program, award number DE-SC0021198 (grant to JBE). SEG was also supported by the National Science Foundation Graduate Research Fellowship, the University of California Eugene Cota-Robles Fellowship, and the College of Agriculture and Environmental Sciences (UC Davis) Dean's Circle Award.

## References

1.Fernandes PM, Botelho HS. A review of prescribed burning effectiveness in fire hazard reduction. Int J Wildland Fire. 2003;12(2):117.

2.Kolden CA. We're Not Doing Enough Prescribed Fire in the Western United States to Mitigate Wildfire Risk. Fire. 2019 Jun;2(2):30.

3.Davis KT, Peeler J, Fargione J, Haugo RD, Metlen KL, Robles MD, et al. Tamm review: A meta-analysis of thinning, prescribed fire, and wildfire effects on subsequent wildfire severity in conifer dominated forests of the Western US. Forest Ecology and Management. 2024 Jun 1;561:121885.

4.Jose E, Agarwal P, Zhuang J. A data-driven analysis and optimization of the impact of prescribed fire programs on wildfire risk in different regions of the USA. Nat Hazards. 2023 Aug 1;118(1):181–207.

5.Ryan KC, Knapp EE, Varner JM. Prescribed fire in North American forests and woodlands: history, current practice, and challenges. Frontiers in Ecology and the Environment. 2013;11(s1):e15–24.

6.Wiedinmyer C, Hurteau MD. Prescribed Fire As a Means of Reducing Forest Carbon Emissions in the Western United States. Environ Sci Technol. 2010 Mar 15;44(6):1926–32.

7.A Large and Persistent Carbon Sink in the World's Forests [Internet]. [cited 2024 Jul 26]. Available from: https://www.science.org/doi/10.1126/science.1201609

8.Wear DN, Coulston JW. From sink to source: Regional variation in U.S. forest carbon futures. Sci Rep. 2015 Nov 12;5(1):16518.

9.Kuypers MMM, Marchant HK, Kartal B. The microbial nitrogen-cycling network. Nat Rev Microbiol. 2018 May;16(5):263–76.

10.Daly AB, Jilling A, Bowles TM, Buchkowski RW, Frey SD, Kallenbach CM, et al. A holistic framework integrating plant-microbe-mineral regulation of soil bioavailable nitrogen. Biogeochemistry. 2021 Jun 1;154(2):211–29.

11.Trivedi P, Anderson IC, Singh BK. Microbial modulators of soil carbon storage: integrating genomic and metabolic knowledge for global prediction. Trends in Microbiology. 2013 Dec 1;21(12):641–51.

12.Williamson KE, Radosevich M, Wommack KE. Abundance and Diversity of Viruses in Six Delaware Soils. Applied and Environmental Microbiology. 2005 Jun 1;71(6):3119–25.

13.Emerson JB. Soil Viruses: A New Hope. mSystems. 2019 May 28;4(3):e00120-19, /msystems/4/3/msys.00120-19.atom.

14.Williamson KE, Fuhrmann JJ, Wommack KE, Radosevich M. Viruses in Soil Ecosystems: An Unknown Quantity Within an Unexplored Territory. Annu Rev Virol. 2017 Sep 29;4(1):201–19.

15.Brum JR, Sullivan MB. Rising to the challenge: accelerated pace of discovery transforms marine virology. Nat Rev Microbiol. 2015 Mar;13(3):147–59.

16.Liang X, Radosevich M, DeBruyn JM, Wilhelm SW, McDearis R, Zhuang J. Incorporating viruses into soil ecology: A new dimension to understand biogeochemical cycling. Critical Reviews in Environmental Science and Technology. 2024 Jan 17;54(2):117–37.

17.Pressler Y, Moore JC, Cotrufo MF. Belowground community responses to fire: meta-analysis reveals contrasting responses of soil microorganisms and mesofauna. Oikos. 2019;128(3):309–27.

18.Fischer MS, Patel NJ, de Lorimier PJ, Traxler MF. Prescribed fire selects for a pyrophilous soil sub-community in a northern California mixed conifer forest. Environmental Microbiology. 2023;25(11):2498–515.

19.Pulido-Chavez MF, Randolph JWJ, Zalman C, Larios L, Homyak PM, Glassman SI. Rapid bacterial and fungal successional dynamics in first year after chaparral wildfire. Molecular Ecology. 2023;32(7):1685–707.

20.Whitman T, Whitman E, Woolet J, Flannigan MD, Thompson DK, Parisien MA. Soil bacterial and fungal response to wildfires in the Canadian boreal forest across a burn severity gradient. Soil Biology and Biochemistry. 2019 Nov 1;138:107571.

21.Certini G. Effects of fire on properties of forest soils: a review. Oecologia. 2005 Mar;143(1):1–10.

22.Butler OM, Elser JJ, Lewis T, Mackey B, Chen C. The phosphorus-rich signature of fire in the soil-plant system: a global meta-analysis. Niu S, editor. Ecol Lett. 2018 Mar;21(3):335–44.

23.Alcañiz M, Outeiro L, Francos M, Farguell J, Úbeda X. Long-term dynamics of soil chemical properties after a prescribed fire in a Mediterranean forest (Montgrí Massif, Catalonia, Spain). Science of The Total Environment. 2016 Dec;572:1329–35.

24.Harvey AE, Neuenschwander LF. Proceedings - Management and productivity of western-montane forest soils [Internet]. Ogden, UT: U.S. Department of Agriculture, Forest Service, Intermountain Research Station; 1991 [cited 2019 May 17] p. INT-GTR-280. Report No.: INT-GTR-280. Available from: https://www.fs.usda.gov/treesearch/pubs/33908

25.Mataix-Solera J, Guerrero C, García-Orenes F, Bárcenas GM, Torres MP. Forest fire effects on soil microbiology. Fire effects on soils and restoration strategies. 2009;5:133–75.

26.DeBano LF. The role of fire and soil heating on water repellency in wildland environments: a review. Journal of Hydrology. 2000 May 29;231–232:195–206.

27.Hartford R, Frandsen W. When It's Hot, It's Hot… Or Maybe It's Not! (Surface Flaming May Not Portend Extensive Soil Heating). Int J Wildland Fire. 1992;2(3):139.

28.Bailey AW, Anderson ML. Fire Temperatures in Grass, Shrub and Aspen Forest Communities of Central Alberta. Journal of Range Management. 1980 Jan;33(1):37.

29.Bruns TD, Chung JA, Carver AA, Glassman SI. A simple pyrocosm for studying soil microbial response to fire reveals a rapid, massive response by Pyronema species. Suen G, editor. PLoS ONE. 2020 Mar 4;15(3):e0222691.

30.Enright DJ, Frangioso KM, Isobe K, Rizzo DM, Glassman SI. Mega-fire in redwood tanoak forest reduces bacterial and fungal richness and selects for pyrophilous taxa that are phylogenetically conserved. Molecular Ecology. 2022;31(8):2475–93.

31.Jończyk E, Kłak M, Międzybrodzki R, Górski A. The influence of external factors on bacteriophages—review. Folia Microbiol. 2011 May;56(3):191–200.

32.Kimura M, Jia ZJ, Nakayama N, Asakawa S. Ecology of viruses in soils: Past, present and future perspectives. Soil Science and Plant Nutrition. 2008 Feb;54(1):1–32.

33.Geonczy SE, Hillary LS, Santos-Medellín C, Fudyma JD, Sorensen JW, Emerson JB. Virome responses to heating of a forest soil suggest that most dsDNA viral particles do not persist at 90°C [Internet]. bioRxiv; 2024 [cited 2024 May 13]. p. 2024.05.01.592093. Available from: https://www.biorxiv.org/content/10.1101/2024.05.01.592093v1

34.Parks SA, Dillon GK, Miller C. A New Metric for Quantifying Burn Severity: The Relativized Burn Ratio. Remote Sensing. 2014 Mar;6(3):1827–44.

35.Brady MK, Dickinson MB, Miesel JR, Wonkka CL, Kavanagh KL, Lodge AG, et al. Soil Heating in Fire ( SHEFIRE ): A model and measurement method for estimating soil heating and effects during wildland fires. Ecological Applications. 2022 Sep;32(6):e2627.

36.Agee JK, Skinner CN. Basic principles of forest fuel reduction treatments. Forest Ecology and Management. 2005 Jun 6;211(1):83–96.

37.York RA, Levine J, Russell K, Restaino J. Opportunities for winter prescribed burning in mixed conifer plantations of the Sierra Nevada. Fire Ecology. 2021 Nov 6;17(1):33.

38.Fossum CA, Collins BM, Stephens CW, Lydersen JM, Restaino J, Katuna T, et al. Trends in prescribed fire weather windows from 2000 to 2022 in California. Forest Ecology and Management. 2024 Jun 15;562:121966.

39.Knapp EE, Keeley JE, Ballenger EA, Brennan TJ. Fuel reduction and coarse woody debris dynamics with early season and late season prescribed fire in a Sierra Nevada mixed conifer forest. Forest Ecology and Management. 2005 Apr 5;208(1):383–97.

40.Santos-Medellin C, Zinke LA, ter Horst AM, Gelardi DL, Parikh SJ, Emerson JB. Viromes outperform total metagenomes in revealing the spatiotemporal patterns of agricultural soil viral communities. ISME J. 2021 Jul;15(7):1956–70.

41.Levine JI, Collins BM, York RA, Foster DE, Fry DL, Stephens SL. Forest stand and site characteristics influence fuel consumption in repeat prescribed burns. Int J Wildland Fire. 2020;29(2):148.

42.SoilWeb: An Online Soil Survey Browser | California Soil Resource Lab [Internet]. [cited 2024 Jul 10]. Available from: https://casoilresource.lawr.ucdavis.edu/gmap/

43.Letey J, Carrillo MLK, Pang XP. Approaches to characterize the degree of water repellency. Journal of Hydrology. 2000 May 29;231–232:61–5.

44.Haney Test Interpretation Guide v1.0 [Internet]. [cited 2024 Apr 10]. Available from: https://www.wardlab.com/wp-content/uploads/2020/02/Haney-Rev-1.0-Interpretation-Guide-PDF-1.pdf

45.Haney Report Definitions-New.pdf [Internet]. [cited 2024 Jul 4]. Available from: http://mvtl.com/_static/web/assets/media/pdf/Haney%20Report%20Definitions-New.pdf

46.Santos-Medellín C, Estera-Molina K, Yuan M, Pett-Ridge J, Firestone MK, Emerson JB. Spatial turnover of soil viral populations and genotypes overlain by cohesive responses to moisture in grasslands. Proceedings of the National Academy of Sciences. 2022 Nov 8;119(45):e2209132119.

47.Nicolas AM, Jaffe AL, Nuccio EE, Taga ME, Firestone MK, Banfield JF. Soil Candidate Phyla Radiation Bacteria Encode Components of Aerobic Metabolism and Co-occur with Nanoarchaea in the Rare Biosphere of Rhizosphere Grassland Communities. mSystems. 2021 Aug 17;6(4):10.1128/msystems.01205-20.

48.Santos-Medellín C, Blazewicz SJ, Pett-Ridge J, Firestone MK, Emerson JB. Viral but not bacterial community successional patterns reflect extreme turnover shortly after rewetting dry soils. Nat Ecol Evol. 2023 Sep 28;1–14.

49.Edwards J, Santos-Medellín C, Sundaresan V. Extraction and 16S rRNA Sequence Analysis of Microbiomes Associated with Rice Roots. Bio Protoc. 2018 Jun 20;8(12):e2884.

50.Thompson LR, Sanders JG, McDonald D, Amir A, Ladau J, Locey KJ, et al. A communal catalogue reveals Earth's multiscale microbial diversity. Nature. 2017;551(7681):457–63.

51.Bolger AM, Lohse M, Usadel B. Trimmomatic: a flexible trimmer for Illumina sequence data. Bioinformatics. 2014 Aug 1;30(15):2114–20.

52.Bushnell B. BBTools software package. 2014 [cited 2023 Oct 25]. BBMap. Available from: https://sourceforge.net/projects/bbmap/

53.Li D, Liu CM, Luo R, Sadakane K, Lam TW. MEGAHIT: an ultra-fast single-node solution for large and complex metagenomics assembly via succinct de Bruijn graph. Bioinformatics. 2015 May 15;31(10):1674–6.

54.Kieft K, Zhou Z, Anantharaman K. VIBRANT: automated recovery, annotation and curation of microbial viruses, and evaluation of viral community function from genomic sequences. Microbiome. 2020 Jun 10;8(1):90.

55.Huang Y, Niu B, Gao Y, Fu L, Li W. CD-HIT Suite: a web server for clustering and comparing biological sequences. Bioinformatics. 2010 Mar 1;26(5):680–2.

56.Langmead B, Trapnell C, Pop M, Salzberg SL. Ultrafast and memory-efficient alignment of short DNA sequences to the human genome. Genome Biology. 2009 Mar 4;10(3):R25.

57.Woodcroft BJ. CoverM [Internet]. 2023. Available from: https://github.com/ wwood/CoverM

58.Roux S, Camargo AP, Coutinho FH, Dabdoub SM, Dutilh BE, Nayfach S, et al. iPHoP: An integrated machine learning framework to maximize host prediction for metagenome-derived viruses of archaea and bacteria. PLOS Biology. 2023 Apr 21;21(4):e3002083.

59.Callahan BJ, McMurdie PJ, Rosen MJ, Han AW, Johnson AJA, Holmes SP. DADA2: High-resolution sample inference from Illumina amplicon data. Nat Methods. 2016 Jul;13(7):581–3.

60.Quast C, Pruesse E, Yilmaz P, Gerken J, Schweer T, Yarza P, et al. The SILVA ribosomal RNA gene database project: improved data processing and web-based tools. Nucleic Acids Research. 2013 Jan 1;41(D1):D590–6.

61.R Core Team. R: A language and environment for statistical computing. [Internet]. R Foundation for Statistical Computing, Vienna, Austria.; 2023. Available from: https://www.R-project.org/

62.Oksanen J, Simpson GL, Blanchet FG, Kindt R, Legendre P, Minchin PR, et al. vegan: Community Ecology Package [Internet]. 2022 [cited 2022 Jul 6]. Available from: https://CRAN.R-project.org/package=vegan

63.Krassowski M. ComplexUpset: Create Complex UpSet Plots Using "ggplot2" Components [Internet]. 2021 [cited 2022 Sep 22]. Available from: https://CRAN.R-project.org/package=ComplexUpset

64.Hijmans RJ, Karney (GeographicLib) C, Williams E, Vennes C. geosphere: Spherical Trigonometry [Internet]. 2022 [cited 2024 Jul 4]. Available from: https://cran.r-project.org/web/packages/geosphere/index.html

65.Jr FEH, functions) CD (contributed several functions and maintains latex. Hmisc: Harrell Miscellaneous [Internet]. 2024 [cited 2024 Jul 4]. Available from: https://cran.r-project.org/web/packages/Hmisc/

66.Kolde R. pheatmap: Pretty Heatmaps [Internet]. 2019 [cited 2024 Jul 5]. Available from: https://cran.r-project.org/web/packages/pheatmap/index.html

67.Smokorowski KE, Randall RG. Cautions on using the Before-After-Control-Impact design in environmental effects monitoring programs. Favaro B, editor. FACETS. 2017 May 1;2(1):212–32.

68.Conquest LL. Analysis and Interpretation of Ecological Field Data Using BACI Designs: Discussion. Journal of Agricultural, Biological, and Environmental Statistics. 2000 Sep;5(3):293.

69.Helsel DR. Statistics for Censored Environmental Data Using Minitab and R [Internet]. Newark, UNITED STATES: John Wiley & Sons, Incorporated; 2012 [cited 2024 Apr 25]. Available from: http://ebookcentral.proquest.com/lib/ucdavis/detail.action?docID=818500

70.Roux S, Adriaenssens EM, Dutilh BE, Koonin EV, Kropinski AM, Krupovic M, et al. Minimum Information about an Uncultivated Virus Genome (MIUViG). Nat Biotechnol. 2019 Jan;37(1):29–37.

71.ter Horst AM, Fudyma JD, Sones JL, Emerson JB. Dispersal, habitat filtering, and eco-evolutionary dynamics as drivers of local and global wetland viral biogeography. ISME J. 2023 Nov;17(11):2079–89.

72.Dove NC, Klingeman DM, Carrell AA, Cregger MA, Schadt CW. Fire alters plant microbiome assembly patterns: integrating the plant and soil microbial response to disturbance. New Phytologist [Internet]. [cited 2021 Mar 30];n/a(n/a). Available from: https://nph.onlinelibrary.wiley.com/doi/abs/10.1111/nph.17248

73.Santos-Medellín C, Liechty Z, Edwards J, Nguyen B, Huang B, Weimer BC, et al. Prolonged drought imparts lasting compositional changes to the rice root microbiome. Nat Plants. 2021 Aug;7(8):1065–77.

74.Moreno J, López-González JA, Arcos-Nievas MA, Suárez-Estrella F, Jurado MM, Estrella-González MJ, et al. Revisiting the succession of microbial populations throughout composting: A matter of thermotolerance. Science of The Total Environment. 2021 Jun 15;773:145587.

75.Freches A, Fradinho JC. The biotechnological potential of the Chloroflexota phylum. Applied and Environmental Microbiology. 2024 May 6;90(6):e01756-23.

76.Lucas-Borja ME, Miralles I, Ortega R, Plaza-Álvarez PA, Gonzalez-Romero J, Sagra J, et al. Immediate fire-induced changes in soil microbial community composition in an outdoor experimental controlled system. Science of The Total Environment. 2019 Dec;696:134033.

## Main Figures

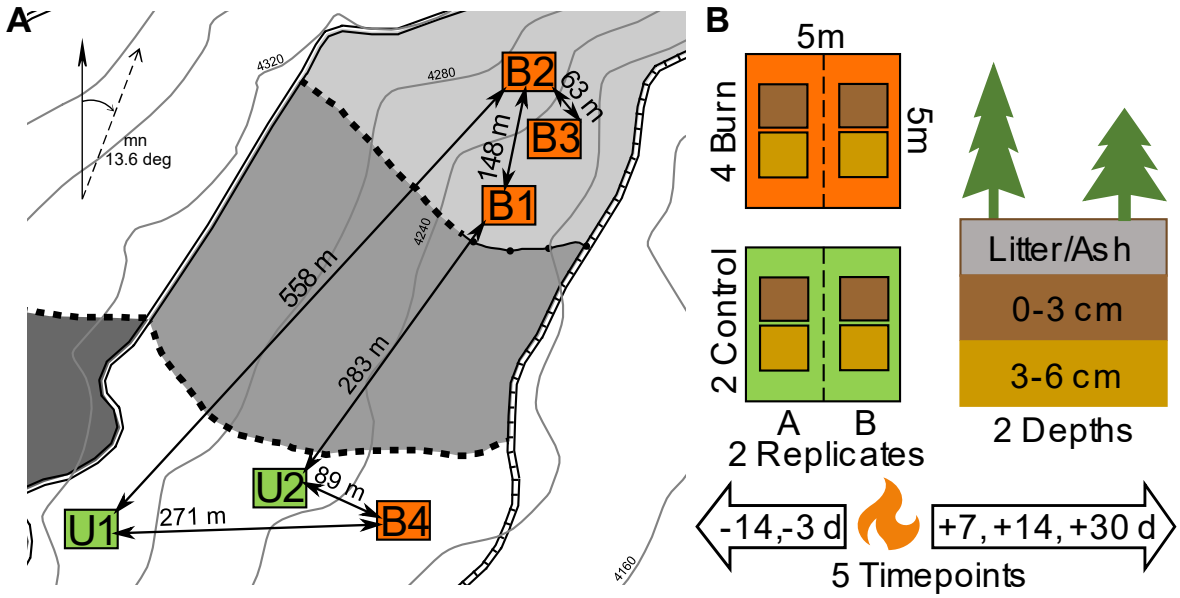


**Figure 6. Experimental design, A.** Map of plot locations with minimum and maximum distances indicated within units and between units. Orange squares indicate burn treatment plots and green squares indicate control plots. The vertical arrow represents true north and the angled arrow represents magnetic north, with a magnetic declination of 13.6 degrees. **B.** Schematic overview, indicating size of all plots, and sampling scheme (4 burn treatment plots and 2 control plots sampled at 2 depths with 2 replicates per plot for five timepoints: two before the fire and three after the fire).

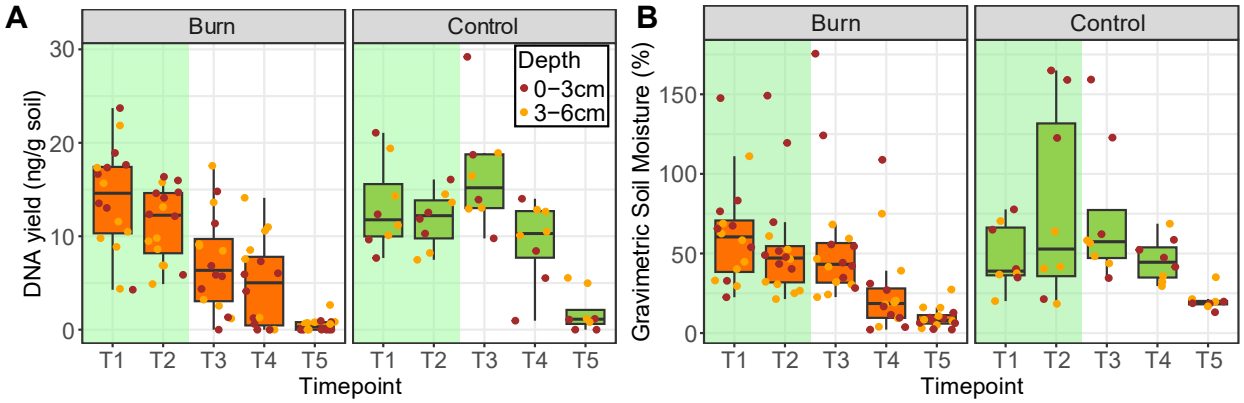


**Figure 7. Viromic DNA yields and soil moisture content, A.** DNA yields per gram of soil for each extracted virome at each timepoint, faceted by burn (left) and control (right) plots, with substitution of 0 ng/g soil for all viromes with yields that were below detection limits. Point colors indicate depth of sample. Box boundaries correspond to 25$^{th}$ and 75$^{th}$ percentiles, and whiskers extend to ±1.5x the interquartile range. **B.** Gravimetric soil moisture percent for each sample at each timepoint, faceted by burn (left) and control (right). Colors and box and whisker parameters are the same as in **A**.

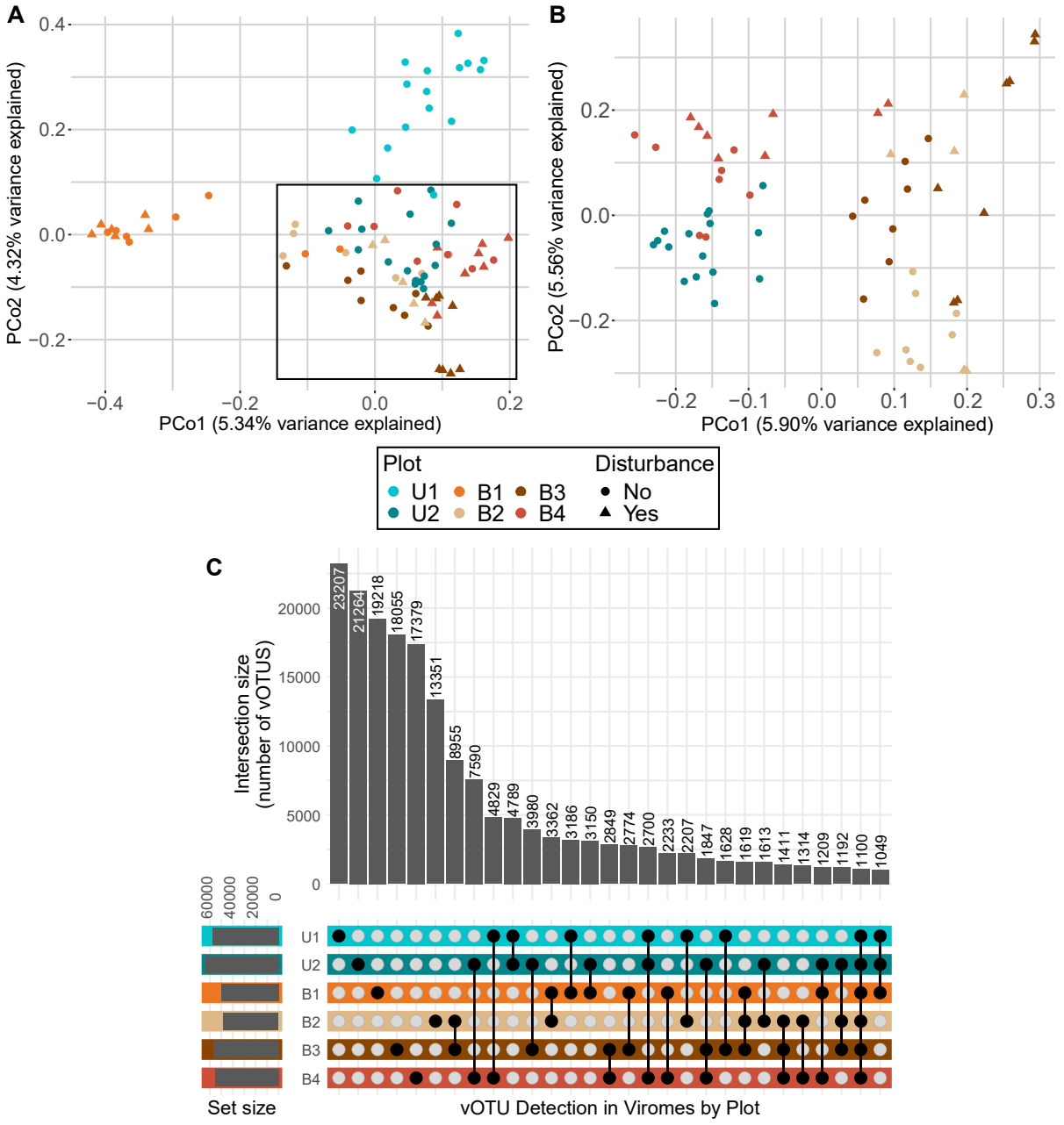


**Figure 8. Spatial structuring of soil viral communities, A/B.** Unconstrained analyses of principal coordinates (PCoA) performed on vOTU Bray-Curtis dissimilarities calculated across viromes, with colors indicating plot and shapes indicating whether or not the sample experienced a burn disturbance. **B**. PCoA excluding samples from the two plots (U1 and B1) with viral communities that separated the most from the rest of the viromes. Inset square in panel **A** approximately outlines panel **B** data. **C.** UpSet plot of vOTU detection patterns across sampled plots, with blackened circles indicating detection in a particular plot and intersection size indicating the number of unique vOTUs with a given detection pattern (found in one or more specific plots).

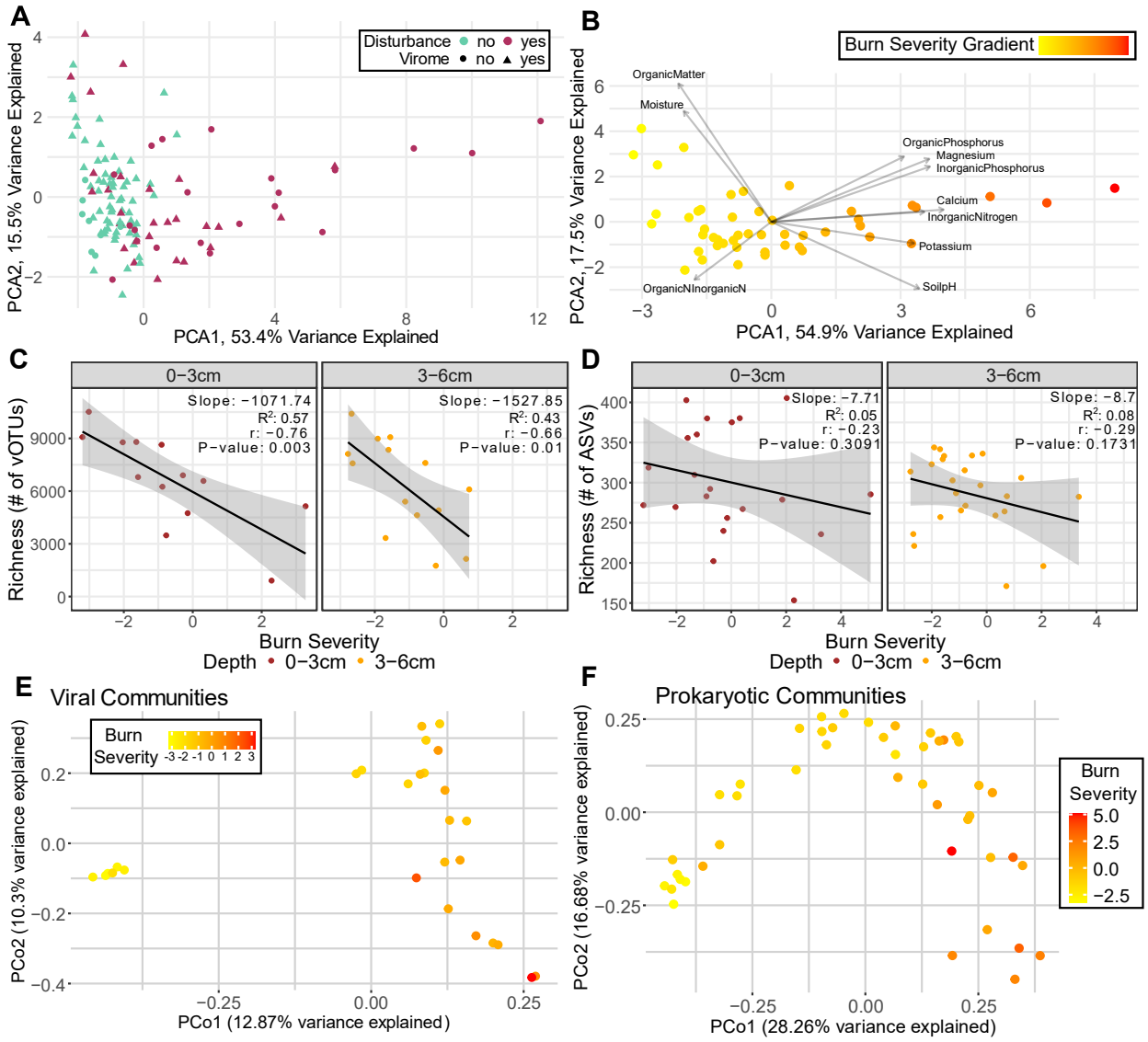


**Figure 9. Burn severity as a function of soil chemistry and its effects on viral and prokaryotic communities, A.** Principal component analysis (PCA) of z-transformed burn-relevant chemical properties (same as vectors in **B**) for each sample. Colors indicate disturbance (burned or not burned) and shapes indicate whether a virome was sequenced for that sample. **B**. Subset of **A**, with only burned samples (burgundy points in **A**). Colors indicate the PCA1 scores (burn severity gradient), and vectors indicate direction and magnitude of loadings. **C,D**. Richness of each burned virome (**C**) and 16S rRNA gene ASV profile (**D**) across the burn severity gradient. Trend lines display the least squares linear regression model. **E/F.** Principal Coordinates Analyses (PCoA) performed on viral community Bray-Curtis dissimilarities calculated only for viromes from burned plots (**E**) and prokaryotic community Bray-Curtis dissimilarities calculated only for 16S rRNA gene amplified samples from burned plots (**F**). Color gradient corresponds to chemistry PC1 scores (the burn severity index) from panel **B**.

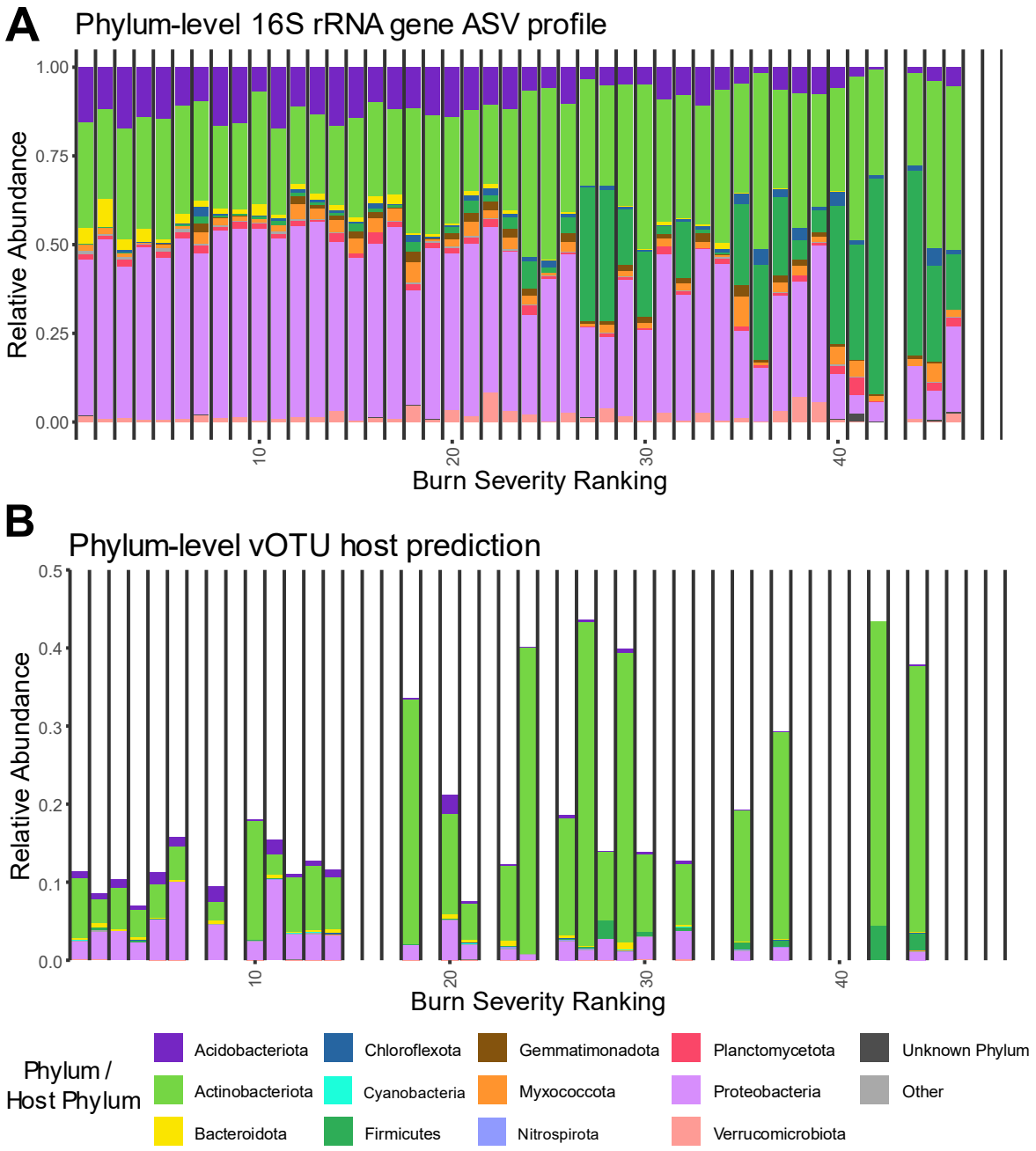


**Figure 10. Dynamics along burn severity gradient for prokaryotic taxa and for groups of viruses according to their predicted host, A.** Phylum-level relative abundances in 16S rRNA gene profiles from burned samples. Each stacked bar is a sample. Missing bars indicate samples that did not amplify or meet the rarefaction threshold. Samples are in rank order of burn severity. The 10 most abundant phyla are colored, with all lower abundance phyla collapsed into "other." **B.** Relative abundances of vOTUs with a host prediction in burned samples, grouped and colored by predicted host phylum (same legend as **A**). Each stacked bar is a virome, and missing bars indicate viromes that were not sequenced due to low or undetectable DNA yields. Viromes are in rank order of burn severity.

## Supplementary Figures

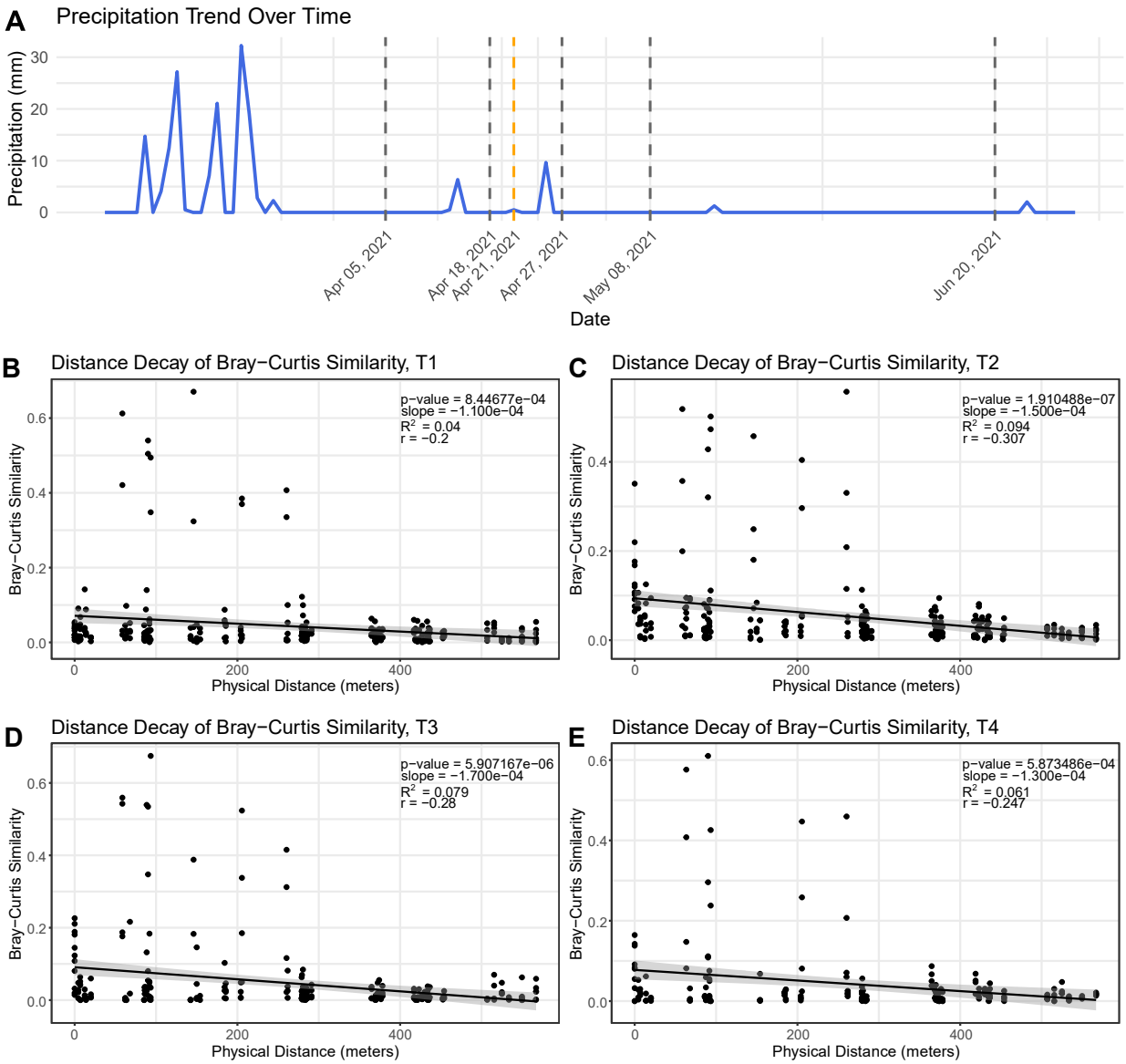


**Supplementary Figure 3. A.** Amount of precipitation in millimeters measured each day between March 01, 2021 to June 30, 2021, with sampling dates highlighted with gray vertical lines and the prescribed burn date highlighted with an orange vertical line. **B-E.** Relationship between pairwise viral community Bray–Curtis similarity and pairwise spatial distance between samples, separated by timepoint to avoid time as a confounding factor [T1 (**B**), T2 (**C**), T3 (**D**), and T4 (**E**)]. Each point is a pair of samples. Trend lines display the least squares linear regression model. Inset statistics correspond to the Pearson's correlation coefficient (r), $R^2$, the linear regression slope, and the associated P value.

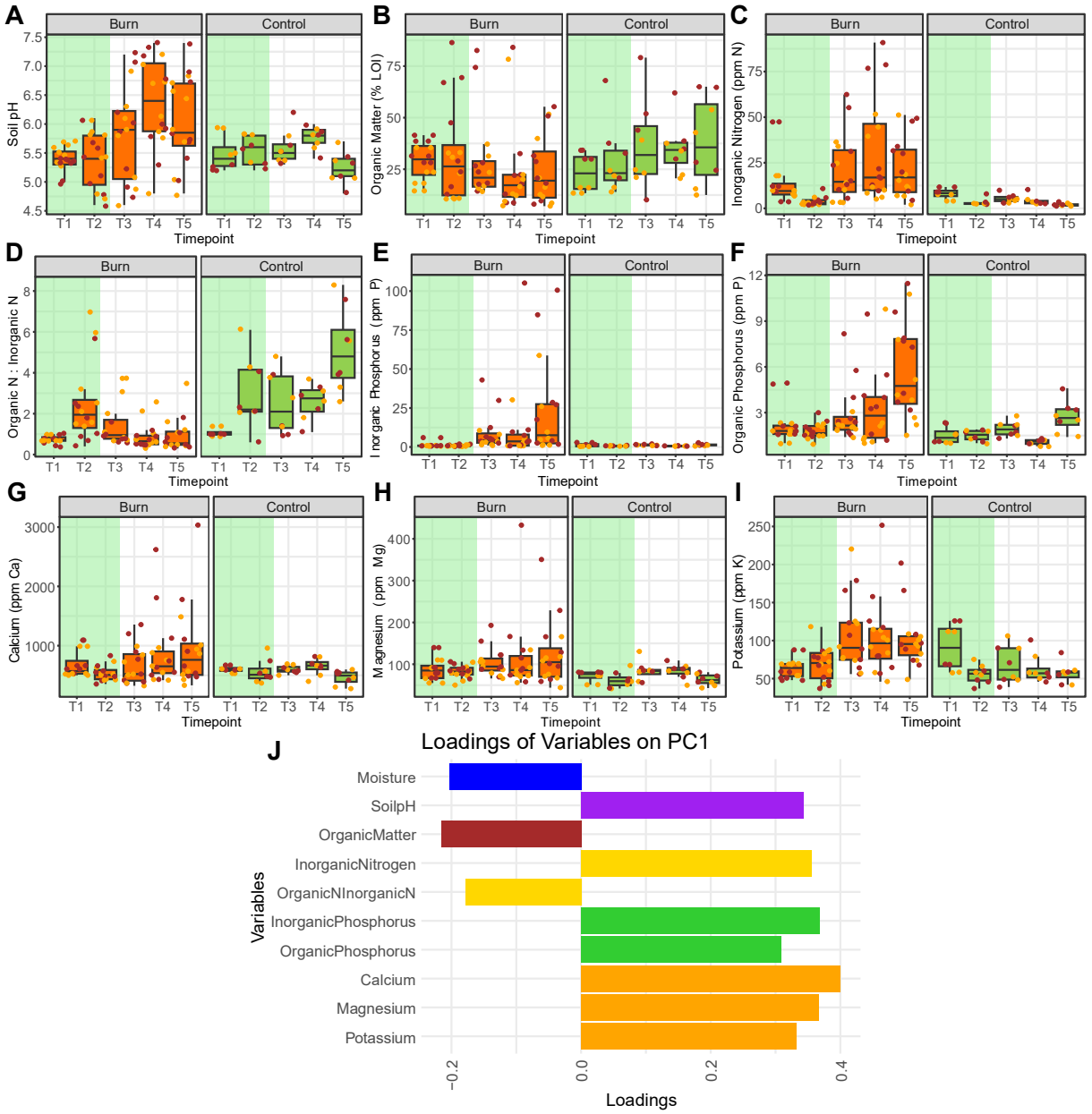


**Supplementary Figure 4. A-I.** Burn-relevant soil chemical properties for each sample over time, faceted by burn (left) and control (right) plots. Point colors indicate depth of sample, same as in **Figure 2**. Box boundaries correspond to 25$^{th}$ and 75$^{th}$ percentiles, and whiskers extend to ±1.5x the interquartile range. **J.** Principal component 1 (PC1) of the PCA in panel (**9B**) (the burn severity gradient) with bars representing the loadings along PC1 for each of the burn-relevant soil properties with different colors for either individual or groups of properties. Group colors: yellow = nitrogen properties, green = phosphorus properties, and orange = micronutrients. For organic matter, LOI = loss on ignition (method).

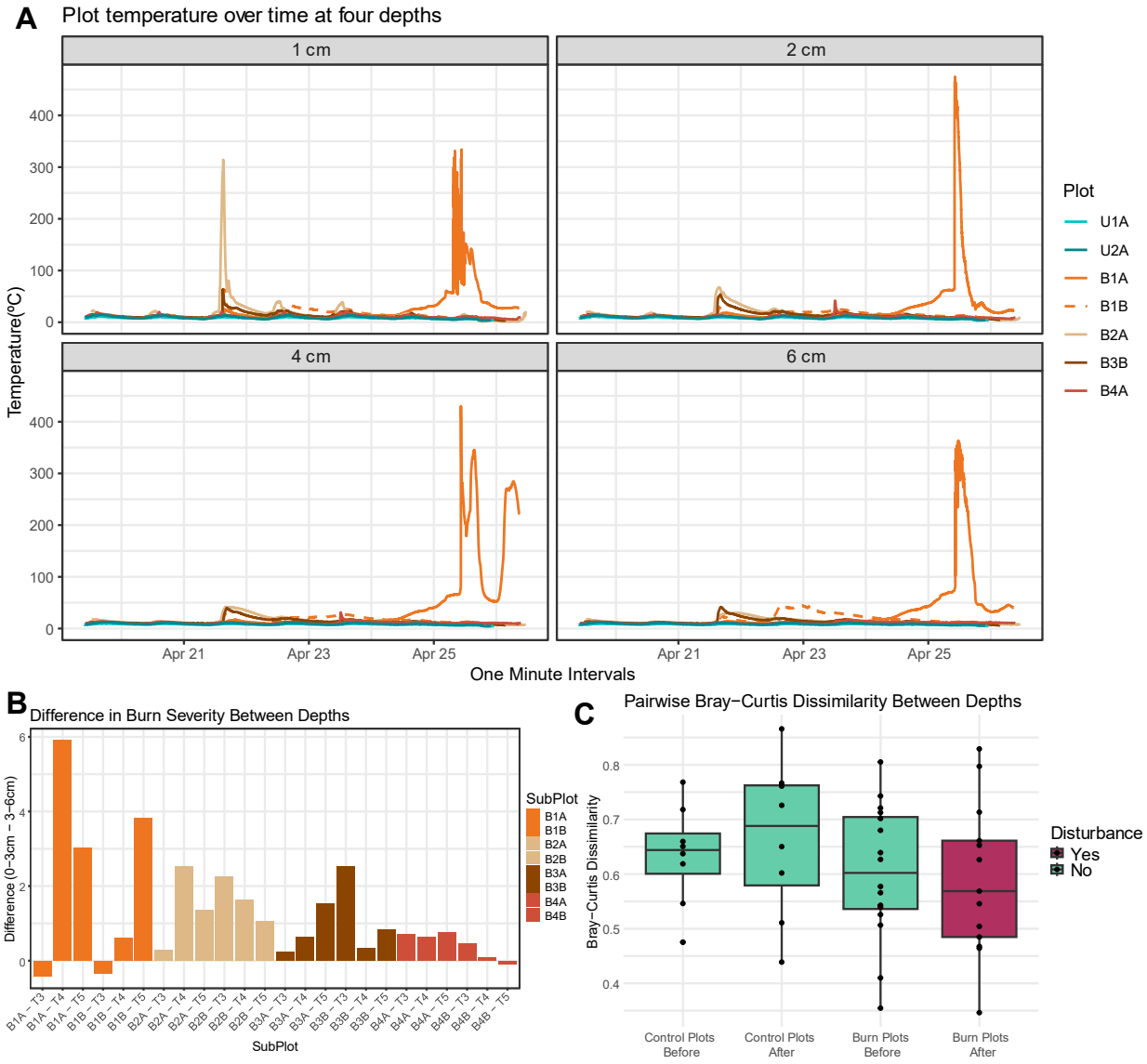


**Supplementary Figure 5**. **A**. Time series temperature measurements from dataloggers placed at each plot (with two sets of data retrieved from plot B1) over the course of the prescribed burn. Figures are faceted by probe depth. Lines are colored by plot location. **B**. Difference in burn severity between depths (upper depth severity minus lower depth severity) in burned plots, with each bar representing a subplot and timepoint and bars grouped and colored by plot. **C.** Boxplots representing the pairwise Bray-Curtis dissimilarity of viral communities between the two sample depths for each plot replicate at each timepoint. Box boundaries correspond to 25$^{th}$ and 75$^{th}$ percentiles, and whiskers extend to ±1.5x the interquartile range.

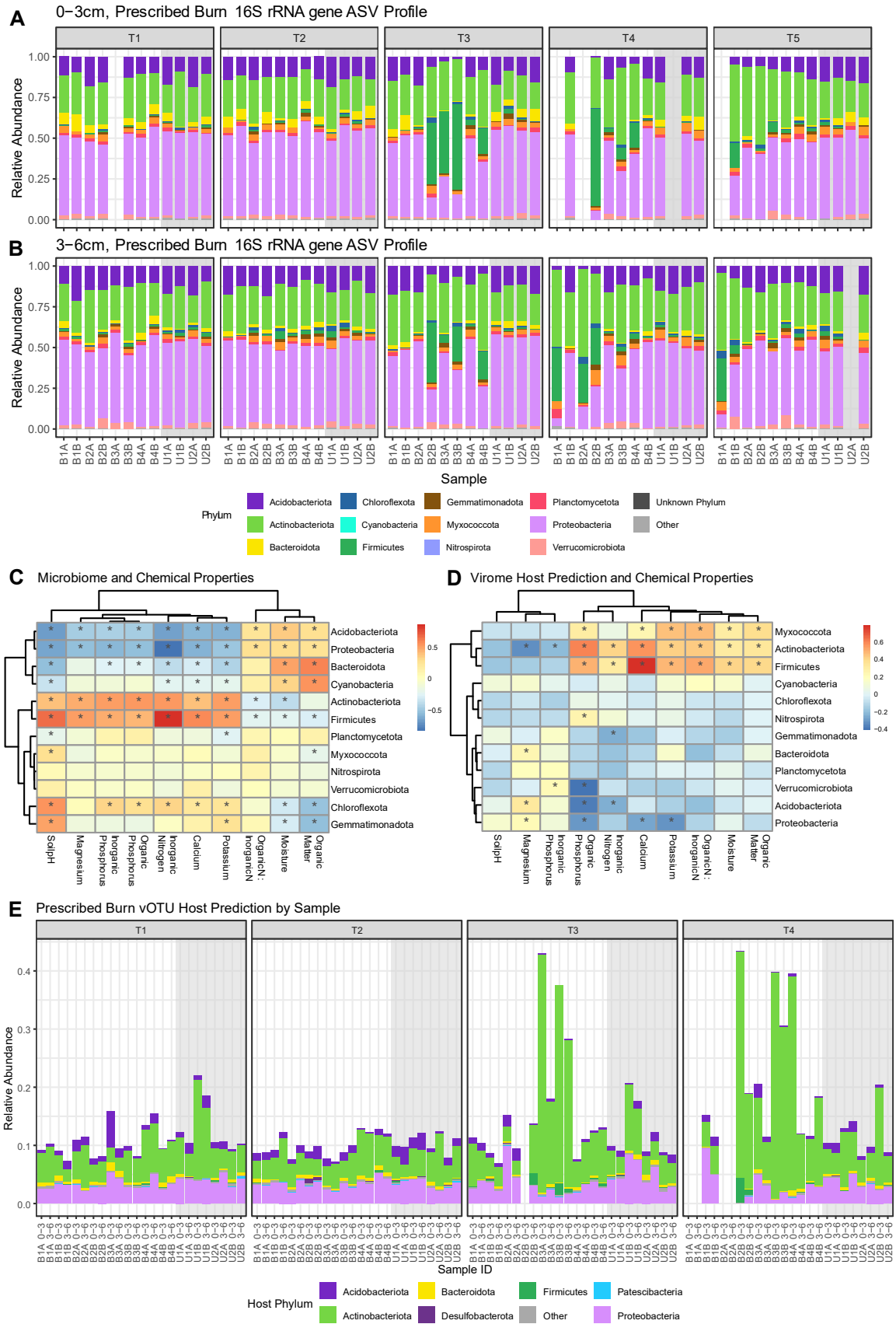
A
0−3cm, Prescribed Burn 16S rRNA gene ASV Profile
T1
T2
T3
T4
T5
Relative Abundance
1.00
0.75
0.50
0.25
0.00
B
3−6cm, Prescribed Burn 16S rRNA gene ASV Profile
Relative Abundance
Sample
Phylum
Acidobacteriota
Actinobacteriota
Bacteroidota
Chloroflexota
Cyanobacteria
Firmicutes
Gemmatimonadota
Myxococcota
Nitrospirota
Planctomycetota
Proteobacteria
Verrucomicrobiota
Unknown Phylum
Other
C
Microbiome and Chemical Properties
Acidobacteriota
Proteobacteria
Bacteroidota
Cyanobacteria
Actinobacteriota
Firmicutes
Planctomycetota
Myxococcota
Nitrospirota
Verrucomicrobiota
Chloroflexota
Gemmatimonadota
SoilpH
Magnesium
Phosphorus
Inorganic Phosphorus
Organic Phosphorus
Inorganic Nitrogen
Calcium
Potassium
Organic:Inorganic N
Moisture
Organic Matter
D
Virome Host Prediction and Chemical Properties
Myxococcota
Actinobacteriota
Firmicutes
Cyanobacteria
Chloroflexota
Nitrospirota
Gemmatimonadota
Bacteroidota
Planctomycetota
Verrucomicrobiota
Acidobacteriota
Proteobacteria
E
Prescribed Burn vOTU Host Prediction by Sample
T1
T2
T3
T4
Relative Abundance
Sample ID
Host Phylum
Acidobacteriota
Actinobacteriota
Bacteroidota
Desulfobacterota
Firmicutes
Other
Patescibacteria
Proteobacteria

**Supplementary Figure 6. A/B.** Phylum-level relative abundances in 16S rRNA gene profiles of all samples from 0-3 cm (**A**) and 3-6 cm (**B**). Each stacked bar is a sample. Missing bars indicate samples that did not amplify or meet the rarefaction threshold. Stacked bars are faceted by timepoint and grouped within each timepoint by plot. The gray box behind bars indicates control samples. The most abundant phyla are colored, with all other low abundance phyla collapsed into "other." **C-D.** Hierarchical clustering and heatmap visualizing the correlation analysis of soil properties and relative abundances of prokaryotic phyla (**C**) or vOTU groups with a given phylum-level host prediction (**D**). Gradient of colors indicate Pearson's correlation coefficient. Negative correlations correspond to dark blue and positive correlations correspond to dark red. Asterisks indicate a significant correlation ($p < 0.05$). **E.** Relative abundances of groups of vOTUs according to their phylum-level host predictions for all sequenced viromes. Each stacked bar is a virome. Missing bars indicate viromes that were not sequenced due to low or undetectable DNA yields. Stacked bars are faceted by timepoint and grouped within each timepoint by plot, with the sample depth indicated in the sample label. All other parameters are the same as (**A/B**).

## Chapter Three: Soil viral and prokaryotic communities shifted significantly after wildfire in chaparral and woodland habitats


### Abstract

Increased wildfire activity in Mediterranean chaparral and woodland habitats warrants more research into fire-driven biotic changes in soil, given that soil microbes contribute to ecosystem succession by way of organic matter decomposition, nutrient cycling, and promoting plant growth. Viruses of prokaryotes apply pressure to microbial communities, making their responses to fire also important for understanding post-fire ecology. Leveraging viromes and 16S rRNA gene amplicon sequencing, here we studied viral and prokaryotic community responses to wildfire in woodland and chaparral soils at five timepoints over one year following the California LNU Complex wildfire. We also compared post-fire samples to unburned controls at the three last timepoints, beginning five months after the fire. Viromic DNA yields were low-to-undetectable (indicative of low viral particle abundances), particularly for the first post-fire timepoint, and comparisons to controls suggest a return to baseline viral particle abundances within five months of the wildfire. Viral and prokaryotic community composition and soil chemistry differed significantly in burned samples compared to controls from both habitats. Compared to controls, a greater proportion of viral 'species' (vOTUs) from a burned Mediterranean conifer forest were detected in both burned habitats here, suggesting fire-associated habitat filtering. Published viromes collected from the same sites nine months pre-fire were more similar to controls than to post-fire viromes. Together, these results indicate significant changes in soil viral and prokaryotic communities due to wildfire.

## Introduction

The current increase in global fire activity, driven by climate change, land use change, and fire suppression policies, warrants a better understanding of fire's effects on biogeochemical processes and ecosystem resiliency in Mediterranean shrubland and woodland habitats (1–3). This includes the impact on prokaryotic communities, which are significant drivers of soil biogeochemical cycling, with major roles in organic matter decomposition and nutrient cycling (4,5). Changes in soil properties, which often occur after a disturbance like a wildfire (6), are well known to drive bacterial community shifts (7). One indirect impact of fire is a decrease in soil moisture, which can impact microbial communities, especially in habitats with low precipitation already (8). Soil viruses are also known to be impacted by drought and heat (9,10). What are not so well known are the long-term impacts of wildfire on viral community composition and the roles that viruses may play in the complex feedback loops among microbial communities, disturbance dynamics, and biogeochemical processes.

Wildfires can transform landscapes, and sometimes act as an ecosystem "reset", driving primary and secondary plant succession (11). Some habitats are wildfire mediated, including chaparral, with vegetation that evolved with fire that has adaptations both conducive and sometimes dependent on a certain frequency of fire activity (12). Post-fire soil bacterial community shifts can influence ecosystem successional rates (13), which makes soil microbial dynamics post-fire of great interest, given the threat of loss of habitat after wildfires (13,14). Studies with high-resolution temporal sampling have shown rapid bacterial community change post-fire, including both dramatic shifts immediately post-fire and rampant community compositional changes over time (12). Pyrophilous bacteria and fungi have been identified for their proliferation after fire, which has been attributed to traits that confer success in a post-fire environment, such as heat tolerance, xerotolerance, and spore and sclerotia formation (15,16). Additionally, pyrophilous bacteria seem to be phylogenetically conserved, which may mean they are both adapted to and ubiquitous across habitats that have experienced a fire disturbance (17).

While bacterial succession after wildfire has been studied in chaparral (12), little is known about the communities in woodland habitats that are often found close to chaparral. Additionally, there is little known about the viruses in these same systems in general (18), especially with regard to post-fire response. Here we present a one-year temporal study on viral and prokaryotic communities in woodland and chaparral soils following a wildfire. Our aim was to compare responses between the two habitats over time while also comparing community responses to dynamics in non-fire-impacted controls. Additionally, we sought to place the viruses detected in post-fire samples in biogeographic context, assessing where these viruses may have been found previously and whether the detection patterns might suggest conserved viral adaptations to fire.

## Materials and Methods

*Study site description:*

The LNU Lightning Complex fires burned 147,000 ha in northern California and were active for 46 days from 17 August 2020 to 2 October 2020 (19). On 4 November 2020 (approximately one month post-fire), we set up four 5x5 m plots at Quail Ridge Natural Reserve, CA, which burned at low-to-moderate severity in all locations throughout the field site, determined via the Monitoring Trends in Burn Severity (MTBS) dataset (20). Two plots were in burned chaparral habitats and two in burned woodland habitats. Plots were spatially paired, meaning that each chapparal plot was located close to (within 85 m of) a spatially paired woodland plot. These plots were all considered burned plots. On 12 March 2021, we set up an additional four burned plots (two chaparral and two woodland, which were spatially paired within 150 m of each other) at McLaughlin Natural Reserve, CA and four control plots (two chaparral and two woodland, which were not spatially paired due to the constraint of sampling locations that had not been burned by the wildfire). We also leveraged seven viromes from seven sites collected in November 2019 as part of a separate study (18), allowing us to make pre-burn comparisons for the Quail Ridge site, which burned completely in the LNU Complex fires.

Overall, there were 19 sampling locations (**Supplementary Table 21**). Chaparral sites had loamy soil with minimal horizon development, with surface mineral soil (A horizon) extending down to 5 to 15 cm. Woodland sites had predominantly loamy clay-enriched soil with an A horizon down to 25 cm. There was no organic horizon at any of the sites (21). Chamise was the dominant vegetation for all chaparral sites, and oak and pine trees were the dominant vegetation for woodland sites.

*Soil sampling:*

We collected two replicates per time point in each plot by dividing the plot in half along the middle, then dividing the subplot into eight sampling units, and collecting soil (0-6 cm depth) in corresponding sampling units at each timepoint (e.g., the top right of the right subplot and the top right of the left subplot for a single timepoint). The distance between replicate samples within each plot was approximately 3.75 m. We homogenized and sieved (8 mm) all samples separately. Samples were stored on ice and transported back to the lab and promptly placed at 4°C until DNA extraction two to three days after sample collection. We sampled five timepoints at Quail Ridge and three timepoints at McLaughlin (corresponding with the final three timepoints at Quail Ridge), with all timepoints two to three months apart, yielding a total of 88 samples.

*Viromic DNA extraction and quantification:*

Within two or three days after sample collection (12 samples were randomly processed each day), we extracted viromic DNA from all samples, as previously described (9,22). Briefly, to 10 g of each soil sample, we added 9 mL of protein-supplemented phosphate-buffered saline solution (PPBS: 2% bovine serum albumin, 10% phosphate-buffered saline, 1% potassium citrate, and 150 mM $MgSO_4$, pH 6.5). Samples were vortexed until homogenized and then placed on a horizontal shaker at 300 RPM at 4°C for 10 min. Supernatant was transferred into a new tube, and then 9 mL of PPBS was added to the soil remaining in the original tube, repeating the process for a total of three soil resuspensions and elutions, ending with a total of three

volumes of supernatant pooled together in a new centrifuge tube. The pooled supernatant was then centrifuged at 8 min at 7840 RPM at 4°C, collecting the progressively clearer supernatant and discarding the concentrated soil particles, for a total of three centrifugations and supernatant collections. The final supernatant was filtered through a 5 μm polyethersulfone (PES) membrane filter (PALL, Port Washington, NY, USA) to filter out larger soil particles, and then the filtrate went through a 0.22 μm PES membrane filter (PALL) to exclude most cellular organisms (apart from ultra-small bacteria (10,23)). Viral-sized particles and DNA remaining in the filtrate were concentrated into a pellet using the Optima LE-80K ultracentrifuge with a 50.2 Ti rotor (Beckman-Coulter, Brea, CA, USA) at 32,000 RPM at 4°C for 2 h 25 min. The pellet was resuspended in 200 μL of 0.02 μm filtered ultrapure water and treated with DNase (briefly, incubation at 37°C for 30 min after adding 10 units of RQ1 RNase-free DNase, Promega, Madison, WI, USA). We then extracted DNA using the DNeasy PowerSoil Pro kit (Qiagen, Hilden, Germany), following the manufacturer's protocol, with the addition of a 10 min incubation at 65°C prior to cell lysis, which also served as the 'stop' incubation for the DNase treatment. DNA quantification was performed using the Qubit dsDNA HS Assay and Qubit 4 fluorometer (ThermoFisher, Waltham, MA, USA). Due to low (30 viromes) or undetectable DNA yields (below 0.1 ng/μl or 0.49 ng/g soil) (19 viromes) now known to be expected for dry, heated, and recently burned soils (9,10), a subset of 39 viromes was prepared for library construction and sequencing.

*Total DNA extraction and quantification:*

For each sample, 0.25 g of soil was added directly to the DNeasy PowerSoil Pro kit (Qiagen) for total DNA extraction, following the manufacturer's protocol, with the addition of a 10 min incubation at 65°C prior to cell lysis. DNA quantification was performed using the Qubit dsDNA HS Assay and Qubit 4 fluorometer (ThermoFisher).

*Virome library preparation and sequencing:*

Sequencing of all 39 viromes was performed by the DNA Technologies and Expression

Analysis Core at the University of California, Davis Genome Center (Davis, CA, USA). Metagenomic libraries were constructed with the DNA Hyper Prep kit (Kapa Biosystems-Roche, Basel, Switzerland) and sequenced (paired-end, 150 bp) using the NovaSeq S4 platform (Illumina, San Diego, CA, USA) to a requested depth of 10 Gbp per virome.

*Amplicon library preparation and sequencing:*

We performed 16S rRNA gene amplicon sequencing on all total DNA extractions with a dual-indexing strategy (24). To amplify the V4 region of the 16S rRNA gene, we used the Platinum Hot Start PCR Master Mix (ThermoFisher) with the 515F/806R universal primer set. We followed the Earth Microbiome Project's PCR protocol (25), which included an initial denaturation step at 94°C for 3 min, 35 cycles of 94°C for 45 s, 50°C for 60 s, and 72°C for 90 s, and a final extension step at 72°C for 10 min. We cleaned libraries with AmpureXP magnetic beads (Beckman-Coulter), quantified amplicons with a Qubit 4 fluorometer (ThermoFisher), and then pooled all bead-purified products together in equimolar concentrations. The libraries were submitted to the DNA Technologies and Expression Analysis Core at the University of California, Davis Genome Center and sequenced (paired-end, 250 bp) using the MiSeq platform (Illumina).

*Soil physicochemical measurements:*

During sample collection, in-field soil temperature measurements were taken at each sampling location, and water repellency was measured by wetting a sample with a single drop of deionized water and counting how many seconds it took until the drop had fully infiltrated into the soil (26) (**Supplementary Table 22**). For the remaining soil physicochemical measurements, we note that there were some methodological differences among time points, which we clarify in detail here. In particular, differences between T0 (from our prior work at the same site) and T1-T5 are in part on account of not anticipating a need to compare these datasets, as well as differences in protocols before T0 and during (T1-T5) the COVID-19 pandemic. Differences within the T1-T5 dataset were largely for cost-effectiveness, as we learned in real

time about costs and options at different testing facilities. For T1-5, we calculated gravimetric soil moisture of each sample, by weighing out 10 g of soil into an aluminum weigh dish and measuring the weight after 24 hours in a drying oven at 105°C. For T0, gravimetric soil moisture was calculated by weighing out 10 g of soil and allowing it to dry completely in a biological hood for up to several days before weighing again. For T0 (from our prior study), soil samples were sent to Ward Laboratories (Kearney, NE, USA) for basic soil tests. For T1, we sent a soil sample from each sample site (at this point, only the 8 samples from Quail Ridge) to A&L Western Agricultural Laboratories (Modesto, CA, USA) for basic soil chemistry analysis as well as the University of California Davis Analytical Lab (Davis, CA, USA) for additional soil chemistry analysis. For timepoints T2-T5, we homogenized subplot replicate soil samples and sent a representative 200 g of field-condition soil (not dried) to Ward Laboratories for a suite of soil chemistry analyses under the Haney Soil Health Analysis package (27,28). Analysis was done by using the soil properties that we have available for all timepoints, which includes: gravimetric soil moisture (difference in method described above, soil pH (1:1 soil/water suspension), organic matter (percentage weight loss-on-ignition), nitrate (T0-1 was KCl-extracted and T2-5 was Haney-extracted), inorganic phosphorus (Olsen method for T0-1 and Haney-extracted and quantified by flow injection analysis for T2-5), and potassium, calcium, magnesium, and sodium (T0-1 was ammonium-acetate extracted and T2-5 was Haney-extracted). All Haney-extracted nutrients were quantified using inductively coupled argon plasma (ICAP) atomic emission spectroscopy (**Supplementary Table 23**).

*Virome bioinformatic processing:*

Raw reads were trimmed using Trimmomatic v0.39 (29) with a minimum q-score of 30 and a minimum read length of 50 bases. We used BBMap v39.01 (30) to remove PhiX sequences. Each virome was assembled separately with MEGAHIT v1.2.9 (31) in the metalarge mode with a minimum contig length of 10,000 bp. Assembled contigs were analyzed with VIBRANT v1.2.0 (32) with the -virome flag to identify viral contigs. All output viral contigs (low,

medium, and high quality) from all samples were iteratively clustered to form a representative set of vOTUs. We used CD-HIT v4.8.1 (33) to cluster viral contigs at 95% shared nucleotide identity and 85% alignment coverage (breadth). Quality-filtered raw reads from all viromes were then mapped against the representative set of vOTUs using Bowtie 2 v2.4.1 (34) in sensitive mode. Lastly, we used CoverM v0.5.0 (35) to quantify vOTU relative abundances in each virome and generated a trimmed mean coverage table and a count table for downstream analyses (0.75 minimum covered fraction). Host taxonomy of all vOTUs was predicted using iPHoP v1.1.0 (36), with default parameters (minimum cutoff score of 90) (**Supplementary Table 24**).

*Read mapping to additional databases:*

We mapped reads to the PIGEON v2.0 database (37,38) and separately to viral contigs from Blodgett Forest in Northern California (9). We then identified contigs that were found in each database and then clustered these contigs with the rest of the dataset at 95% average nucleotide identity (ANI), using CD-HIT (33).

*16S rRNA gene amplicon sequence bioinformatic processing:*

We used DADA2 v1.12.1 (39) to demultiplex 16S rRNA gene amplicon reads and perform quality assessment, read merging, and chimera removal. For quality filtering, we used the filterAndTrim() function with the following parameters: truncLen = c(0,0), maxN = 0, maxEE = c(2,2), truncQ = 2, rm.phix = TRUE. All other processing was with default settings. Amplicon sequence variants (ASVs) were assigned taxonomy by using the DADA2 RDP classifier, using the SILVA database v138.1 as reference (40).

*Statistical and ecological analyses:*

R v4.4.1 was used to perform all ecological and statistical analyses (41). Input for all analyses of viral communities or vOTUs was the trimmed mean coverage vOTU table. We normalized the vOTU abundance table by using the decostand function (method = “total”, MARGIN = 2) from the Vegan package v2.6-6.1 (42) and removed singletons, (vOTUs detected in only one sample). With a DADA2-generated abundance table for 16S rRNA gene amplified

single variants (ASVs), we filtered out mitochondria and chloroplasts and removed singletons (ASVs that only appeared in a single sample). We calculated Bray-Curtis dissimilarities with vegdist (method = "bray"), performed PERMANOVAS with adonis2, and performed PERMDISPs with betadisper and permutest, all functions from the Vegan package. We performed multidimensional scaling and retrieved true eigenvalues to calculate PCoA points with the cmdscale function (base stats). To perform PCA analysis, we used the princomp function (base R). Upset pots were created with the ComplexUpset v1.3.3 package using species abundance tables that were transformed into presence-absence tables (43). We determined distance between plots with the geosphere v1.5-18 package (44). We added two datasets collected from a mixed conifer forest (9) to the PIGEON v2.0 database, increasing the total number of vOTUs from 515,763 to 787,780. For the Blodgett addition, we identified vOTUs that were only found in burned forest samples, vOTUs that were only found in undisturbed forest samples, and vOTUs that were found in both burned and unburned forest samples and labeled them accordingly. We then used this updated version to determine the proportion of vOTUs that had mapped to the PIGEON v2.0 database and the Blodgett Forest datasets in each habitat. Statistical analyses are documented in **Supplementary Tables 25-27**.

## Results and Discussion

*Study design and dataset features*

The intention for this study was to assess time-resolved changes in dsDNA viral and prokaryotic communities after a wildfire, comparing the response in two habitats (chaparral and woodland) to control (not burned) plots. We set up a total of 12 5x5 m plots, 8 burned and 4 control, with half of the plots in chaparral habitat and the other half in woodland habitat (**Figure 11A**). Over the course of 10 months (or one year since the start of the wildfire), we sampled five timepoints (T1-T5) at Quail Ridge Natural Reserve (CA) and three timepoints at McLaughlin Natural Reserve (CA) (corresponding with T3-T5 at Quail Ridge) for a total of 88 samples. For comparison, we also leveraged a pre-burn dataset of seven viromes from the same

field sites collected in November 2019 (9 months pre-burn) (18).

We initially generated 88 DNase-treated viromes and used the viromic DNA yields to estimate patterns of viral particle abundances (10) and determine which viromes to sequence (**Figure 11B**). Yields were below detection limits for all samples at T1 (all of which were burned samples), indicating low viral particle abundances (10), consistent both with the dry season at the time of sampling and the potential long-term temperature and moisture impacts of the fire (45,46), all of which have been shown to reduce viromic DNA yields (9,10). For the three time points with control samples (T3-T5), there was no significant difference in viromic DNA yields between burned and control samples at any of the time points (Kruskal-Wallis, T3: $P = 0.2446$, T4: $P = 0.2534$, T5: $P = 0.1581$), suggesting a return to baseline viral particle abundances within 5 months of the fire (the first control timepoint). By T4 and T5, viromic DNA yields had decreased significantly in both chaparral and woodland habitats in both control and burned samples (Kruskal-Wallis, $P < 0.05$ for all conditions), presumably reflecting the transition into the dry season in the Mediterranean climate, which has previously been shown to substantially reduce the abundance of free viral particles (10). Due to undetectable and low DNA yields, we elected not to sequence 49 of the viromes, which, to preserve statistical power for comparisons, reduced the number of time points considered for our viral community analysis. We sequenced 39 viromes, including all viromes from Quail Ridge (burned) from T2-T4 except one (Chaparral, T2) and all viromes from McLaughlin T3, which included the control viromes. We also extracted total DNA from all 88 samples and amplified the 16S rRNA gene region to profile prokaryotic communities. All 88 samples amplified and were sequenced, but one sample yielded insufficient sequencing data (Quail Ridge, Chaparral, T5), so it was removed from the analysis during rarefaction. We recovered 5,097 ASVs over the entire dataset (**Supplementary Table 28**), which reduced to 4,933 ASVs after rarefying to a common depth of 17,700 reads per sample and removing singletons.

In our bioinformatic analyses, we also included seven viromes that were collected from

chaparral and woodland habitats at both Quail Ridge and McLaughlin in November 2019 (18), nine months prior to the fire. Paired 16 rRNA gene amplicon profiles were planned for that dataset, but, due to the COVID shutdown, they were never generated). The viromes served as pre-fire controls and increased the number of vOTUs used for read mapping-based detection in our dataset. In total, we amassed 77,869 putative viral contigs > 10 kbp as identified by VIBRANT (32), with 77,433 de novo assembled from this study and 436 from the 2019 viromes. We also mapped reads to vOTUs from the PIGEON v2.0 database (38) and from viromes generated from our recent prescribed burn study in a forest (Chapter 2), resulting in detection of 1,644 viral contigs. All recovered viral contigs were then clustered into a dereplicated set of 71,046 vOTUs (**Supplementary Table 29**), which was reduced to 37,926 vOTUs after removing singletons (vOTUs detected in only one sample).

*Viral communities differed significantly in burned and unburned samples and between habitats, whereas fire homogenized prokaryotic communities across habitats*

Since soil chemical properties are a good indicator of fire impact (6), we first compared the profile of chemical properties across soil samples. A principal component analysis revealed significant separation of burned samples from post-fire controls based on soil chemistry ($p = 0.04$ by PERMANOVA) (**Figure 11C**). The loadings in the direction of the burned samples relate to post-fire responses found elsewhere, including increased pH (47) and increased available phosphorus (6,11). We then compared beta-diversity of viral and prokaryotic communities in post-fire and control samples to see whether they differed significantly. Burn condition (burned or unburned) significantly structured viral communities (explaining 13.1% of the variation, $p < 0.001$ by PERMANOVA) (**Figure 12A**). Habitat explained 5.82% of the variation ($p < 0.001$ by PERMANOVA), still playing a part in viral community structuring, as had been observed previously (18). Despite large spatial differences in sampling locations, spatial distance (plot location) did not seem to obscure treatment effects on viral communities as substantially as has been observed in other studies (22,48), including our analysis of viral

community responses to a prescribed burn in a California mixed conifer forest (Chapter 2) ($p < 0.001$ by PERMANOVA for plot location across all viromes and $p < 0.001$ across all prokaryotic profiles). This means that plots with the same condition or the same habitat were found to respond similarly, overcoming plot-specific variability. While we did see viral community compositional structuring by habitat in control samples, as in prior work (18), habitat had a more pronounced influence on viral community composition post-fire (interaction of habitat and burn condition explained 8.1% of the variation in the data, $P < 0.001$ by PERMANOVA). The dispersion of viral communities was significantly greater in burned viromes than in controls ($p = 0.006$ by PERMDISP), meaning that burned viral community composition had greater variability than the control samples. When considering vOTU detection patterns in each habitat, 30% of the 37,926 vOTUs were detected only in post-fire burned woodland and 13% only in post-fire control woodland. For chaparral, 23% were found only in post-fire burned locations and 11% only in post-fire control locations. Only 11% of vOTUs were uniquely found in both burned habitats and 1.3% in both control habitats. This signifies that it is likely unique vOTUs that are driving community differences in the burned habitats, rather than shifts in the relative abundances of shared vOTUs (**Supplementary Figure 7A**).

For prokaryotic communities, burn condition explained 12% of the variation, habitat explained 8.2%, and the interaction between burn condition and habitat explained 5.6% (all $p < 0.001$ by PERMANOVA) (**Figure 12B**). In terms of dispersion, prokaryotic communities in woodland and chaparral were more similar to each other in burned samples than control samples, suggesting a homogenizing effect of fire on prokaryotic communities despite habitat differences ($p = 0.002$ by PERMDISP). Given the distinct separation between control and burned samples in soil chemical properties, prokaryotic, and viral communities across space, time, and habitat, this wildfire likely had a more homogenous impact on the landscape than did a prescribed burn in our previous study of a forest habitat (Chapter 2), likely attributable to overall greater fire severity . While heterogenous burn severity over short distances best

explained community compositional responses in the previous study, with low-severity burned communities appearing similar to unburned controls and generally only high-severity communities exhibiting a significant response to burn, here the response was more apparent across burned samples.

*Taxonomic shifts in burned versus control samples differed by habitat*

To assess whether viral infection dynamics may have changed after wildfire, we next compared viromes according to predicted host taxonomic profiles between burned and unburned samples, leveraging data from T3 (March 2021, approximately five months since the fire), from which we could make these direct comparisons (due to low DNA yields, an insufficient number of viromes was sequenced from other time points). Relative to the woodland habitat, more significant shifts in the relative abundances of viral groups according to predicted host taxonomy were observed for chaparral, which showed a significant increase in the relative abundances of phages predicted to infect Actinobacteria after wildfire and significant decreases in the relative abundances of putative phages of Acidobacteriota and Nitrospirota (Kruskal-Wallis, $p < 0.05$) (**Figure 12C**). The woodland results were less consistent, with some comparisons showing an increase in putative phages of Actinobacteria, but not uniformly across burn samples. Only the relative abundances of viruses predicted to infect Cyanobacteria had a significant change (Kruskal-Wallis, $p < 0.05$) between burned and control viromes in the woodland habitat (**Figure 12D**).

We were able to compare the relative abundances of prokaryotic phyla in control and burned samples for all three timepoints from which control samples were collected (T3-T5). In chaparral specifically, multiple prokaryotic phyla remained significant differences in burned samples as compared to control samples until T5 (August 2021, approximately one year since the fire), with some significantly different between burned and control samples across all timepoints (**Figures 12E & G**). The relative abundances of Actinobacteriota and Firmicutes were significantly higher in burned samples at each timepoint, perhaps reflective of the ability of

members of these phyla to form spores as survival structures (49,50). Increased relative abundances of Firmicutes have been previously observed in the first year after a wildfire in chaparral (12) and forest ecosystems (51), as well as in heated soil (9). Although there was a significant shift in the relative abundances of viruses predicted to infect Nitrospirota, a phylum of nitrite-oxidizing bacteria that typically dominates in arid ecosystems (52), members of this phylum were at very low relative abundance in the prokaryotic data and did not exhibit the same pattern as their viruses. In woodland habitats (**Figures 12F & H**), similar to the patterns in the viruses when grouped by predicted hosts, differences in prokaryotic communities between burned and control samples were less pronounced and were observed at fewer time points. Firmicutes were significantly more abundant in burned samples (only at T4 and T5), similar to our observations in chaparral (Kruskal-Wallis, $p < 0.05$). In general, the woodland habitat did not exhibit as pronounced a response to the fire, in terms of phylum-level shifts in the relative abundances of prokaryotes or their predicted phages.

Since there were several timepoints that did not have sufficient control data comparisons, we were unable to compare community compositional change between burned and unburned soils over the entire time series. However, we were able to determine if there was significant compositional changes for viruses (based on host-prediction data) or prokaryotes as the days since fire increased (**Supplementary Figures 7B-E**). In chaparral, there were significant changes in the relative abundance of viruses predicted to infect Actinobacteria (decrease) and Bacteroidota (increase) over time, while in woodland, Bacteroidota and Proteobacteria significantly decreased over time (Spearman's, $p < 0.05$). All other viruses of a particular host-predicted phyla that significantly changed across timepoints (Kruskal-Wallis, $p < 0.05$) had trends that were non-monotonic over time. For prokaryotes, most phyla that significantly changed across timepoints (Kruskal-Wallis, $p < 0.05$) also had non-monotonic relationships with days since fire, potentially reflecting seasonal changes. Only Actinobacteria significantly increased over time in both chaparral and woodland and Acidobacteriota decreased

over time in woodland (Spearman's, $p < 0.05$).

*Biogeographic context suggests that some viral taxa were preferentially detected in post-fire datasets and thus may be fire-adapted*

To assess biogeographic patterns of fire-impacted vOTUs, we performed read mapping of this LNU viromic dataset to other vOTU databases to see whether our viromes included vOTUs that had been previously detected elsewhere, including in our other fire-related studies. We detected a total of 1,644 such vOTUs, with 760 from a mixed conifer forest soil as part of our studies from Blodgett Forest, CA (9) (Chapter 2) and 884 from the PIGEON v2.0 database (38). The overall composition of vOTUs in the PIGEON v2.0 database together with the Blodgett Forest vOTUs reflected primarily aqueous (freshwater and marine), forest, and agricultural sources (**Figure 13A**). Other than vOTUs from our November 2019 viromes from these sites, which we had already included in this study (and therefore removed from the database, leaving a total of 787,363 vOTUs), the PIGEON v2.0 database did not contain any vOTUs known to originate from chaparral or woodland habitats, though some vOTUs were from samples labeled as 'terrestrial (soil)' in the original publication (53), which could conceivably have included these habitats. When separated by habitat and burn condition, a large percentage of vOTUs detected in burned chaparral (total vOTUs = 527) (**Figure 13B**) and burned woodland (total vOTUs = 912) (**Figure 13C**) viromes were originally found in burned mixed conifer forest (31.3% and 18.9% respectively). Conversely, when considering the composition of vOTUs found in the control viromes (612 total vOTUs for chaparral and 543 total vOTUs for woodland), burned mixed conifer forest was a much smaller fraction (6.3% for chaparral – **Figure 13D** to almost undetectable at 0.6% for woodland – **Figure 13E**). This suggests that there may be specific groups of viral 'species' that commonly persist in post-fire environments, certainly in part due to survival and/or rapid colonization and growth of their hosts (10), but also perhaps due to their own inherent survival traits (e.g., as genomes inside spore-forming hosts and/or as durable virions) (54,55).

## Conclusion

In this study, we compared viral and prokaryotic community responses to wildfire in chaparral and woodland habitats over one year. Many of our viromes had low-to-undetectable viromic DNA yields, suggesting that post-fire conditions in arid climates likely have low extracellular viral biomass. Of the 39 viromes that we were able to sequence, significant differences were observed between burned and control viromes for both habitats, alongside significant changes in soil chemical properties and prokaryotic community composition. Wildfire increased dispersion in viral community beta-diversity for both habitats, while there was an opposite, homogenizing effect on prokaryotic community composition, with prokaryotic communities from different habitats more similar in burned samples than in controls. At T3 (the only timepoint from which control viromes were sequenced), significant increases in the relative abundances of viruses predicted to infect Actinobacteriota and decreases in putative Nitrospirota and Acidobacteriota phages were evident in chaparral, while only viruses predicted to infect Cyanobacteria significantly decreased in woodland. As for prokaryotic shifts, only Actinobacteria and Firmicutes were consistently significantly more abundant in burned chaparral samples at all timepoints than the controls (suggesting increased survival of spore-formers), with no consistent changes in woodland. Additionally, there seemed to be a degree of habitat filtering on viral 'species' in burned ecosystems, regardless of habitat, given that a substantial percentage of vOTUs in burned chaparral and woodland were also found previously in burned forest.

In summary, wildfire had a clear impact on viral community composition, including changes in the relative abundances of viruses predicted to infect bacteria from spore-forming phyla, which were at higher abundance in burned samples. Thus, the shifts in viral community composition post-fire were at least partially attributable to shift their host abundances, but perhaps some of these viruses were also inherently more durable (fire-resistant). Higher temporal resolution in both burned and unburned viromic data will help us to better

characterize these compositional shifts over time and compare them with prokaryotic community shifts, enhancing our understanding of viral-host dynamics post-fire.

## Data Availability

All raw sequences have been deposited in the NCBI Sequence Read Archive under the BioProject accession PRJNA1147726. The database of dereplicated vOTUs is available at https://zenodo.org/records/12740558. All scripts are available at https://github.com/seugeo/wildfire.


## Acknowledgements

This chapter will be submitted for peer-reviewed publication with the following anticipated coauthors: Anneliek ter Horst and Joanne Emerson. Additionally, we thank Cathy Koehler at McLaughlin Natural Reserve and Shane Waddell at Quail Ridge Natural Reserve for advising on field sampling logistics and coordinating site visits, and Jane Fudyma, Kristin Kawecki, and David Robles for help with soil collection. Thanks to Valerie Eviner and Jorge Rodrigues for helpful comments on a draft version of the manuscript. Funding for this work was provided by the U.S. Department of Energy (DOE), Office of Science, Office of Biological and Environmental Research (BER), Genomic Science Program, award number DE-SC0021198 (grant to JBE). SEG was also supported by the National Science Foundation Graduate Research Fellowship, the University of California Eugene Cota-Robles Fellowship, and the College of Agriculture and Environmental Sciences (UC Davis) Dean's Circle Award.


## References


1.Bowman DMJS, Balch JK, Artaxo P, Bond WJ, Carlson JM, Cochrane MA, et al. Fire in the Earth System. Science. 2009 Apr 24;324(5926):481.

2.Riley KL, Loehman RA. Mid-21st-century climate changes increase predicted fire occurrence and fire season length, Northern Rocky Mountains, United States. Ecosphere. 2016;7(11):e01543.

3.Moritz MA, Batllori E, Bradstock RA, Gill AM, Handmer J, Hessburg PF, et al. Learning to coexist with wildfire. Nature. 2014 Nov;515(7525):58–66.

4.Crowther TW, van den Hoogen J, Wan J, Mayes MA, Keiser AD, Mo L, et al. The global soil community and its influence on biogeochemistry. Science. 2019 Aug 23;365(6455):eaav0550.

5.Schimel J, Schaeffer SM. Microbial control over carbon cycling in soil. Front Microbiol [Internet]. 2012

Sep 26 [cited 2024 Aug 10];3. Available from: https://www.frontiersin.org/journals/microbiology/articles/10.3389/fmicb.2012.00348/full

6.Gómez-Rey MX, Couto-Vázquez A, García-Marco S, González-Prieto SJ. Impact of fire and post-fire management techniques on soil chemical properties. Geoderma. 2013 Mar;195–196:155–64.

7.Fierer N, Jackson RB. The diversity and biogeography of soil bacterial communities. Proceedings of the National Academy of Sciences. 2006 Jan 17;103(3):626–31.

8.Yang X, Zhu K, Loik ME, Sun W. Differential responses of soil bacteria and fungi to altered precipitation in a meadow steppe. Geoderma. 2021 Feb 15;384:114812.

9.Geonczy SE, Hillary LS, Santos-Medellín C, Fudyma JD, Sorensen JW, Emerson JB. Virome responses to heating of a forest soil suggest that most dsDNA viral particles do not persist at 90°C [Internet]. bioRxiv; 2024 [cited 2024 May 13]. p. 2024.05.01.592093. Available from: https://www.biorxiv.org/content/10.1101/2024.05.01.592093v1

10.Santos-Medellín C, Blazewicz SJ, Pett-Ridge J, Firestone MK, Emerson JB. Viral but not bacterial community successional patterns reflect extreme turnover shortly after rewetting dry soils. Nat Ecol Evol. 2023 Sep 28;1–14.

11.Butler OM, Elser JJ, Lewis T, Mackey B, Chen C. The phosphorus-rich signature of fire in the soil-plant system: a global meta-analysis. Niu S, editor. Ecol Lett. 2018 Mar;21(3):335–44.

12.Pulido-Chavez MF, Randolph JWJ, Zalman C, Larios L, Homyak PM, Glassman SI. Rapid bacterial and fungal successional dynamics in first year after chaparral wildfire. Molecular Ecology. 2023;32(7):1685–707.

13.Graham EB, Knelman JE, Schindlbacher A, Siciliano S, Breulmann M, Yannarell A, et al. Microbes as Engines of Ecosystem Function: When Does Community Structure Enhance Predictions of Ecosystem Processes? Front Microbiol [Internet]. 2016 Feb 24 [cited 2024 Aug 10];7. Available from: https://www.frontiersin.org/journals/microbiology/articles/10.3389/fmicb.2016.00214/full

14.Driscoll DA, Armenteras D, Bennett AF, Brotons L, Clarke MF, Doherty TS, et al. How fire interacts with habitat loss and fragmentation. Biological Reviews. 2021;96(3):976–98.

15.Fischer MS, Patel NJ, de Lorimier PJ, Traxler MF. Prescribed fire selects for a pyrophilous soil sub-community in a northern California mixed conifer forest. Environmental Microbiology. 2023;25(11):2498–515.

16.Whitman T, Whitman E, Woolet J, Flannigan MD, Thompson DK, Parisien MA. Soil bacterial and fungal response to wildfires in the Canadian boreal forest across a burn severity gradient. Soil Biology and Biochemistry. 2019 Nov 1;138:107571.

17.Enright DJ, Frangioso KM, Isobe K, Rizzo DM, Glassman SI. Mega-fire in redwood tanoak forest reduces bacterial and fungal richness and selects for pyrophilous taxa that are phylogenetically conserved. Molecular Ecology. 2022;31(8):2475–93.

18.Durham DM, Sieradzki ET, Ter Horst AM, Santos-Medellín C, Bess CWA, Geonczy SE, et al. Substantial differences in soil viral community composition within and among four Northern California habitats. ISME Communications. 2022 Dec 1;2(1):100.

19.LNU Lightning Complex | CAL FIRE [Internet]. [cited 2024 Jul 8]. Available from: https://www.fire.ca.gov/incidents/2020/8/17/lnu-lightning-complex

20.Direct Download | MTBS [Internet]. [cited 2024 Aug 3]. Available from: https://mtbs.gov/direct-download

21.SoilWeb: An Online Soil Survey Browser | California Soil Resource Lab [Internet]. [cited 2024 Jul 10]. Available from: https://casoilresource.lawr.ucdavis.edu/gmap/

22.Santos-Medellín C, Estera-Molina K, Yuan M, Pett-Ridge J, Firestone MK, Emerson JB. Spatial turnover of soil viral populations and genotypes overlain by cohesive responses to moisture in grasslands. Proceedings of the National Academy of Sciences. 2022 Nov 8;119(45):e2209132119.

23.Nicolas AM, Jaffe AL, Nuccio EE, Taga ME, Firestone MK, Banfield JF. Soil Candidate Phyla Radiation Bacteria Encode Components of Aerobic Metabolism and Co-occur with Nanoarchaea in the Rare Biosphere of Rhizosphere Grassland Communities. mSystems. 2021 Aug 17;6(4):10.1128/msystems.01205-20.

24.Edwards J, Santos-Medellín C, Sundaresan V. Extraction and 16S rRNA Sequence Analysis of Microbiomes Associated with Rice Roots. Bio Protoc. 2018 Jun 20;8(12):e2884.

25.Thompson LR, Sanders JG, McDonald D, Amir A, Ladau J, Locey KJ, et al. A communal catalogue reveals Earth's multiscale microbial diversity. Nature. 2017;551(7681):457–63.

26.Letey J, Carrillo MLK, Pang XP. Approaches to characterize the degree of water repellency. Journal of Hydrology. 2000 May 29;231–232:61–5.

27.Haney Test Interpretation Guide v1.0 [Internet]. [cited 2024 Apr 10]. Available from: https://www.wardlab.com/wp-content/uploads/2020/02/Haney-Rev-1.0-Interpretation-Guide-PDF-1.pdf

28.Haney Report Definitions-New.pdf [Internet]. [cited 2024 Jul 4]. Available from: http://mvtl.com/_static/web/assets/media/pdf/Haney%20Report%20Definitions-New.pdf

29.Bolger AM, Lohse M, Usadel B. Trimmomatic: a flexible trimmer for Illumina sequence data. Bioinformatics. 2014 Aug 1;30(15):2114–20.

30.Bushnell B. BBTools software package. 2014 [cited 2023 Oct 25]. BBMap. Available from: https://sourceforge.net/projects/bbmap/

31.Li D, Liu CM, Luo R, Sadakane K, Lam TW. MEGAHIT: an ultra-fast single-node solution for large and complex metagenomics assembly via succinct de Bruijn graph. Bioinformatics. 2015 May 15;31(10):1674–6.

32.Kieft K, Zhou Z, Anantharaman K. VIBRANT: automated recovery, annotation and curation of microbial viruses, and evaluation of viral community function from genomic sequences. Microbiome. 2020 Jun 10;8(1):90.

33.Huang Y, Niu B, Gao Y, Fu L, Li W. CD-HIT Suite: a web server for clustering and comparing biological sequences. Bioinformatics. 2010 Mar 1;26(5):680–2.

34.Langmead B, Trapnell C, Pop M, Salzberg SL. Ultrafast and memory-efficient alignment of short DNA sequences to the human genome. Genome Biology. 2009 Mar 4;10(3):R25.

35.Woodcroft BJ. CoverM [Internet]. 2023. Available from: https://github.com/ wwood/CoverM

36.Roux S, Camargo AP, Coutinho FH, Dabdoub SM, Dutilh BE, Nayfach S, et al. iPHoP: An integrated machine learning framework to maximize host prediction for metagenome-derived viruses of archaea and bacteria. PLOS Biology. 2023 Apr 21;21(4):e3002083.

37.Ter Horst AM, Santos-Medellín C, Sorensen JW, Zinke LA, Wilson RM, Johnston ER, et al. Minnesota peat viromes reveal terrestrial and aquatic niche partitioning for local and global viral populations. Microbiome. 2021 Nov 26;9(1):233.

38.ter Horst AM, Fudyma JD, Sones JL, Emerson JB. Dispersal, habitat filtering, and eco-evolutionary dynamics as drivers of local and global wetland viral biogeography. ISME J. 2023 Nov;17(11):2079–89.

39.Callahan BJ, McMurdie PJ, Rosen MJ, Han AW, Johnson AJA, Holmes SP. DADA2: High-resolution sample inference from Illumina amplicon data. Nat Methods. 2016 Jul;13(7):581–3.

40.Quast C, Pruesse E, Yilmaz P, Gerken J, Schweer T, Yarza P, et al. The SILVA ribosomal RNA gene database project: improved data processing and web-based tools. Nucleic Acids Research. 2013 Jan 1;41(D1):D590–6.

41.R Core Team. R: A language and environment for statistical computing. [Internet]. R Foundation for Statistical Computing, Vienna, Austria.; 2023. Available from: https://www.R-project.org/

42.Oksanen J, Simpson GL, Blanchet FG, Kindt R, Legendre P, Minchin PR, et al. vegan: Community

Ecology Package [Internet]. 2022 [cited 2022 Jul 6]. Available from: https://CRAN.R-project.org/package=vegan

43.Krassowski M. ComplexUpset: Create Complex UpSet Plots Using “ggplot2” Components [Internet]. 2021 [cited 2022 Sep 22]. Available from: https://CRAN.R-project.org/package=ComplexUpset

44.Hijmans RJ, Karney (GeographicLib) C, Williams E, Vennes C. geosphere: Spherical Trigonometry [Internet]. 2022 [cited 2024 Jul 4]. Available from: https://cran.r-project.org/web/packages/geosphere/index.html

45.Cooperdock SC, Hawkes CV, Xu DR, Breecker DO. Soil Water Content and Soil Respiration Rates Are Reduced for Years Following Wildfire in a Hot and Dry Climate. Global Biogeochemical Cycles. 2020;34(12):e2020GB006699.

46.Santana VM, Bradstock RA, Ooi MKJ, Denham AJ, Auld TD, Baeza MJ. Effects of soil temperature regimes after fire on seed dormancy and germination in six Australian Fabaceae species. Aust J Bot. 2010 Oct 27;58(7):539–45.

47.Alcañiz M, Outeiro L, Francos M, Farguell J, Úbeda X. Long-term dynamics of soil chemical properties after a prescribed fire in a Mediterranean forest (Montgrí Massif, Catalonia, Spain). Science of The Total Environment. 2016 Dec;572:1329–35.

48.Santos-Medellin C, Zinke LA, ter Horst AM, Gelardi DL, Parikh SJ, Emerson JB. Viromes outperform total metagenomes in revealing the spatiotemporal patterns of agricultural soil viral communities. ISME J. 2021 Jul;15(7):1956–70.

49.Santos-Medellín C, Liechty Z, Edwards J, Nguyen B, Huang B, Weimer BC, et al. Prolonged drought imparts lasting compositional changes to the rice root microbiome. Nat Plants. 2021 Aug;7(8):1065–77.

50.Moreno J, López-González JA, Arcos-Nievas MA, Suárez-Estrella F, Jurado MM, Estrella-González MJ, et al. Revisiting the succession of microbial populations throughout composting: A matter of thermotolerance. Science of The Total Environment. 2021 Jun 15;773:145587.

51.Smith NR, Kishchuk BE, Mohn WW. Effects of Wildfire and Harvest Disturbances on Forest Soil Bacterial Communities. Applied and Environmental Microbiology. 2008 Jan;74(1):216–24.

52.Ramond JB, Jordaan K, Díez B, Heinzelmann SM, Cowan DA. Microbial Biogeochemical Cycling of Nitrogen in Arid Ecosystems. Microbiology and Molecular Biology Reviews. 2022 Apr 7;86(2):e00109-21.

53.Paez-Espino D, Eloe-Fadrosh EA, Pavlopoulos GA, Thomas AD, Huntemann M, Mikhailova N, et al. Uncovering Earth’s virome. Nature. 2016 Aug;536(7617):425–30.

54.Dennehy JJ, Abedon ST. Bacteriophage Ecology. In: Harper DR, Abedon ST, Burrowes BH, McConville ML, editors. Bacteriophages [Internet]. Cham: Springer International Publishing; 2021 [cited 2024 Aug 10]. p. 253–94. Available from: https://link.springer.com/10.1007/978-3-319-41986-2_8

55.Paepe MD, Taddei F. Viruses’ Life History: Towards a Mechanistic Basis of a Trade-Off between Survival and Reproduction among Phages. PLOS Biology. 2006 Jun 13;4(7):e193.

## Main Figures

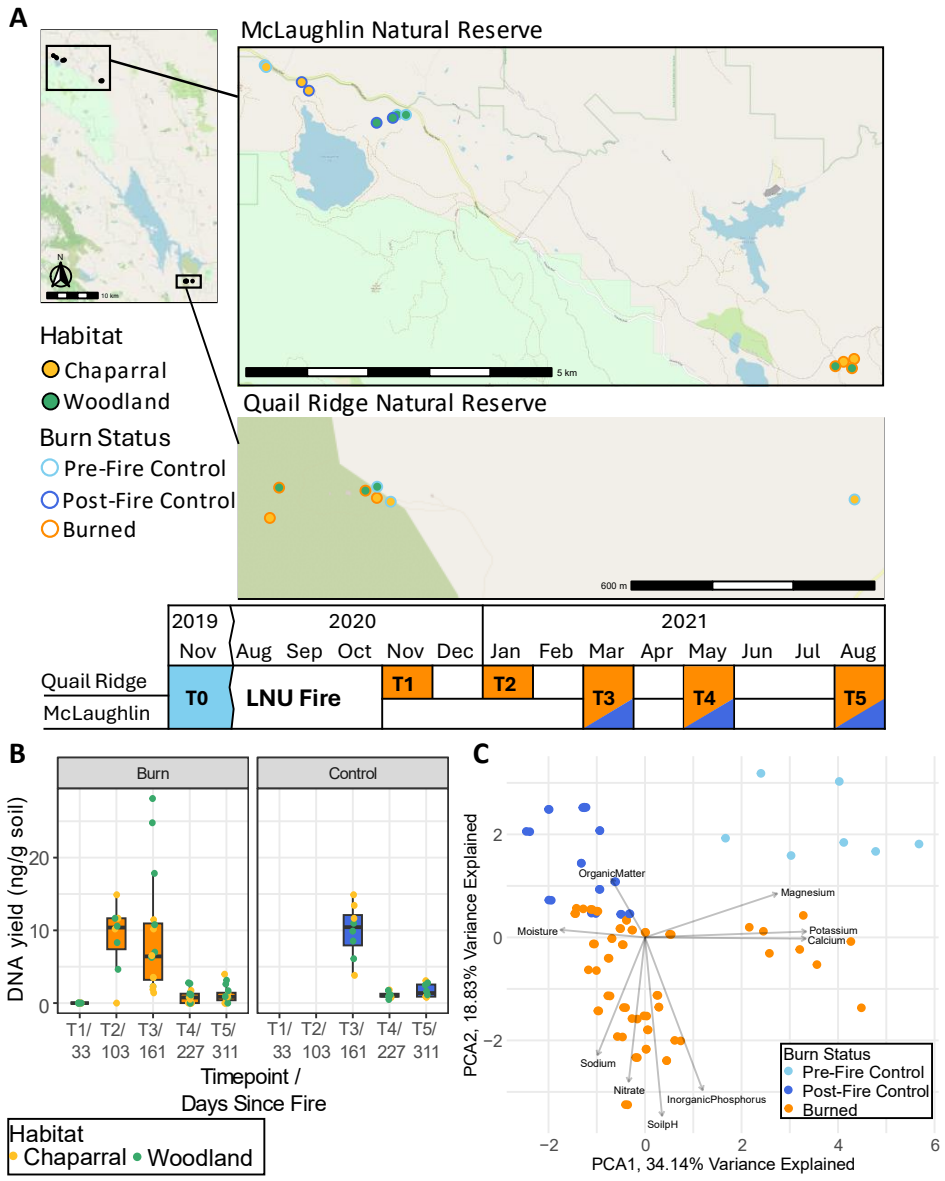


**Figure 11. A.** Map of plot locations in the main map and point fill indicating habitat and point outline indicating burn status in the subset maps, for a total of 12 plots. Two replicate cores were collected from each plot (each point in the map) at each sampled time point (except for the pre-fire controls). Table shows timeline of sample collection in each natural reserve. **B.** DNA yields for all viromes over time (labels show time point / days since fire), separated by burned (left facet) and control (right facet) plots. Dot color indicates habitat. Box boundaries correspond to 25$^{th}$ and 75$^{th}$ percentiles, and whiskers extend to ±1.5x the interquartile range. T1 and T2 were not collected for control plots but remain as "blanks" in the graph for easier comparisons to burned plots T3-T5. T0 (not plotted) was 322 days before the fire. **C.** Principal component analysis (PCA) of z-transformed chemical properties for each sample, with color indicating burn status.

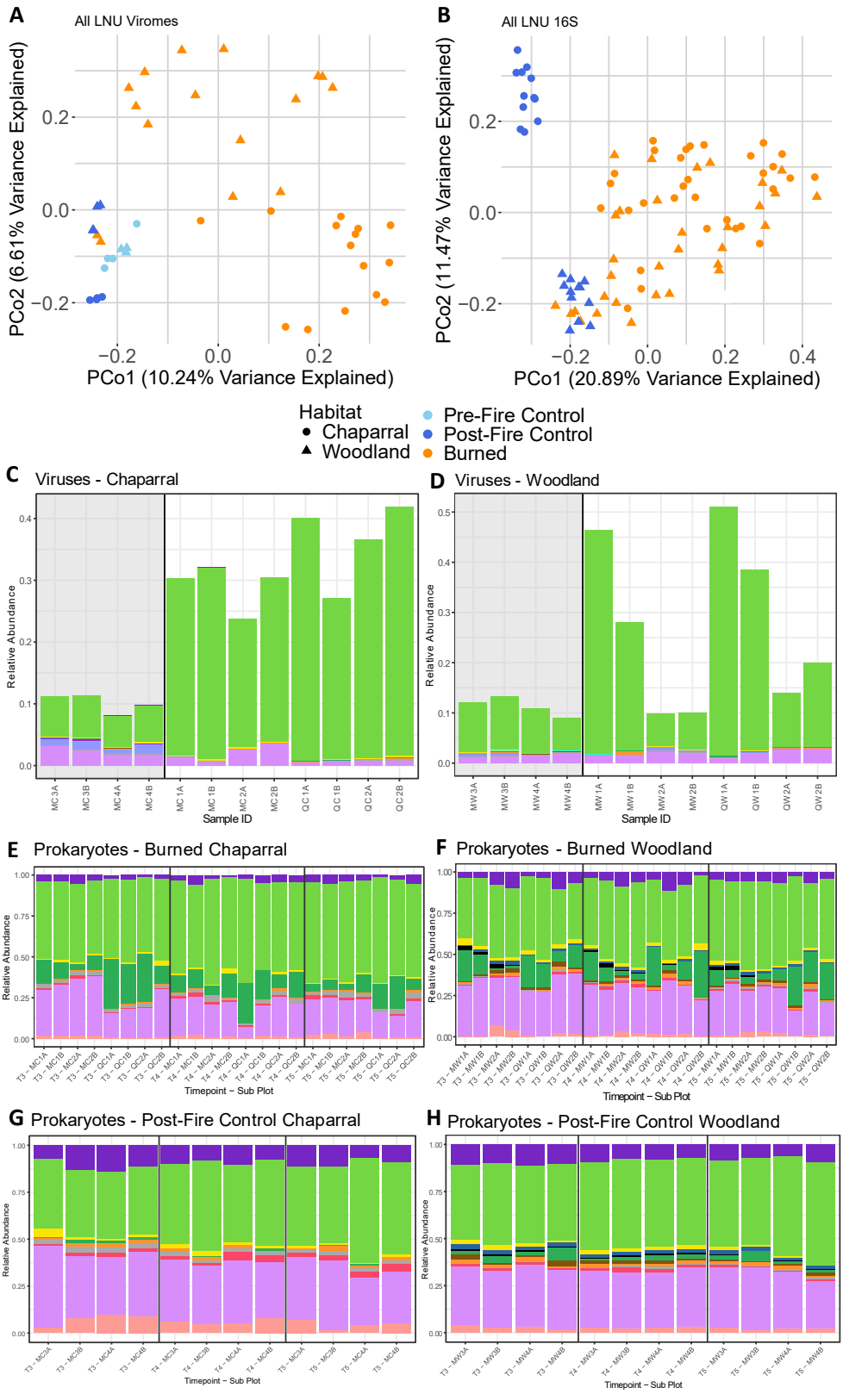
A
All LNU Viromes
PCo2 (6.61% Variance Explained)
PCo1 (10.24% Variance Explained)
B
All LNU 16S
PCo2 (11.47% Variance Explained)
PCo1 (20.89% Variance Explained)
Habitat
Chaparral
Woodland
Pre-Fire Control
Post-Fire Control
Burned
C
Viruses - Chaparral
D
Viruses - Woodland
Relative Abundance
Sample ID
E
Prokaryotes - Burned Chaparral
F
Prokaryotes - Burned Woodland
Timepoint – Sub Plot
G
Prokaryotes - Post-Fire Control Chaparral
H
Prokaryotes - Post-Fire Control Woodland
Host Phylum / Phylum
Acidobacteriota
Actinobacteriota
Bacteroidota
Cyanobacteria
Chloroflexota
Crenarchaeota
Firmicutes
Gemmatimonadota
Myxococcota
Nitrospirota
Planctomycetota
Proteobacteria
Verrucomicrobiota
mixed
Other

**Figure 12. A/B.** Unconstrained analyses of principal coordinates (PCoA) performed on vOTU (**A**) and prokaryotic ASV (**B**) Bray-Curtis dissimilarities calculated across all viromes or ASV gene profiles, respectively, with color indicating burn condition and shape indicating habitat. **C/D.** Relative abundances of vOTUs labeled with their phylum-level host predictions for chaparral (**C**) and woodland (**D**) habitats. Each stacked bar is one virome. Less abundant host phyla are collapsed into the "other" group. The gray box behind bars indicates control samples. **E-H.** Phylum-level relative abundances in 16S rRNA gene profiles from total DNA amplicon libraries of all samples over time faceted by chaparral burned (**E**), woodland burned **(F),** chaparral post-fire control **(G)** and woodland post-fire control (**H**). Each stacked bar is one sample, and all other parameters are like **C/D**.

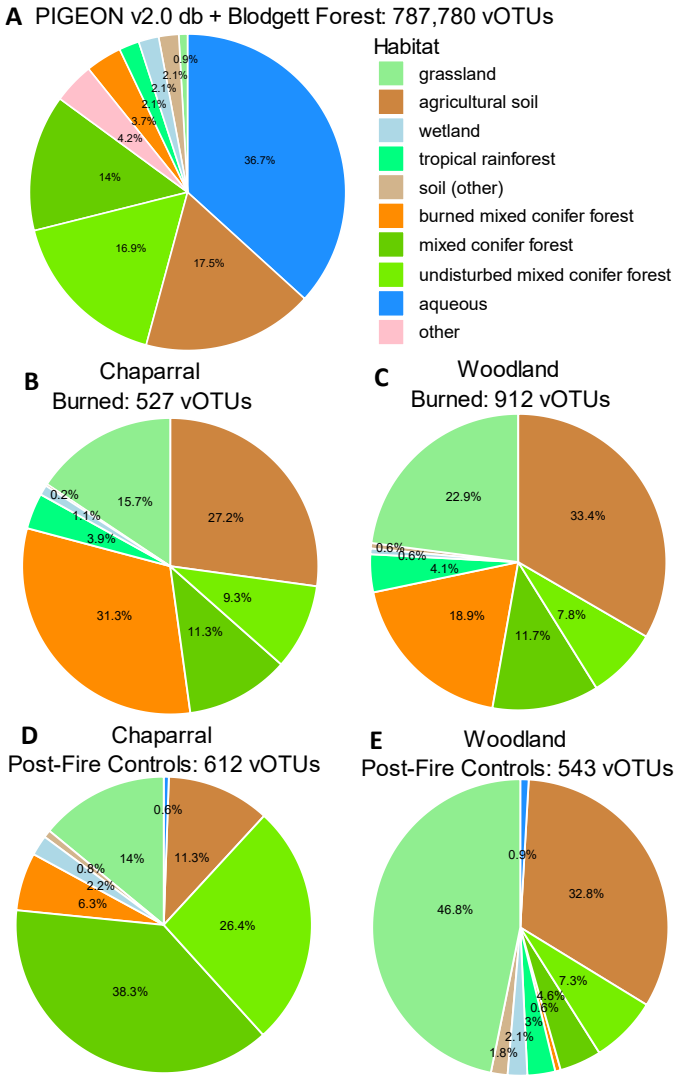


**Figure 13. A.** Habitat composition (percentages) of 787,780 vOTUS from the combined set of vOTUs from the of PIGEON v2.0 database (db) and the Blodgett Forest prescribed burn and laboratory heating (9) studies, colored by original source environment. **B-E.** Relative proportions of the vOTUs from (**A**) that were detected in our dataset, separated by the habitat (chaparral or woodland) and burn status (burn or control) in which they were detected.

## Supplementary Figures

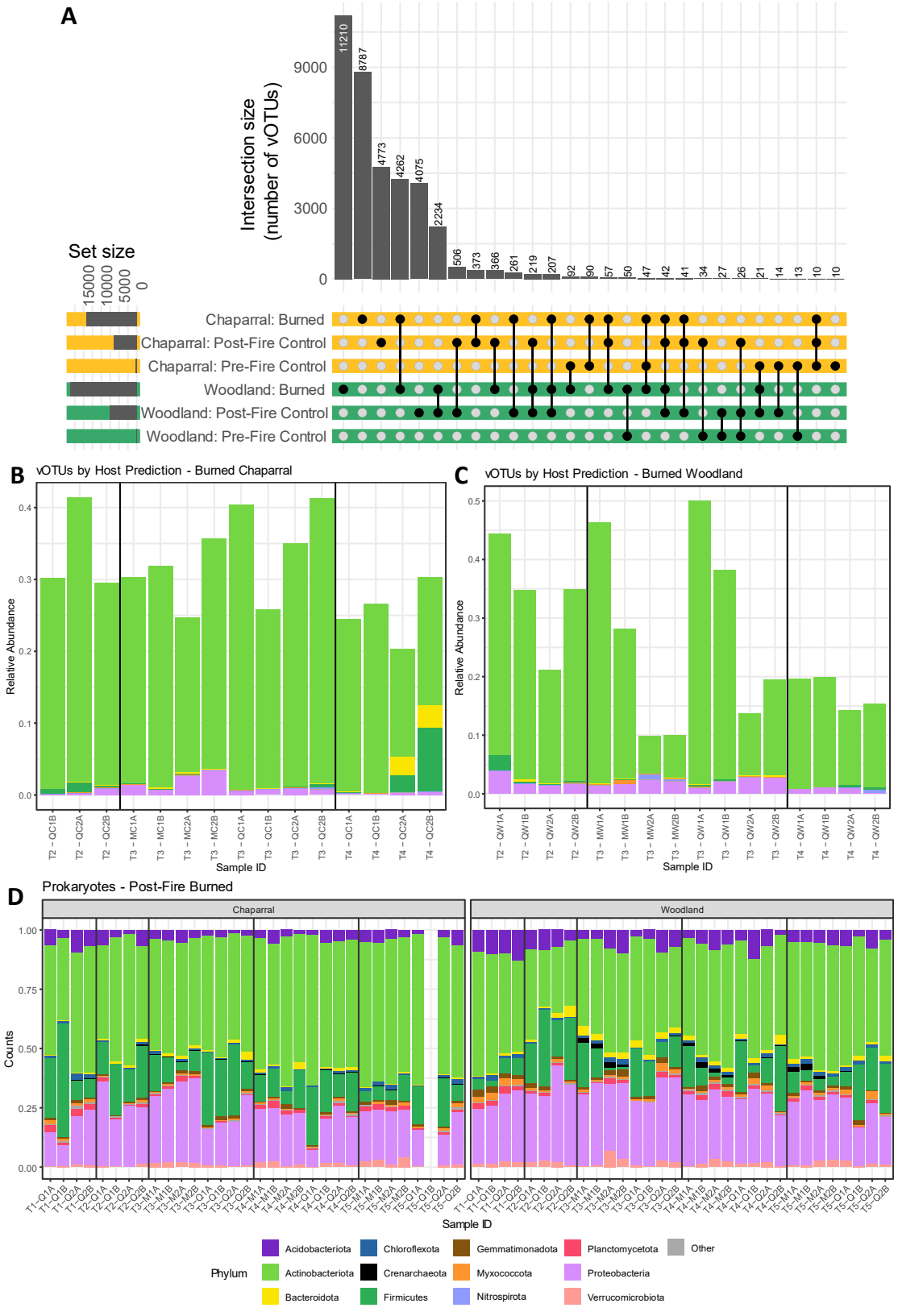

**Supplementary Figure 7. A.** UpSet plot of vOTU detection patterns across plots with blackened circles indicating detection in a particular habitat with a particular condition (burned, pre-fire control, and post-fire control) and intersection size indicating the number of vOTUs with a given detection pattern (detected in one or more habitat/burn condition combinations). **B/C.** Time series showing the relative abundances of vOTUs grouped by their phylum-level host predictions for burned chaparral (**B**) and burned woodland (**C**) time points. Each bar is a virome, and vertical black lines separate time points. All lower abundance vOTU groups (according to host phyla) are collapsed into an "other" group. **D.** Time series showing relative abundances of prokaryotic phyla, faceted by habitat (chaparral – left, woodland – right) from burned samples from all timepoints. Each bar is a sample, with the missing bar representing a sample that failed amplification and was not sequenced. Vertical black lines separate time points. All lower abundance phyla are collapsed into an "other" group.